REACTOR MATERIALS

A Quarterly Technical Progress Review

Prepared for DIVISION OF TECHNICAL INFORMATION, USAEC, by
R. W. DAYTON, E. M. SIMONS, and ASSOCIATES, BATTELLE MEMORIAL INSTITUTE

Fall 1964

● VOLUME 7

● NUMBER 3

TECHNICAL PROGRESS REVIEWS

To meet the needs of industry for concise summaries of current atomic developments, the Atomic Energy Commission is publishing this series, Technical Progress Reviews. Issued quarterly, each of the reviews digests and evaluates the latest findings in a specific area of nuclear technology and science.

The five journals published in this series are:

Isotopes and Radiation Technology, P. S. Baker, A. F. Rupp, and associates, Oak Ridge National Laboratory

Nuclear Safety, Wm. B. Cottrell, W. H. Jordan, and associates, Oak Ridge National Laboratory

Power Reactor Technology, W. H. Zinn and J. R. Dietrich, General Nuclear Engineering Corporation

Reactor Fuel Processing, Stephen Lawroski and associates, Chemical Engineering Division, Argonne National Laboratory

Reactor Materials, R. W. Dayton, E. M. Simons, and associates, Battelle Memorial Institute

Each journal may be purchased from the Superintendent of Documents, U. S. Government Printing Office, Washington, D. C., 20402. *Isotopes and Radiation Technology* at $2.00 per year for subscription or $0.55 for individual issues; the other four journals at $2.50 per year and $0.70 per issue. See back cover for remittance instructions and foreign postage requirements.

The views expressed in this publication do not necessarily represent those of the United States Atomic Energy Commission, its divisions or offices, or of any Commission advisory committee or contractor.

Availability of Reports Cited in This Review

Unclassified AEC reports are available for inspection at AEC depository libraries and are sold by the Office of Technical Services, Department of Commerce, Washington, D. C., 20230. Some of the reports cited are not available owing to their preliminary nature; however, the information contained in them will eventually be made available in formal progress or topical reports.

Unclassified reports issued by other Government agencies or private organizations should be requested from the originator.

Unclassified British and Canadian reports may be inspected at AEC depository libraries. British reports are sold by the British Information Service, 45 Rockefeller Plaza, New York, N. Y.; Canadian reports (AECL series) are sold by the Scientific Document Distribution Office, Atomic Energy of Canada, Ltd., Chalk River, Ontario, Canada.

Classified U. S. and foreign reports identified in this journal as Classified may be purchased by properly cleared Access Permit Holders from the Division of Technical Information Extension, U. S. Atomic Energy Commission, P. O. Box 1001, Oak Ridge, Tenn., 37831. Such reports may be inspected at classified AEC depository libraries.

REACTOR MATERIALS

A REVIEW OF RECENT DEVELOPMENTS

Prepared for DIVISION OF TECHNICAL INFORMATION, USAEC,
by R. W. DAYTON, E. M. SIMONS, and ASSOCIATES,
BATTELLE MEMORIAL INSTITUTE

FALL 1964

VOLUME 7

NUMBER 3

Foreword

Reactor Materials is one of a series of quarterly technical progress reviews broadly covering the field of nuclear science and technology. Under the auspices of the USAEC Division of Technical Information, *Reactor Materials* is prepared by Battelle personnel from worldwide literature. It covers properties, behavior, and fabrication processes of materials applicable to nuclear reactor components and associated equipment.

The reader will recognize that the scope of this Review is too broad to permit detailed coverage of every topic. Rather, the authors and editors attempt to combine the highlights of significant new developments into an information summary of current research for both management and the technical specialist. As a rule, enough of the results are presented to define the research and summarize the findings. For readers desiring more information on any particular topic, a complete set of references is provided at the end of each section.

Each quarter, a number of bibliographies, monographs, and books appear on subjects within the scope of *Reactor Materials*. Although the main purpose of this Review is to call attention to findings that are new and significant, such publications are noted in the text because they often represent excellent compilations of available information on important materials topics.

R. W. DAYTON
E. M. SIMONS
R. W. ENDEBROCK
Battelle Memorial Institute

DEPOSITED BY THE
UNITED STATES OF AMERICA

Contents

Foreword

I Fuel and Fertile Materials 149
Uranium Metal and Alloys 149
Plutonium 152
Thorium and Its Alloys 154
Metal-Ceramic Fuels 156
Coated-Particle Materials 158
Uranium Oxides 162
Carbide and Nitride Fuels 163
Mechanism of Corrosion of Fuel Alloys 164
Basic Studies of Irradiation Effects in Fuel Materials 164
References 166

II Moderator Materials 169
Graphite 169
Beryllium Metal and Alloys 172
Beryllium Oxide 173
Solid Hydrides 174
References 175

III Nuclear Poisons 177
Metallic Poison Materials 177
Dispersion Poison Materials 177
References 178

IV Cladding and Structural Materials . 179
Corrosion 179
Metal-Water Reactions 184
Radiation Effects in Nonfuel Materials 185
Selected Mechanical Properties of Cladding and Structural Materials . . 191
Selected Metallurgical Aspects of Cladding and Structural Materials . . 194
Diffusion Studies 195
Ceramic Technology 196
References 197

V Special Fabrication Techniques . . . 201
Melting, Casting, and Hot and Cold Working 201
Cladding 202
Metals Joining 204
Nondestructive Testing 206
References 207

Issued quarterly by the U. S. Atomic Energy Commission. Use of funds for printing this publication approved by the Director of the Bureau of the Budget on October 14, 1963.

Section

I

Reactor Materials

Fuel and Fertile Materials

Uranium Metal and Alloys

Unalloyed Uranium

A new book entitled *Uranium*[1] has been published. This, the latest book to appear on uranium, contains information on the preparation of uranium metal from ore, fabrication, physical properties, deformation and preferred orientation, recovery, recrystallization and grain growth, mechanical properties, effects of irradiation and thermal cycling, and corrosion of uranium. In addition, binary and ternary phase diagrams for important uranium alloys are presented, along with alloy property and diffusion data.

In work performed at Battelle[2] for the National Lead Co. of Ohio, levels and distribution of residual stresses were determined in specimens representative of six normal steps and four alternative steps in the manufacture of hollow uranium fuel elements. To obtain the data, an electrochemical procedure was developed for the rapid and controlled removal of metal from the bores of the specimens. A definite correlation was noted between residual-stress levels and specific manufacturing-process steps. Distinct differences in residual stresses were noted between oil- and water-quenched specimens. Stresses in water-quenched specimen were in the 40,000- to 50,000-psi range, whereas oil-quenched specimens were about one-quarter of this stress. However, in the final production step, the canning procedure, the effects of earlier stressing were almost completely canceled, final stresses being in the 15,000- to 20,000-psi range.

In measurements after various mechanical and thermal treatments, internal friction and Young's modulus went through a maximum and minimum, respectively, with increasing severity of quenching from a beta temperature. Beta-heat-treated and furnace-cooled uranium, when cold reduced, exhibited monotonic increases and decreases, respectively, in internal friction and modulus for reductions up to 12%. Uranium that was hot forged and rolled and then cold reduced in increments up to 46% in area showed an initial rapid reduction in modulus and then a leveling off with increasing degree of cold work. The internal friction fluctuated, showing that there was no relation to degree of working.

In another study,[3] tensile tests and exhaustive metallographic examinations were conducted in an effort to relate the mechanical properties, the chemical compositions, and the structures of five grades of uranium to their irradiation stability. Subsequent tensile tests were conducted on seven other types of uranium containing various levels of iron, aluminum, and silicon. Special attention was given to the mode of fracture exhibited by the various materials and to the existence of grain-boundary phases and intergranular fracture. No evidence was noted of grain-boundary failure at temperatures up to 450°C. Most or all failures were precipitated by secondary phases not associated with the grain boundaries. No definite connection was noted between the chemical composition and the tensile properties of the materials which could be related to their irradiation stability. A supplementary study concerned with the substructure and fine-particle distribution in cast uranium was also undertaken. The major accomplishment of this study was the development of metallographic techniques. Particularly interesting were the microstructures revealed by vacuum-cathodic etching.

The plastic behavior of polycrystalline uranium has been investigated by the French.[4] Traction tests were used to study the effect of

temperature between 20 and −196°C on the plastic behavior of uranium. The rupture stress and the elongation at rupture both decrease when the temperature is lowered but pass through a plateau that marks the transition from intercrystalline to transcrystalline rupture.

The surface tension of uranium at its melting point has been determined by the French[5] to be 1500 dynes/cm.

The behavior of helium in cyclotron-irradiated and -heated uranium and several uranium alloys was studied at Nuclear Metals.[6] The observed bubbles were classified in two groups: class I bubbles, having diameters less than 1 μ and densities of the order of 10^{13} to 10^{15}/cm^3, and class II bubbles, having diameters of 10 to 150 μ and densities of the order of 10^3 to 10^5/cm^3. Bubbles of intermediate size were not seen. The number and distribution of class I bubbles appear to be related to the availability of nucleation sites. Activation energy for nucleation and growth of class I bubbles in gamma-phase uranium was determined to be 20 kcal/mole at temperatures between 900 and 1070°C. This value was found to be in good agreement with that reported for the self-diffusion of gamma uranium.

In the dilute alloys of uranium examined, class I bubbles were, for the most part, smaller in size and greater in number than those in unalloyed uranium subjected to the same annealing conditions. In uranium metal richer in additions, class II bubbles formed less easily during gamma-phase anneals. Postirradiation thermal-cycling treatments did not, in general, alter the formation of bubbles in materials included in this study. (M. S. Farkas)

Alpha-Phase Uranium Alloys

The Russians have issued two books in the uranium-alloy field: *Structure and Properties of Uranium, Thorium, and Zirconium Alloys*[7] and *The Structure of Alloys of Certain Systems Containing Uranium and Thorium.* The latter is available in translated form. These books contain 75 technical papers on the constitution and the thermal, mechanical, and corrosion properties of uranium, thorium, and zirconium. Uranium-alloy systems specifically reported include U-Cr, U-Mo, U-Nb, U-Zr, U-Al-Fe, U-Al-Si, U-Cr-Mo, U-Mo-Nb, U-Mo-Zr, U-Nb-Ti, U-Nb-Zr, U-Ti-Zr, and U-Mo-Nb-Zr. These books are of particular interest to uranium metallurgists because they present information and data on alloys not previously available.

The uranium-osmium system was investigated by the English.[9] The principle features of the system are the high solubility of osmium in gamma uranium and the existence of four intermetallic compounds: U_3Os, U_2Os, U_5Os, and UOs_2.

Table I-1 COMPOSITION OF ALLOYS IRRADIATED, DESCRIPTION OF DISPERSED PHASES, AND PERCENT DENSITY CHANGE AFTER IRRADIATION AND POSTIRRADIATION ANNEALING[13]

Alloy	Composition, wt.% U	Mo	Si	Particles/cm^3	Particle size, μ	Total density change, % After irradiation	After annealing 5 hr at 650°C	After annealing 20 hr at 650°C	After annealing 20 hr at 650°C and 10 hr at 680°C
				Capsule NAA-60-1					
A	100					3.7	25.8	26.9	
B	Balance	4.4				−0.8	−1.2	11.0	16.1
C	Balance	4.0	0.1	10^{10}	2	1.2	1.3	1.2	1.6
D	Balance	4.0	0.1	4×10^{12}	0.2	0.6	0.8	0.5	1.3

Alloy	Composition, wt.% U	Mo	Sn	Particles/cm^3	Particle size, μ	Total density change, % After irradiation	After annealing 18 hr at 550°C	After annealing 72 hr at 550°C	After annealing 72 hr at 550°C and 24 hr at 600°C
				Capsule NAA-60-2					
A2	100					9.1	29.4	30.0	
E	Balance	10.3				1.4	1.9	2.3	1.7
F	Balance	10.5	0.04	2×10^{13}	0.3	0.5	0.7	0.7	1.2
G	Balance	10.5	0.04	(As cast)		1.0	1.0	1.0	1.8

The system uranium-UAl_2-UFe_2 has been investigated by the Germans.[10] The results indicate that extended three-phase equilibria exist. Uranium solid solutions show a limited ternary solubility, but the intermetallic compounds UAl_2, $U(Fe,Al)_2$, UFe_2, and U_6Fe do not.

The kinetics of the isothermal decomposition of a gamma-phase uranium–6 at.% molybdenum alloy at 670 to 390°C are discussed in an English report.[11] Four different decomposition modes were found; one of these, involving the formation of a fine granular structure, has not been reported before for alloys of similar composition.

Other studies conducted by the English[12] on the transformation of uranium-molybdenum alloys containing 0.9 to 4.17 at.% molybdenum have been reported. Cooling at various rates from the gamma phase was investigated by an end-quenching technique. It was shown that there is direct transformation from gamma to alpha or alpha plus gamma for alloys containing 2.5 at.% or more of molybdenum and that the gamma grain size has an effect on the decomposition product. The sequence of phases observed at various cooling rates was elucidated.

Investigators at North American Aviation Science Center[13] have reported results of irradiation and postirradiation annealing on uranium, uranium-molybdenum, uranium-molybdenum-silicon, and uranium-molybdenum-tin alloys. The objective of the program was to test the hypothesis that swelling may be controlled in nuclear fuels containing a fine dispersion of a second phase. The compositions of the samples irradiated are given in Table I-1 along with the particle density, size, density change after irradiation, and density change after postirradiation annealing. The specimens in the NAA-60-1 capsule were irradiated to 0.4 at.% burnup at a calculated central temperature of 300°C, whereas the specimens in NAA-60-2 received 0.6 at.% burnup at 400°C.

The results indicate that considerable reduction in swelling at moderate burnups has been achieved in these alloys. The ternary additions, although effective in the uranium–10 wt.% molybdenum alloy, provide outstanding swelling resistance in the uranium–4 wt.% molybdenum alloys and are most helpful in the form of a fine dispersion.

Uranium alloys with molybdenum contents between 3 and 10 wt.% were subjected to capsule irradiation tests by Atomics International.[14] Burnups up to 10,000 Mwd/ton of uranium at temperatures between 800 and 1500°F were achieved.

The results shown in Fig. I-1 indicate that molybdenum has a considerable effect in reducing the swelling due to irradiation. For example, 3 wt.% molybdenum reduces the swelling from 25%, for pure uranium, to 7% at ~3000 Mwd/ton at 1270°F. Further swelling resistance can be gained by increasing the molybdenum content, but the amount gained becomes successively smaller. At higher irradiation levels the amount of swelling rapidly becomes greater, and larger amounts of molybdenum are required to provide similar resistance. A limit of 7% swelling, at 900°F and an irradiation of 7230 Mwd/ton, requires the use of 10 wt.% molybdenum in the alloy. The burnup rates were in the range of 2.0 to 4.0 × 10^{13} fissions/(cm^3)(sec).

Small ternary additions of silicon and aluminum were shown to have a noticeable effect in reducing swelling when added to a uranium–3 (or 4) wt.% molybdenum alloy base. Under the conditions of the present experiment, 0.26

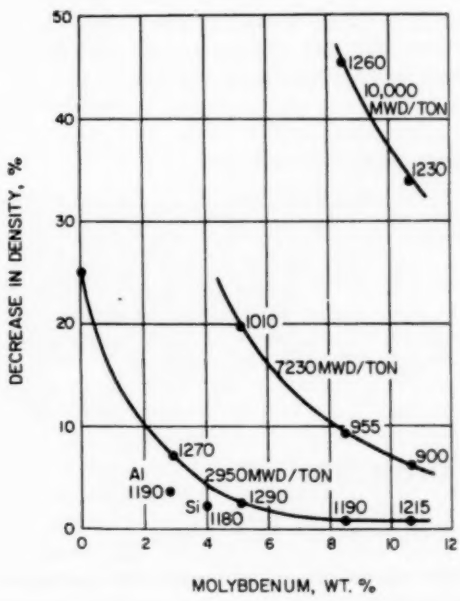

Fig. I-1 Effect of molybdenum content on swelling of uranium alloys.[14] The average central temperature (°F) of the specimens during irradiation is shown by each point.

wt.% silicon or 0.38 wt.% aluminum was equivalent to 1 to $1\frac{1}{2}$ wt.% molybdenum.

The Swedish[15,16] have released the results of two literature surveys. One is on the aqueous corrosion of uranium and its alloys; the other is concerned with radiation effects on solid uranium-based nuclear fuel materials.

(M. S. Farkas)

Gamma-Phase Uranium Alloys

The oxidation behavior of the uranium–10 wt.% molybdenum alloy in moist air (20,000 ppm H_2O) was studied at Argonne.[17] At 300°C the oxidation rate was linear at 1.74×10^{-3} mg of oxygen/(cm^3)(min) for the first 80 to 100 min, after which the reaction became parabolic. The transition is believed to be caused by the formation of a protective oxide coating. At 400 and 450°C the reaction was parabolic, with rate constants of 5.5 and 14 mg of oxygen/(cm^2)(min), respectively. At 500 and 600°C the reactions were linear throughout the runs, with rate constants of 0.039 and 0.31 mg of oxygen/(cm^2)(min), respectively. At 700°C a nearly cubic oxidation process was observed for the first 200 min, followed by an accelerating reaction that led to a final rate of about 0.07 mg of oxygen/(cm^2)(min). In general, oxidation rates for this alloy are at least an order of magnitude lower than for unalloyed uranium.

(A. A. Bauer)

Dilute Uranium Alloys

Phillips Petroleum[18] investigators report that aluminum-clad fuel plates containing cores of 20 to 35 wt.% uranium at UAl_3 dispersed in aluminum-alloy powder performed better than UO_2 fuel elements during irradiation under Materials Testing Reactor (MTR) and Engineering Test Reactor (ETR) conditions.

(M. S. Farkas)

Plutonium

Plutonium Metal and Alloys

The effects of various mechanical and thermal treatments on the transformation of retained phases in alpha plutonium have been determined at Hanford by measuring the density changes for periods up to 2 years.[19] The density of as-cast plutonium continually increased with time and continued to increase while standing at room temperature for 2 years. Density increases were less and rates of transformation were slower for higher purity plutonium. Both thermal cycling the plutonium between high-alpha temperature and subzero temperatures and hydrostatic pressing in the alpha phase can produce metal that contains no retained phases. It was also noted that isothermal beta-to-alpha transformation high in the alpha phase resulted in essentially no retained phases, whereas a significant amount of retained phase is observed after an isothermal transformation at subzero temperatures.

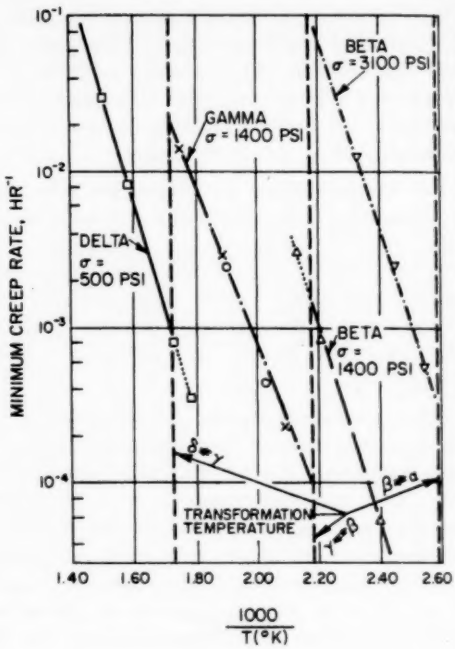

Fig. I-2 Effect of temperature on the steady-state creep rate of beta, gamma, and delta plutonium at the indicated compressive stresses.[19]

The effect of temperature on the steady-state creep rate of beta, gamma, and delta plutonium was determined. The data are plotted in Fig. I-2. Activation energies for creep of the beta, gamma, and delta phases were calculated to be 31, 24, and 31 kcal/mole, respectively.

The homogenization behavior of cast gallium-stabilized delta plutonium has been investigated at Los Alamos.[20] The cored alloy, containing 1.00 to 1.05 wt.% gallium, could be homogenized in the following minimum times: 500 hr at

Table I-2 PENETRATIONS OF URANIUM–10 WT.% PLUTONIUM–10 WT.% FIZZIUM INTO VANADIUM, VANADIUM–10 WT.% TITANIUM, AND VANADIUM–20 WT.% TITANIUM ALLOYS[17]

	Penetrations, μ					
	Vanadium		V–10 wt.% Ti		V–20 wt.% Ti	
Temp., °C	17 days	42 days	7 days	17 days	7 days	17 days
550	Nil	Nil				
600	Nil	Nil	2	3	2	2
650		1	4	5	4	4

425°C, 60 hr at 500°C, and 16 hr at 525°C. Mechanically working the alloy decreased homogenization time at 500°C to 14 hr. The following approximate diffusion equation was calculated:

$$D = (65 \pm 5) \exp(-40{,}100/RT) \text{ cm}^2/\text{sec}$$

Liquidus temperatures of plutonium-iron alloys containing 15 to 30 at.% iron as determined by differential thermal analysis indicated that the peritectic isotherm terminates at 13.5 at.% iron rather than at 11 at.% iron as reported by other investigators.[21]

Solubility limits of scandium in delta plutonium increased from 19.8 at.% at 350°C to 22.5 at.% at 650°C. Densities of the arc-cast plutonium-scandium alloys were essentially a linear function of the atomic composition.

Argonne[17] is continuing work on the development of uranium-plutonium-fizzium fuel alloys. A major second phase in uranium–10 wt.% plutonium–10 wt.% fizzium alloy, oil quenched from 775°C, comprised about 8 vol.% of the alloy and consisted of about 40 wt.% each of uranium and zirconium and about 10 wt.% each of plutonium and ruthenium. In a similar uranium–10 wt.% plutonium–10 wt.% fissium alloy, the major second phase comprised about 10 vol.% of the alloy and corresponded to U_2Ru in composition.

Results of preliminary compatibility tests of the uranium–10 wt.% plutonium–10 wt.% fizzium alloy with vanadium, vanadium–10 wt.% titanium, and vanadium–20 wt.% titanium are given in Table I-2. (V. W. Storhok)

Plutonium Compounds

Results of a study[22] of the plutonium-carbon phase diagram detail the $Pu + 2PuC \rightleftharpoons Pu_3C_2$ peritectoid reaction. Other Argonne workers[23] indicate that plutonium will precipitate as Pu_2C_3 from liquid-metal systems high in magnesium content. Since uranium is not soluble in such media, the liquid-metal concept of copreparing the mixed carbides seems unfeasible. The addition of carbon from organic binders in excess of 0.5 wt.% added to PuC causes formation of sesquicarbide during sintering. Results show that PuC can be sintered to 93% of theoretical density in vacuum after 2 hr at 1400°C. This same reference[23] indicates that the addition of a nickel sintering aid will introduce unidentified secondary phases that can in turn be reduced by vacuum annealing at 2200°C. The nickel additive does not appreciably affect the thermal coefficient of linear expansion; values of 11.9×10^{-6}/°C and 12.3×10^{-6}/°C are typical of pure $(U_{0.8}Pu_{0.2})C_{0.95}$ and the same material with 0.1 wt.% nickel, respectively.[24] The melting point of this composition is 2480 ± 20°C. Conclusions drawn[25] are that the vapor pressure of uranium over the solid solution $(U_{0.8}Pu_{0.2})C_{0.95}$ is 5×10^{-4} atm at 2600°K and 1×10^{-6} atm at 2100°K. It is of interest to note that arc-cast PuC fractured[26,27] under irradiation at 650°C after a 0.1 metal at.% burnup, whereas pressed and sintered material did not fracture but released 12% of the theoretical fission gas produced.

It has been established by workers at Nuclear Materials[28] that less than 50 ppm of SiO_2 must be maintained to permit sintering of mechanically blended UO_2 and PuO_2 to high density. The same workers have reported a maximum electrical resistivity for a UO_2–10 wt.% PuO_2 mixture which can probably be correlated with a corresponding melting-point anomaly reported by Hanford several years ago.

PuO_2 can be sintered to a high density in dry CO_2 after 6 hr at 1650°C with no suboxide formation; however, similar sintering in dry argon caused[29] decomposition to PuO_{2-x} and alpha Pu_2O_3. The halides are now removed[25] by heating in moist air for 1 hr between 650 and 700°C, whereas subsequent drying at 900°C is required for complete water removal.[30]

Hanford has indicated that beta Pu_2O_3 is compatible with tungsten, molybdenum, tantalum, niobium, and vanadium for 24 hr at 1650°C in helium atmospheres. Irradiation studies at Hanford have shown[31] that, in UO_2 pellets coaxially enriched with a plutonium–15 wt.% zirconium alloy wire, the wire disappeared, pre-

sumably by oxidation and dissolution in the UO_2. $(Th,Pu)O_2$ irradiation specimens have demonstrated behavior similar to other actinide oxide systems. Their thermal conductivity appears to be less than that of UO_2.

PuN containing 5 wt.% PuO_2 has been sintered to 97% of theoretical density in $1\frac{1}{4}$ hr at 1800°C in $\frac{2}{3}$ atm of nitrogen, and an 80 vol.% UN–20 vol.% PuN pellet formed a solid solution but did not densify in 5 hr under similar conditions.

(W. M. Pardue)

Thorium and Its Alloys

Work performed by the Russians[8] has recently become available on phase diagrams of thorium with uranium, plutonium, cerium, hafnium, zirconium, titanium, niobium, vanadium, beryllium, magnesium, aluminum, carbon, lead, bismuth, and selenium. Isothermal ternary diagrams are presented for the thorium-zirconium-uranium system at various temperatures from 550 to 1000°C.

Hardness of extruded thorium billets containing 4, 7, and 13 vol.% dispersed ThO_2 was measured at Oak Ridge.[32] Data are presented in Table I-3.

Table I-3 HARDNESS OF EXTRUDED THORIUM BILLETS[32]

Temp., °C	Hardness values, DPHN*	
	4 vol.% ThO_2	7 vol.% ThO_2
Ambient	129	148
300	54	67
600	31	31
800	13	13

*Diamond Pyramid Hardness Number.

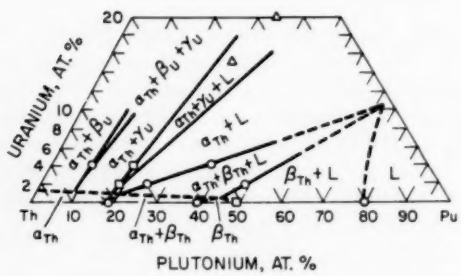

Fig. I-3 Preliminary phase diagram[17] of thorium-plutonium-uranium at 700°C. Phase boundaries: ○, by X-ray diffraction; □, by X-ray diffraction and metallography; ×, by microprobe analysis; Δ, other alloys.

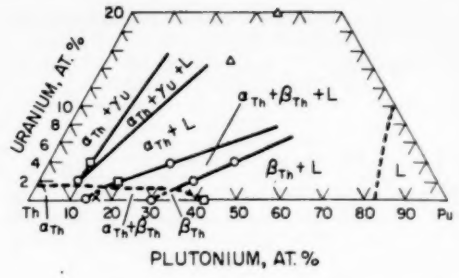

Fig. I-4 Preliminary phase diagram[17] of thorium-plutonium-uranium at 900°C. Phase boundaries: ○, by X-ray diffraction; □, by X-ray diffraction and metallography; ×, by microprobe analysis; Δ, other alloys.

Table I-4 COMPOSITION OF THE ALPHA PHASE IN AN ALLOY OF 45 WT.% THORIUM–20 WT.% URANIUM–35 WT.% PLUTONIUM[17]

Quenching temp., °C	Composition of alpha phase, wt.%			
	By microprobe analysis		From phase diagram	
	Plutonium	Uranium	Plutonium	Uranium
700	18.2	0.6	18.5	1.0
900	15.6	0.4	16.0	1.2

Peterson[33] reports that a solution of 2 g of ammonium chloride, 100 ml of formic acid, and 6 ml of water produced a smooth scratch-free surface on thorium when electropolished at 20 volts for 60 sec. Polishing of arc-melted thorium by this method revealed extensive twinning before other details of the microstructure were revealed.

Preliminary phase relations in the thorium-plutonium-uranium system have been reported for isotherms at 700 and 900°C by Argonne investigators.[17] These ternary diagrams are presented in Figs. I-3 and I-4. The composition of the alpha phase in a thorium–20 wt.% uranium–35 wt.% plutonium alloy as determined from the phase diagram and by microprobe analysis is shown in Table I-4. The lowering of the $\alpha \rightarrow \beta$ transformation of thorium by plutonium additions reported by the Russians could not be confirmed.

Hanford workers[34] have reported that Zircaloy-2-clad thorium–2.5 wt.% uranium–1.0

Table I-5 IRRADIATION HISTORY OF TUBULAR THORIUM–2.5 WT.% URANIUM–1.0 WT.% ZIRCONIUM FUEL ELEMENTS[34]

	Maximum operating conditions							
	Burnup		Temp.,	Surface heat flux		Specific power		Fuel volume
ETR	Fissions/cm³	Mwd/ton	°C	Cal/(sec)(cm²)	Btu/(hr)(sq ft)	Watts/g	Kw/ft	increase,* %
54	2.8×10^{19}	800	585	75	1.0×10^{6}	69	210	0.15
55	5.4×10^{19}	1550	538	68	9.0×10^{5}	62	188	0.15
56	8.6×10^{19}	2475	523	65	8.6×10^{5}	59	180	Not weighed
57	1.2×10^{20}	3400	585	75	1.0×10^{6}	69	210	0.5

*Weight measurements made at the end of cycle 57 showed a total fuel-element-volume increase of 0.3% for the two lower exposure fuel elements.

Table I-6 AS-CAST HARDNESS OF THORIUM-BASE ALLOYS[34]

Nominal alloy composition (balance thorium), wt.%		Addition elements, ppm		Hardness,* R_F
Uranium	Zirconium	Aluminum	Beryllium	
2.5	1.0	0	0	91, 91
2.5	2.0	0	0	73, 85, 84
2.5	2.0	500		86, 89
2.5	2.0	1000		90, 92
2.5	2.0	2000		92
2.5	2.0		500	80
2.5	2.0		1000	81
2.5	2.0		2000	79, 89
2.5	5.0	0	0	85, 88
2.5	5.0	500		86
2.5	5.0	1000		86
2.5	5.0	2000		91
2.5	5.0		500	88
2.5	5.0		1000	86
2.5	5.0		2000	81
5.0	2.0	0	0	79
5.0	2.0	500		90
5.0	2.0	1000		86
5.0	2.0	2000		97
5.0	2.0		500	89
5.0	2.0		1000	77
5.0	2.0		2000	87
5.0	5.0	0	0	84, 90
5.0	5.0	500		90
5.0	5.0	1000		88
5.0	5.0	2000		92
5.0	5.0		500	92
5.0	5.0		1000	91
5.0	5.0		2000	89

*Average of five measurements except where multiple readings are given.

wt.% zirconium alloy fuels completed four cycles in the ETR P-7 facility. The maximum operating conditions and measured volume changes for the four irradiation cycles are given in Table I-5.

The hardness of as-cast, 100-g, arc-melted thorium-uranium-zirconium alloys containing small additions of aluminum and beryllium has been measured. Hardness values are shown in Table I-6. (R. L. Martin)

Metal-Ceramic Fuels

Dispersion Fuels

To test the reference fuel of the Advanced Test Reactor (ATR) as well as alternative materials, Phillips Petroleum workers[35] fabricated fuel plates for irradiation in the ETR. Cores containing 32 to 54 wt.% U_3O_8, UO_2, and UAl_3, plus 0.19 wt.% B_4C in a matrix of X8001 and the matrix metal. All the samples containing UAl_3 appeared to be in good condition at the end of testing. A small amount of fission-gas voids could be seen in the microstructures; however, no blistering was evident.

Oak Ridge reports[36] mechanical-property data for two aluminum alloys (X8001 and 6061) and a fuel dispersion (35 wt.% U_3O_8–X8001 aluminum). The creep properties of these materials in uniaxial tension were measured in aluminum, were clad with 6061-0 and X8001 with 15 to 20% cold work. All the samples were anodized to produce thermal-barrier coatings of Al_2O_3 so that the fuel temperature of interest in the ATR core could be obtained during irradiation in the ETR. This also provided a simulation of corrosion conditions anticipated in the ATR. The irradiation consisted of two 6-week cycles, and the conditions are summarized in Table I-7.

Table I-7 FUEL COMPOSITIONS TESTED FOR THE ATR[35]

Fuel composition,* wt.%	Cladding material	Average heat flux,† 10^6 Btu/(hr)(sq ft)	Average temp.,† °C	Burnup, 10^{21} fissions/cm^3	General results
35 U_3O_8	X8001-H12	0.8	171	0.66	Satisfactory
35 U_3O_8	6061-0	0.8	186	0.69	Satisfactory
32 UO_2	X8001-H12	0.6	141	0.51	Satisfactory
32 UO_2	6061-0	0.6	155	0.53	Satisfactory
40 UAl_3	X8001-H12	1.0	175	0.75	Satisfactory
40 UAl_3	6061-0	1.0	180	0.77	Satisfactory
54 UAl_3	6061-0	1.3	178	1.0	Satisfactory
44 U_3O_8	6061-0	1.3	176	1.0	Blistered
41 UO_2	6061-0	1.5	180	1.1	Blistered

*X8001 aluminum powder plus B_4C used as matrix materials.
†At beginning of irradiation.

The combinations of high temperature (uranium-aluminum fuels) and high burnups at high fission rates represent a range of testing previously not attempted. Blisters developed in all the high weight percent UO_2 and U_3O_8 plates that were irradiated to 1×10^{21} fissions/cm^3, although no fission breaks were detected by the ETR monitor. Examination of the UO_2 and U_3O_8 plates irradiated at 0.5×10^{21} fissions/cm^3 disclosed no evidence of blistering, nor was there any indication of damage in the 35 wt.% U_3O_8 samples irradiated to about 0.7×10^{21} fissions/cm^3. Microstructure of the irradiated plates indicated considerable void formation (fission gas) within the UO_2 and U_3O_8 fuel particles, as well as extensive reaction between the oxides

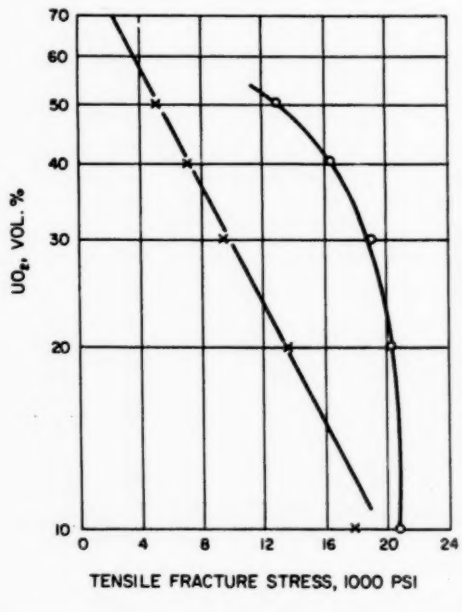

Fig. I-5 Relation of fracture stresses to UO_2-tungsten dispersion compositions.[25] ○, compaction direction parallel to applied load. ×, compaction direction perpendicular to applied load.

the temperature range 206 to 316°C for maximum strains of 1% and times of 450 hr. Tensile properties were measured from 21 to 316°C, and elastic and dynamic moduli were obtained at room temperature. Results indicate that the 6061-0 material was stronger in short-time tension and creep than the X8001-0 material. Cold working of X8001 increased the tensile strength, and the recovery of the cold-worked X8001 and 6061 alloys was investigated and compared to the overaging of 6061 in T6 condition. The fuel dispersion clad with X8001 was stronger in creep and tension than the matrix X8001 material.

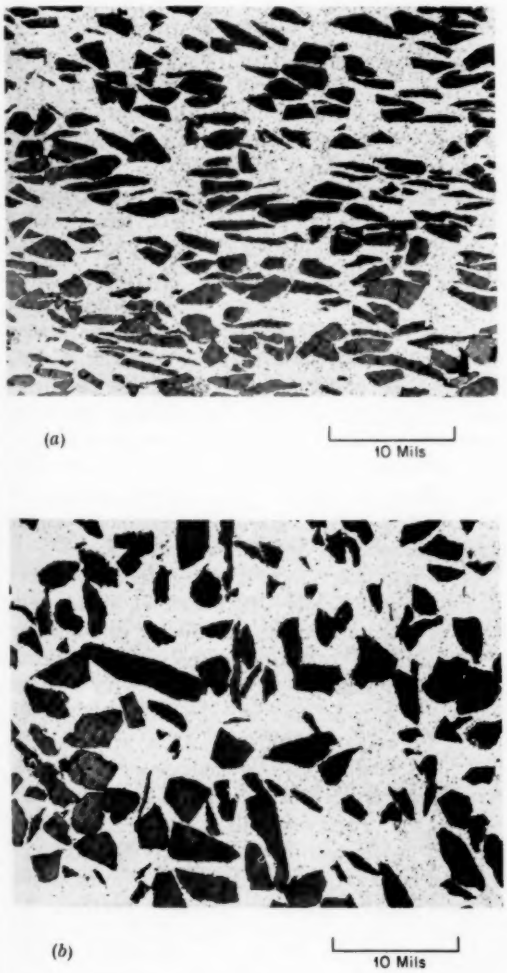

Fig. I-6 Microstructures of 40 vol.% UO_2–tungsten dispersions after pneumatic impaction.[38] (*a*) Parallel to compaction direction. (*b*) Perpendicular to compaction direction.

An etching study has been initiated at Georgia Institute of Technology[37] to identify the resulting phases by metallographic examinations of UO_2 and U_3O_8-aluminum dispersions after undergoing heat-treatments and irradiation tests. Two methods of distinguishing UAl_3 and UAl_4 are being investigated. Preliminary studies indicated that the stain colors resulting from an etchant solution (0.5% HF in water) were stable and reproducible. After etching, electron-microprobe analysis identified the blue phase as UAl_4 and the clear outlined phase as UAl_3.

Hanford reports[25,38] that UO_2-tungsten dispersions were fabricated by pneumatically impacting the powder mixtures at 300,000 psi and 1200°C with a Dynapak machine. The fracture stresses of the samples varied from 22,000 to 14,000 psi as the composition varied from pure tungsten to 50 vol.% UO_2–tungsten. The fracture stresses were found to be directionally dependent upon the orientation of UO_2 grains that occurred during the specimen's preparation. The fracture stresses vs. volume percent UO_2 for a tensile stress perpendicular and parallel to the compaction direction were reported as shown in Fig. I-5. Metallographic studies of the 40 vol.% UO_2–tungsten dispersion showed preferential alignment of the fused UO_2 grains in the tungsten matrix, as shown in Fig. I-6. The measured densities of these specimens were a minimum of 96% of theoretical.

(D. L. Stoltz)

Cermet Fuels

Workers at General Electric[39] have conducted creep-rupture tests at 2260°C on 60 vol.% UO_2–tungsten cermet specimens. The specimens were isostatically pressed, hydrogen sintered for 1 hr at 2500°C, and machined to a 0.100-in. diameter. The tests were initially performed in a hydrogen atmosphere; however, they are currently being conducted in a helium atmosphere to minimize the loss of surface UO_2, which had been substantial in the reducing atmosphere. Second-stage creep rates of 10^{-6} to 10^{-5} sec^{-1} were measured at stresses of 400 to 1000 psi. Although the technique has been improved, the samples indicated a significant density reduction due to UO_2 surface depletion, and the data appear to be conservative.

(D. E. Kizer)

Coated-Particle Fuel Materials

Particle Coating

A PyC coating called Triplex, applied to nuclear fuel particles by General Atomic[40] consists of an inner buffer-zone layer of spongy PyC overcoated with successive layers of laminar and columnar PyC. The Triplex coating combines the crack-interrupting qualities of the laminated coating with the stress-relieving feature of the buffer-zone coating. Preliminary irradiation results indicate that this coating has a high degree of irradiation stability.

Reuter[41] obtained data at National Carbon which show that a duplex PyC coating has uranium-migration resistance superior to that of the laminar type PyC. The data, given in Table I-8, show the alpha activity measured at the surface of the two types of heat-treated particles. The duplex coating consists of a porous inner layer and a dense outer layer with a well-ordered graphitic structure.

Table I-8 COUNT RATES IN THE 2300°C MIGRATION TEST[41]

Coating type	Count rate, alphas/(min)(g of coated particles)		
	As coated	After 1 hr at 2300°C	After 2 hr at 2300°C
Onion skin	0	525	12,900
Duplex	4	299	1,232

Efforts are being continued at Battelle[42–44] to optimize coatings of Al_2O_3, BeO, and PyC applied to nuclear fuel particles. The major portion of the recent experimental coating work is concentrated on the improvement of BeO coatings applied to UO_2 particles. The present objectives are: (1) to identify the coating conditions required to deposit a randomly oriented, fine-grained structure and (2) to retard grain growth in the coated product which occurs on heating at elevated temperatures. One experimental approach is to determine the effect of coating-process variables on the structure of the deposited BeO. A second approach is to deliberately add contaminants to the coating. Preliminary results indicate that the contaminants Al_2O_3, SiO_2, or ZrO_2 are ineffective as grain-growth inhibitors in concentrations of 4 to 15 wt.%. MgO was also ineffective in concentrations of 0.4 to 6 wt.%. (N. D. Veigel)

Irradiation and Evaluation of Coated-Particle Fuels

OXIDE-BASE FUEL

Studies of pyrolytic carbon-coated UO_2 are continuing at Battelle.[42–44] A graphite-matrix specimen of 200-μ, 92% dense UO_2 coated with 5 μ of Al_2O_3 and overcoated with 118 μ of columnar pyrolytic carbon has been irradiated to an estimated burnup of 1.3×10^{21} fissions/cm^3 or 8 at.% at 1050°C without coating failure. The fission-gas-release fractions remained in the order of 10^{-7} throughout the irradiation. With the success of this material, other pyrolytic carbon-containing coatings on porous UO_2 substrates are being evaluated. A specimen[44] similar to that discussed above, but having the Al_2O_3 layer replaced with BeO, has resisted failure in an irradiation to about 1 at.% burnup at 100°C. Another specimen[42] having no inner oxide layer in the coating has also performed well at 100°C. This material had a thinner coating than the others (10 μ of laminar PyC and 75 μ of columnar PyC), and its performance, at 100°C at least, was better than that observed earlier for comparable thickness coatings on dense UC_2 particles. It will be interesting to learn if thin pyrolytic carbon coatings on porous UO_2 particles will remain intact during irradiations at elevated temperatures.

An irradiation of a graphite-matrix specimen of 200-μ, 80% dense UO_2 particles coated with 60 μ of Al_2O_3 has continued during this quarter at Battelle.[42–44] The specimen temperature, which is permitted to fluctuate with reactor power, has remained at about 900°C except during reactor shutdowns, when it drops to 60°C. No coating failure has occurred after an estimated burnup of 8 at.% of the uranium.

A paper reviewing the status of coated-particle fuels has been recently published.[45] Many of the early irradiation data are discussed in this paper. Another article[46] reviews the in-pile performance of coated particles as of fall 1963.

CARBIDE-BASE FUEL

Fission-gas-release data obtained at Oak Ridge in irradiations of pyrolytic carbon-coated

UC_2 particles are summarized in a recent paper by Reagan, Carlsen, and Carroll.[47] Results are presented for three types of pyrolytic carbon coatings (columnar, laminar, and duplex) and for uncoated UC_2 particles. The data show the duplex coatings to be superior to the laminar and columnar coatings.

Studies are in progress at Battelle to determine the optimum coating thickness for multilayered pyrolytic carbon coatings on UC_2 particles.[43,44] Uranium carbide particles 200 μ in diameter coated with 20 to 30 μ of porous PyC, 9 μ of laminar PyC, and various thicknesses of columnar PyC have been evaluated in-pile at 100°C. Specimens with total coating thicknesses of 60 and 80 μ have exhibited over 10% failure in 2-week irradiations at a thermal-neutron flux of 1×10^{13} neutrons/(cm^2)(sec). With a coating thickness of 110 μ, no failure occurred; therefore the critical thickness is somewhere between 80 and 110 μ. This was also found earlier to be the case at 100°C with monolithic pyrolytic carbon coatings.

The relative magnitude of each effect that might contribute to cracking of pyrolytic carbon coatings on $(Th,U)C_2$ particles has been estimated by General Atomic.[40,48] In Table I-9 the various effects are listed, with the stresses estimated for each effect under a certain set of conditions. The calculations are reported to be only semiquantitative, but they do provide an estimate of the relative importance of the different effects. The main contributors to cracking of the coatings would appear to be swelling of the carbide particle and possibly fission-recoil damage to the pyrolytic carbon, fast-neutron-induced shrinkage of the pyrolytic carbon, and fission-gas pressure. (C. W. Townley)

Table I-9 SUMMARY OF ESTIMATED STRESSES IN PYROLYTIC CARBON COATINGS ON $(Th,U)C_2$ PARTICLES AT 1400°C AFTER 10% BURNUP OF HEAVY-METAL ATOMS[40]

(Carbide-Particle Diameter, 200 μ; Pyrolytic Carbon-Coating Thickness, 100 μ; Elastic Behavior Assumed; Modulus of Pyrolytic Carbon Taken as 3×10^6 Psi)

Effect	Strain (circumferential) in inner layers of pyrolytic carbon coating, %	Tensile stress in pyrolytic carbon coating at particle-coating interface, 1000 psi
Fission-product-induced expansion of $(Th,U)C_2$	18	150
Fission-recoil-induced damage to inner regions of pyrolytic carbon	4*	33
Fast-neutron-induced contraction of pyrolytic carbon	3†	25
Pressure buildup due to volatile fission products		20
Differential thermal expansion between pyrolytic carbon and $(Th,U)C_2$	‡	‡
Thermal annealing of pyrolytic carbon	‡	‡

*Assuming fission recoils are a factor of 10 more damaging than fast neutrons.

†Estimated for an exposure of 3×10^{21} neutrons/cm^2 ($E > 0.18$ Mev).

‡Contributes to tensile stress in coating, but, since contribution is small compared with that of other effects, no estimate has been made.

Coated-Particle Fuel-Materials Compatibility

One of the more important phenomena that limit the useful life of a coated fuel particle operating under normal reactor conditions is the compatibility of the fuel material with the applied coating at the reactor operating temperature. One of the systems that has received much attention in the past has involved the use of mixed carbide crystals coated with pyrolytic carbon. In such systems the compatibility of the fuel material with the coating is directly related to the thermal stability of the materials in intimate contact, which is, in many cases, related to the diffusion of various constituents through the pyrolytic carbon coating. The diffusing species consist of fission products or heavy metals within the fuel core. Using a neutron-activation-analysis technique, workers at General Atomic[49] have studied uranium diffusion in bulk pyrolytic graphite (density >90% of theoretical). The diffusion coefficients, shown in Table I-10, indicate that diffusion along the c axis (i.e., perpendicular to the layer planes) is approximately two orders of magnitude greater than the rate observed perpendicular to the c

axis. The log concentration-penetration curves, Figs. I-7 and I-8, show that a nearly linear relation exists for diffusion along the c axis (perpendicular to layer planes). This type of behavior is indicative of grain-boundary diffusion; however, autoradiography failed to reveal localization of uranium along the grain boundaries. The authors suggest that the presence of microcracks (formed during machining operations) could be responsible for the rapid surface diffusion that was observed. Further investigations concerning surface diffusion are in progress.[48] Data at 954°C indicate that the surface diffusion coefficient is on the order of 10^{-5} cm^2/sec. Radial microcracks have been observed by other workers attempting to measure the thermal conductivity of graphite at temperatures[50] above 1000°C. They report radial cracking (perpendicular to the c axis) when the graphite specimens are annealed at temperatures in excess of 1544°C.

Benesovsky, Theisen, and Stecher[51] have studied the migration behavior of carbon-coated UC-ZrC crystals of varying compositions. The coatings were prepared using CH_4 at 2000°C. Annealing treatments included 100 hr at 2000°C followed by 20 hr at 2400°C. After the specimens were annealed, they were analyzed using electron-probe microanalysis. No changes were observed in particles containing ZrC substrates. However, a mixed ZrC-UC crystal containing 10 mole % UC exhibited a diffusion zone extend- 8 μ into the coating. A uranium concentration gradient of 0.3 to 0.2 wt.% was found. In addition, zirconium penetrated into 5 μ of the coating. The effect was more pronounced with the 30 mole % UC mixed crystal, uranium migration in this case penetrating 60 μ of the coating. The above workers reported that both compositions are stable according to the phase diagram of the uranium-zirconium-carbon system.

Interesting is the fact that the presence of as little as 10 mole % UC facilitates migration of the zirconium that has previously remained within the fuel core. The migration resistance of a 65 mole % UC mixed crystal is even lower because, in addition to diffusion processes, disintegration reactions can occur, forming UC_2. The structure of the latter crystal consists of two distinct phases: (1) a light phase containing 43.1 wt.% uranium and 51.3 wt.% zirconium and (2) a dark-gray phase containing 88.9 wt.% uranium and 3.5% zirconium. The zirconium-rich phase does not react with carbon up to the maximum annealing temperatures. The uranium-rich phase, however, begins to react with carbon at approximately 1600°C, forming UC_2. The authors conclude that carbide formation accompanies the migration of uranium into the coating, and the resulting porosity facilitates the transfer mechanism. The diffused species than concentrate in these defect spots.

Studies conducted at General Atomic[40] on pyrolytic carbon-coated UC_2 particles prepared from C_2H_2 and CH_4 have shown that those coatings deposited from CH_4 are more resistant to

Table I-10 URANIUM–PYROLYTIC GRAPHITE DIFFUSION RESULTS[49]

Run	Pyrolytic graphite	Temp., °C	Anneal time, hr	$D_\perp$, cm^2/sec	$D_\parallel$, cm^2/sec	C_s, mg U/g C
1	HTM	1826	231	1×10^{-8}	3×10^{-10}	1.3
2	GE	1826	231	4×10^{-8}	(3×10^{-10})	0.98
3	HTM	2020	49			0.98
4	GE	2020	49			1.2
5	HTM	1902	123	2.3×10^{-7}		1.0
6	HTM	1902	123			
7	HTM	1602	644	3×10^{-10}		
8	HTM	1602	644	(8×10^{-10})	(4×10^{-11})	0.45
B-6*	HTM	2000	115			1.1
B-7	HTM	2150	56			1.8
B-8	HTM	2200	20			2.1

*Specimens B-6 through B-8 were examined on the electron-microprobe analyzer and found to contain a uniform concentration of uranium in the range 1 to 2 mg/g of graphite. Then they were analyzed for average uranium concentration by the neutron-activation-analysis technique; the values of C_s reported represent these average values.

Studies conducted at General Atomic[40] on pyrolytic carbon-coated UC_2 particles prepared from C_2H_2 and CH_4 have shown that those coatings deposited from CH_4 are more resistant to

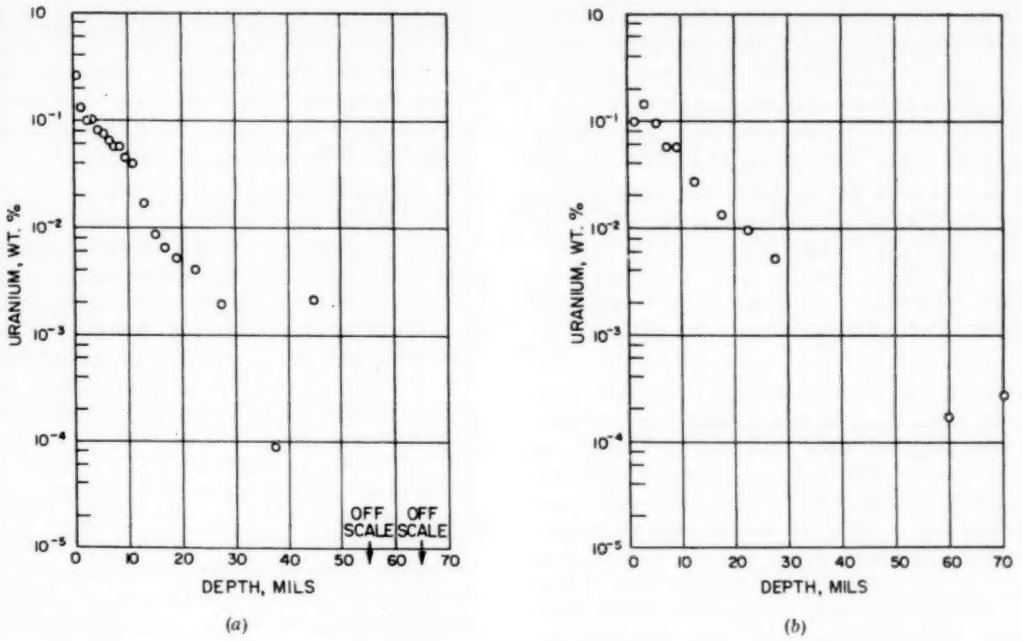

Fig. I-7 Diffusion of uranium in pyrolytic graphite perpendicular to layer planes[49] at 1806°C. (*a*) High Temperature Materials Company pyrolytic graphite. (*b*) General Electric Company pyrolytic graphite.

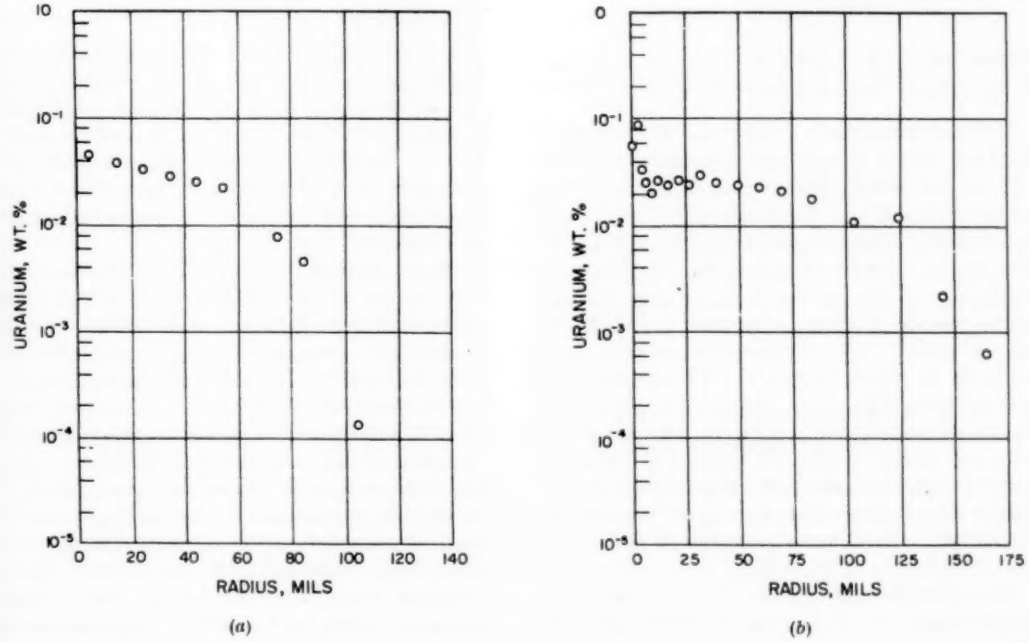

Fig. I-8 Diffusion of uranium in pyrolytic graphite parallel to layer planes[49] at 1806°C. (*a*) High Temperature Materials Company pyrolytic graphite. (*b*) General Electric Company pyrolytic graphite.

Table I-11 SUMMARY OF LONG-TERM THERMAL-STABILITY TESTS OF PYROLYTIC CARBON-COATED (Th,U)C_2 PARTICLES[40]

Temp., °C	Time, hr	Source of pyrolytic carbon coating	Extent of migration, μ
1700	500	C_2H_2	None
1700	500	CH_4	None
1700	3,100	C_2H_2	25
1700	3,100	CH_4	15
1550	7,415	C_2H_2	30
1550	10,208	CH_4	None
1400	10,359	CH_4	None

uranium migration than similar coatings prepared from C_2H_2. Although both types of particles migrated after 3100 hr at 1700°C, as shown in Table I-11, those containing the coatings prepared from C_2H_2 exhibited uranium migration up to 50% of the coating thickness. Coatings prepared from CH_4 had a maximum penetration of approximately 30%. Similar data at 1550°C indicated no migration in CH_4 coatings after 10,208 hr, whereas C_2H_2 coatings exhibited up to 60% penetration after 7415 hr.

(W. F. Pfeifer)

Uranium Oxides

Properties and Behavior of Uranium Oxide Fuels

The low-temperature magnetic properties of uranium oxides have been investigated between 1.5 and 44°K by Leask et al.,[52] using an a-c induction technique. The susceptibility of U_3O_8 was found to exhibit a sharp maximum at 4.2°K, with smaller peaks at 8 and 25.3°K. The susceptibility of UO_2 attains a maximum at 29°K and remains constant between 2 and 25°K. Nagels et al.[53] have measured electrical conductivity in single crystals with compositions varying from $UO_{2.000}$ to $UO_{2.007}$. The activation energy decreases from 0.34 to 0.19 ev with increasing excess oxygen. An attempt to measure the Hall-effect coefficient resulted in no response, indicating that the Hall mobility at 300°K is probably less than 0.015 cm^2/(volt)(sec).

The solubility of helium in UO_2 has been studied at the U. S. Bureau of Standards.[54] At 800°C and a pressure of 110 atm, the solubility of helium in Norton fused UO_2 was found to be 0.06×10^{-6} g of helium per gram of UO_2. For single-crystal UO_2 the solubility was 0.01×10^{-6} g of helium per gram of UO_2. Ferrari[55] has inferred a diffusion coefficient for nitrogen atoms in sintered UO_2 from nitrogen-degassing studies. Over the temperature range from 1000 to 1600°C, diffusion followed the relation:

$$D = 2.25 \times 10^{-9} \exp(-33{,}400/RT) \text{ cm}^2/\text{sec}$$

Italian investigators[56] have observed that the irradiation dose affects the diffusional release of xenon from UO_2 during postirradiation annealing. A significant decrease in xenon release occurred with increasing irradiation exposure.

Studies at General Electric[57] show that grain growth in sintered UO_2 in an argon atmosphere followed the relation:

$$D^2 - D_0^2 = K e^{-E/RT} t^m$$

where D_0 is the initial grain diameter and D is the grain diameter at time t. The exponent m is related to the type of UO_2 and was equal to about one-third for the 91 to 94% dense sintered material that was studied. The activation energy for grain growth was 65 kcal/gram mole.

(R. H. Barnes)

Preparation of Uranium Oxide Fuel Bodies

A final report covering the uranium oxide extrusion studies by French workers[58] has been issued. Fifteen uranium dioxide powders of French and foreign origin were extruded to produce sintered uranium dioxide rods with densities above 10.4 g/cm^3. Fabrication characteristics were carefully noted for several of the powders.

Other French workers[59] have developed a method for preparing UO_2 pellets without the use of binders. In this process the UO_2 powder is initially compacted at approximately 6.5 tsi. This compact is crushed and screened to give a granular feed in the particle-diameter range from 125 to 990 μ. The fines are recycled to the compaction step. Approximately 0.3 wt.% zinc behenate is then added to the granular powder to provide lubrication in the final compaction step. A pressure of 32 tsi is used in this final compaction step to form the pellets. Higher densities were achieved in the sintered UO_2 compacts made by the above method than could be achieved using conventional wet granulation techniques to prepare the power for pressing.

(D. E. Rhodes)

Carbide and Nitride Fuels

Properties

The compatibility of uranium carbide with a variety of metals at temperatures from 1000 to 2400°C for times up to 10 min has been surveyed by Christensen.[60] The data were obtained using UC that varied in composition from very hypostoichiometric (about 4.6 wt.% carbon) to slightly hyperstoichiometric (about 5.1 wt.% carbon), and no allowance for this variable was made in interpreting the results. At 1000°C, stainless steel, Hastelloy F, and Inconel reacted extensively with the carbide. Since these materials melt below 1500°C, none were tested at or above 1500°C. Tantalum, niobium–1 wt.% zirconium alloy, and Zircaloy-2 reacted extensively with UC at 1500°C; tungsten reacted only slightly; and molybdenum and niobium–33 wt.% tantalum–1 wt.% zirconium alloy reacted at intermediate rates. Molten UC was contained by tantalum for 180 sec, but tungsten contained molten UC for only 10 sec. Niobium–1 wt.% zirconium alloy reacted with UC at 2250°C to form five layers identified as: (1) unaffected niobium plus Nb_2C, (2) niobium plus massive Nb_2C, (3) niobium–uranium monocarbide, (4) UC, and (5) unaffected UC plus UC_2. The niobium carbides formed in regions 2 and 3 were formed at the expense of UC_2 removed from region 4.

The reaction of UC_2 with zirconium to form an intermediate layer of ZrC that controls the rate of the reaction is reported.[25] UC reacts with zirconium to form uranium metal and an intermediate layer of ZrC that controls the rate of reaction below the melting point of uranium. The rate of thickening of the ZrC layer is shown in Fig. I-9. The activation energy for this process is 30 kcal/mole.

Thin sections of slightly hyperstoichiometric UC have been examined by Whitton[61] using electron-microscope techniques. The photographs show markings that appear to be dislocations associated with the interfaces between the UC matrix and the UC_2 platelets. The spacing of the dislocation planes was found to be, uniformly, about 300 A, with no indication of pileup. It is suggested that the dislocations derive from a slight mismatch between the basal plane of the UC_2 structure and the {1 0 0} plane of the UC structure; one extra row of atoms occurs in the UC in every 90 rows at the UC-UC_2 interface. These dislocations appear to be relatively immobile and could not be moved by heating the specimens.

The thermal conductivity of UC is not significantly affected by an irradiation of 5200 Mwd/ton at centerline temperatures[25] of 820 to 930°C.

At a burnup of about 14,000 Mwd/ton and at centerline temperatures over 980°C, the free uranium in hypostoichiometric UC (4.2 to 4.4 wt.% carbon) showed a marked tendency to redistribute toward the cooler outer surfaces.[25] Gas bubbles and voids developed in the hot central region.

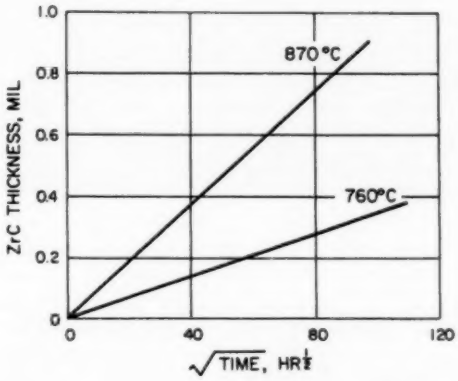

Fig. I-9 Carburization of 3Z1 alloy by hypostoichiometric and hyperstoichiometric UC, contact bonded.[25]

The free energies of formation of ThC and ThC_2 at 900°C are found[25] to be −24 and −28 kcal/mole, respectively.

The homogeneity range of ThC is from 44 to 50 at.% carbon at about 1600°C, according to Henney, Jones, and Hill.[62] The lattice parameter varies correspondingly from 5.305 to 5.344 A.

(W. Chubb)

Fabrication of Refractory Fuels Other Than Uranium Oxides

UC technology has been advanced another significant step in the route from conception to consumer. Atomics International[23] estimated that the overall capacity for supplying usable UC melt stock is about 1200 kg/week. It is indicated that, as a result of a fairly large development program, melt stock can be used with variable carbon content so long as the oxygen content is less than 500 ppm. Actual

experience was gained in casting up to 500 kg/week of UC slugs in the composition range 4.5 to 4.8 wt.% carbon by skull melting in water-cooled copper crucibles with nonconsumable carbon electrodes.

There are indications that stoichiometric UC rods can be made by a zone-refining operation from UC castings of varying composition. Excess uranium in hypostoichiometric rods is moved with the molten zone in an induction apparatus at traverse rates of $\frac{1}{8}$ to $\frac{1}{2}$ in./hr. Some results obtained[25] are shown in the following tabulation of observed compositions:

Initial composition	Final composition of main section	Composition of last zone to freeze
5.2 wt.% C	4.85 wt.% C	5.3 to 5.5 wt.% C
5.0 wt.% C	4.85 wt.% C	5.5 wt.% C
4.5 wt.% C	Single-phase UC	Excess uranium
4.1 wt.% C	Some excess uranium	Excess uranium

(E. O. Speidel)

Mechanism of Corrosion of Fuel Alloys

The beneficial effect of copper additions on the oxidation behavior of uranium has been attributed by Harwell scientists[63] to the formation of a layer of an intermetallic compound, UCu_5, or of copper-containing uranium oxide at the metal/oxide interface. The layer was believed to have formed from the diffusion of copper ions into the metal away from the oxide.

(W. E. Berry)

Basic Studies of Irradiation Effects in Fuel Materials

Metals

At Berkeley[64] it is shown that small bubbles move in a way analogous to Brownian motion with an effective diffusion coefficient that is inversely proportional to their radius to the fourth power. This movement is relevant to the behavior of reactor fuels insofar as it enables small bubbles to coalesce and an estimate to be made of the rate of coalescence. The process influences the spacing of bubbles and enables a more satisfactory estimate to be made of swelling in fissile materials.

As mentioned earlier in the Alpha-Phase Uranium Alloys section, an irradiation experiment has been conducted at North American Science Center[65] to test the effectiveness of finely dispersed phases in reducing swelling. Uranium–4 wt.% molybdenum–0.1 wt.% molybdenum–0.1 wt.% silicon and uranium–10 wt.% molybdenum–0.04 wt.% tin alloys containing finely dispersed phases have been irradiated with appropriate control samples at low temperatures and then postirradiation annealed to induce swelling. The annealing was performed in steps at progressively higher temperatures from 550 to 950°C, with density measurements taken after each step and electron-microscope examinations when warranted. The lowest density changes took place in samples having the finest dispersions, 10^{12} to 10^{13} particles/cm^3. Binary control samples having no dispersions experienced density decreases more than ten times those of equivalent samples with dispersions. After a 750°C anneal, a uranium–4 wt.% molybdenum–0.1 wt.% silicon alloy with a fine dispersion, having experienced a 0.4 at.% burnup, showed only a 1.7% density decrease. A uranium–10 wt.% molybdenum–0.04 wt.% tin alloy showed the same density decrease after an 850°C anneal, following a burnup of 0.6 at.%. Irradiation-induced precipitation was observed in the uranium–4 wt.% molybdenum–0.1 wt.% silicon alloy and is believed to have occurred in the uranium–10 wt.% molybdenum–0.04 wt.% tin alloy, producing a particle density on the order of 10^{14}/cm^3. The greatly improved swelling resistance of the samples with fine dispersions results from the interaction of gas atoms with the original precipitates and with the irradiation-induced precipitates. These precipitates, acting as trapping sites for gas bubbles, stabilized the fission gas in an array of a large number of small bubbles, thereby reducing swelling.

Resistivity and dimensional changes induced by neutron irradiation of different grades of uranium at 77 and 20°K were studied by the French.[66,67] After allowance for growth, which is considerable at these temperatures, there are residual changes in resistivity which reach saturation for deformed uranium irradiated at

77°K and which approach saturation in the other instances. It is impossible to interpret the results in terms of a single fission spike. Rather, it is necessary to postulate two distinct volumes, a small one (0.9×10^{-16} cm^3), corresponding, no doubt, to the annihilation of defect clusters in displacement spikes, and a second, larger one (3 to 6.5×10^{-16} cm^3), corresponding to the recombination of point defects outside displacement spikes. The probable existence of a whole spectrum of volumes for different types of defects is discussed, and it is shown that this generalization does not profoundly modify the foregoing conclusions.

At Harwell,[68] evidence of saturation in 4 wt.% aluminum–delta-stabilized plutonium, after being held at 5°K for over 7000 hr, is reported. Yet, after 7000 hr at ~5°K, the rate of increase in resistance of delta plutonium was still over 25% of its initial rate. It was also noted that the rates of resistance increase do not follow a true exponential law.

A bibliography of radiation effects of solid uranium-based nuclear fuel materials has been compiled in Sweden.[69]

Ceramics

The focusing of momentum by collision sequences was examined at Harwell[70] in UO_2 by means of high-energy ion bombardment. The structure of UO_2 is regarded as a simple face-centered-cubic (fcc) arangement of uranium, with oxygen positioned at the eight equivalent positions (¼, ¼, ¼). As in the fcc structure, the simplest sequence in UO_2 is expected to propagate along the (1 0 0) directions. Under the hard-sphere conditions, focusing occurs when the collision radius R becomes sufficiently large to satisfy the condition $R \geq \frac{1}{4} D^{1\,1\,0}$; thus successive collisions occur before the midway points. Focusing in the (1 0 0) directions of fcc metals results from the interaction with rings of atoms surrounding the sequence. Focusing in the (1 1 1) direction of a fcc structure results from the interaction with a pair of converging lenses; in UO_2, successive uranium atoms in this direction are separated by pairs of oxygen atoms. The results suggest that focusing in UO_2 occurs predominantly in the (1 1 0) and (1 0 0) directions, together with rather weak focusing in the (1 1 1) directions.

Vapor-grown single crystals of nearly stoichiometric UO_2 have been thinned for transmission electron microscopy.[71] The as-grown crystals show a dense pattern of precipitates and may contain loops due to quenched-in vacancies but contain hardly any dislocations. Two models for the production of the loops are proposed. Dislocation networks (small-angle boundaries) are produced on annealing of the crystals. Irregular patterns of dislocations arise when sufficiently thick parts of crystal foils are treated with heat shocks in the microscope by suddenly increasing the beam current. After exposure to 10^{15} neutrons/cm^2, the crystal foils show fission tracks, short segments of straight dislocation lines, and black dots that are partly distributed at random and are partly aligned on fission tracks. Interaction between fission tracks and dislocations has been observed. The conditions for contrast production on fission tracks have been investigated. The experimental findings can be explained by a model of a displacement field around the fission tracks.

The physical behavior of fission-product impurities in irradiated uranium dioxide fuel is reviewed by the British[72] under two main headings: (1) the processes and kinetics governing the escape of fission products from uranium dioxide, both during irradiation and also on subsequent out-of-pile heating; and (2) the physical and microstructural changes produced by the fission products retained in the fuels. In many of the subjects, the experimental data are limited or contradictory, and no final conclusions are possible. Some experiments to rectify the situation are suggested.

On the basis of fission-gas-release data from single-crystal UO_2 specimens, a tentative model was formulated at Oak Ridge[73] for high-temperature fission-gas release. The features of the model are: (1) defects in the UO_2 structure trap impurity atoms, (2) defects are formed by fission-fragment tracks, and (3) the fission-gas release is controlled by the probability of the gas being trapped, rather than by a diffusion process. With this model, qualitative explanations of all observed in-pile gas-release effects are possible.

An irradiation experiment was performed at Chalk River[74] to determine whether the columnar (essentially single-crystal) grains grown in UO_2 fuel elements under irradiation at high heat ratings showed an enhanced thermal conductivity. No indication was found of any alteration in thermal conductivity within the limits of error of the experiment. Although this does

not exclude the possibility that enhanced conductivity can occur in uranium dioxide, it indicates that it is not necessarily a property of single-crystal material. (F. A. Rough)

References

1. J. H. Gittus, *Uranium*, Metallurgy of the Rarer Metals No. 8, Butterworths, Washington, 1963.
2. E. L. Foster (Ed.), Production Uranium Residual Stresses, Internal Friction and Modulus, USAEC Report BMI-1658, Battelle Memorial Institute, Dec. 27, 1963.
3. E. L. Foster (Ed.), A Study of the Tensile Fracture and Microstructure of Uranium, USAEC Report BMI-1664, Battelle Memorial Institute, February 1964.
4. A. Lemogne, J. Morin, and P. Lacombe, Plastic Behavior of Polycrystalline Uranium Between 20°C and −196°C (in French), *Compt. Rend.*, 257: 2032-2035 (September 1963).
5. B. Spriet, Surface Tension of Uranium and Plutonium at the Melting Point (in French), *Mem. Sci. Rev. Met.*, 60: 531-540 (July−August 1963).
6. H. M. Green, A Metallographic Study of Gas Behavior in Uranium Irradiated with Alpha Particles, USAEC Report NMI-7009, Nuclear Metals, Inc., Sept. 28, 1962.
7. O. S. Ivanov (Ed.), Structure and Properties of Uranium, Thorium and Zirconium Alloys, Report JPRS-24347(OTS-64-31154), 1963.
8. E. M. Potapova (Ed.), The Structure of Alloys of Certain Systems Containing Uranium and Thorium, USAEC Translation AEC-tr-5834, 1961.
9. The Uranium-Osmium System, *J. Nucl. Mater.*, 9: 309-319 (August 1963).
10. G. Petzow and R. Tank, The Equilibrium Phases in the Uranium-Aluminum-Iron Alloys in the Partial Domain Uranium-UAl_2-UFe_2, Report MCW-TR-1, December 1963. [Translated from *Z. Metallk.*, 54: 91-98 (1963).]
11. B. W. Howlett, A. J. Eycott, I. K. Kang, and D. R. F. West, The Kinetics of the Isothermal Decomposition of a Gamma-Phase Uranium−6 At.% Molybdenum Alloy, British Report AERE-R-4076, June 1962.
12. R. F. Hills, B. W. Howlett, and B. R. Butcher, Further Studies on the Decomposition of the Gamma Phase in Uranium−Low Molybdenum Alloys, *J. Less-Common Metals*, 5: 369-373 (October 1963).
13. D. Kramer and W. V. Johnston, Postirradiation Annealing of Uranium-Molybdenum Ternary Alloys, *J. Nucl. Mater.*, 9: 213-215 (July 1963).
14. M. P. Johnson and W. A. Holland, Irradiation of Uranium-Molybdenum Base Alloys, USAEC Report NAA-SR-6262, Atomics International, Jan. 30, 1964.
15. W. Uhlmann, The Aqueous Corrosion of Uranium and Some of Its Alloys—A Literature Survey, Swedish Report VDIT-82, December 1963.
16. W. Uhlmann, Radiation Effects on Solid, Uranium-Based Nuclear Fuel Materials—A Bibliography, Vol. 3, No. 4, Swedish Report VDIT-16(3.4), October 1963.
17. Argonne National Laboratory, Reactor Development Program Progress Report, January 1964, USAEC Report ANL-6840, Feb. 15, 1964.
18. G. W. Gibson and D. R. deBoisblanc, Uranium-Aluminum Alloy Powders for Use as Nuclear Reactor Fuels, paper presented at Metallurgical Society of AIME Fall Meeting, Cleveland, Ohio, October 1963, USAEC Report CONF-339-5, Phillips Petroleum Co.
19. Hanford Atomic Products Operation, Metallurgy Research Operation, Quarterly Progress Report, October−December 1963, USAEC Report HW-79766, Jan. 15, 1964.
20. K. A. Johnson, Homogenization of Gallium-Stabilized Delta-Phase Plutonium, USAEC Report LA-2989, Los Alamos Scientific Laboratory, November 1963.
21. Los Alamos Scientific Laboratory, Quarterly Status Report on Plutonium Reactor Fuel Development for Period Ending February 20, 1964, USAEC Report LAMS-3057, March 1964.
22. S. Rosen, M. V. Nevitt, and A. W. Mitchell, Metallographic and X-Ray Observations of Plutonium-Carbon Alloys, *J. Nucl. Mater.*, 10(3): 90-98 (October 1963).
23. The Fourth Uranium Carbide Conference, East Hartford, Conn., May 20−21, 1963, USAEC Report TID-7676, February 1964.
24. D. Stahl, A. Strasser, K. Taylor, and J. Anderson, Out-of-Pile Properties of Mixed Uranium-Plutonium Carbides, USAEC Report UNC-5074 (EURAEC-918), United Nuclear Corp. and Carborundum Co., Dec. 6, 1963.
25. Hanford Atomic Products Operation, January 1964. (Unpublished)
26. J. H. Kittel, L. A. Neimark, R. Carlander, O. L. Kuger, and R. C. Lied, Preliminary Irradiations of PuC and UC-PuC, USAEC Report ANL-6678, Argonne National Laboratory, September 1963.
27. Hanford Atomic Products Operation, Reactor and Fuels Laboratory Monthly Report, September 1963, USAEC Report HW-79046A, Oct. 15, 1963. (Classified)
28. Nuclear Materials & Equipment Corp., Development of Plutonium-Bearing Fuel Materials, Monthly Progress Letter, November 1963, USAEC Report NUMEC-P-66, Dec. 10, 1963.
29. J. A. Leary, W. J. Maraman, W. N. Miner, and F. W. Schonfeld, Quarterly Status Report on Solid Plutonium Fuels Program for Period July 1−September 30, 1963, USAEC Report LAMS-3023, Los Alamos Scientific Laboratory, October 1963.

30. Hanford Atomic Products Operation, Reactor and Fuels Laboratory Monthly Report, November 1963, USAEC Report HW-79726A, Dec. 15, 1963. (Classified)
31. Hanford Atomic Products Operation, Reactor and Fuels Laboratory Monthly Report, December 1963, USAEC Report HW-79999A, Jan. 15, 1964. (Classified)
32. Oak Ridge National Laboratory, Feb. 6, 1964. (Unpublished)
33. H. P. Roth (Comp.), Technical Papers of the Fourteenth Metallographic Group Meeting held at Nuclear Metals, Inc., West Concord, Mass., April 5 and 6, 1960, Report NMI-4996, Jan. 6, 1964, D. T. Peterson, Some Metallographic Observations on Thorium Metal.
34. Hanford Atomic Products Operation, Metallurgy Development Operation, Quarterly Progress Report, July–September 1963, USAEC Report HW-78984, Oct. 18, 1963. (Classified)
35. Phillips Petroleum Co., Materials Testing Reactor—Engineering Test Reactor Technical Branches, Quarterly Report No. 3, July–September 30, 1963, USAEC Report IDO-16932, Feb. 15, 1964.
36. W. R. Martin and J. R. Weir, Mechanical Properties of X8001 and 6061 Aluminum Alloys and Aluminum-Base Fuel Dispersion at Elevated Temperatures, USAEC Report ORNL-3557, Oak Ridge National Laboratory, February 1964.
37. J. D. Fleming, J. W. Johnson, P. Boland, and S. H. Bomar, Materials for High-Temperature Nuclear Engineering Applications, Quarterly Report No. 5, June 1–October 1, 1963, USAEC Report TID-20026.
38. Hanford Atomic Products Operation, Ceramics Research and Development Operation Quarterly Report, July–September 1963, USAEC Report HW-76303.
39. General Electric Co., Advanced Technology Services, 710 Reactor Program Quarterly Report No. 6, USAEC Report GEMP-265, Jan. 31, 1964. (Classified)
40. General Atomic Division, General Dynamics Corp., Development and Utilization of Pyrolytic-Carbon-Coated Fuel for the High-Temperature Gas-Cooled Reactor, USAEC Report GA-4699, November 1963.
41. R. A. Reuter, Duplex-Carbon-Coated Fuel Particles, *Trans. Am. Nucl. Soc.*, 6: 380 (November 1963).
42. Battelle Memorial Institute, Progress Relating to Civilian Applications During December 1963, USAEC Report BMI-1659, Jan. 1, 1964. (Classified)
43. Battelle Memorial Institute, Progress Relating to Civilian Applications During January 1964, USAEC Report BMI-1661, Feb. 1, 1964. (Classified)
44. Battelle Memorial Institute, Progress Relating to Civilian Applications During February 1964, USAEC Report BMI-1665, Mar. 1, 1964. (Classified)
45. R. W. Dayton, J. H. Oxley, and C. W. Townley, Ceramic-Coated-Particle Nuclear Fuels (Review Article), *J. Nucl. Mater.*, 11(1): 1-31 (January 1964).
46. C. W. Townley, N. E. Miller, R. L. Ritzman, and R. J. Burian, In-Pile Performance of Ceramic-Coated-Particle Fuels, *Nucleonics*, 22(2): 43-48 (February 1964).
47. P. E. Reagan, F. L. Carlsen, and R. M. Carroll, Fission-Gas Release from Pyrolytic-Carbon-Coated Fuel Particles During Irradiation, *Nucl. Sci. Eng.*, 18(3): 301-318 (March 1964).
48. W. V. Goeddel, Development and Utilization of Pyrolytic-Carbon-Coated Carbide Fuel for the High-Temperature Gas-Cooled Reactor, USAEC Report GA-4699, General Atomic Division, General Dynamics Corp., November 1963; accepted for publication in *Nuclear Science and Engineering*.
49. General Atomic Division, General Dynamics Corp., Advanced, Graphite-Matrix, Dispersion-Type Fuel Systems, First Annual Report, April 1, 1962–March 31, 1963, USAEC Report GA-4022 (Pt. 1), May 1, 1963.
50. J. Vardi and M. Hoch, Thermal Conductivity of Anisotropic Solids at High Temperatures—The Thermal Conductivity of Molded and Pyrolytic Graphites, *J. Am. Ceram. Soc.*, 46(3): 132 (1963).
51. F. Benesovsky, R. Theisen, and P. Stecher, Diffusion Phenomena on Heat-Treated, Pyrographite-Coated (U,Zr)C Nuclear-Fuel Particles (Uber Diffusion-serscheinunigen on Warmebehandelten, pyrographituberzogenen (U,Zr)C-Kernbrennstoffteilchen), *Planseeber. Pulvermet.*, 2(3): 146-156 (1963).
52. M. J. M. Leask, L. E. J. Roberts, A. J. Walter, and W. P. Wolf, Low-Temperature Magnetic Properties of Some Uranium Oxides, *J. Chem. Soc.*, 4788-4794 (October 1963).
53. P. Nagels, M. Denayer, and J. Devresse, Electrical Properties of Single Crystals of UO_2, *Solid State Commun.*, 1: 35 (June 1963).
54. S. Hasko and R. Szwarc, Noble Gas Solubility and Diffusion in UO_2, USAEC Report TID-19229, Aug. 6, 1963.
55. H. M. Ferrari, Nitrogen Release from UO_2 Pellets at Elevated Temperature, *Nucl. Sci. Eng.*, 17: 503 (December 1963).
56. G. Frigerio and T. Gerevini, The Dependence upon the Irradiation Dose of the Apparent Diffusion Rates of Xenon in UO_2, *J. Nucl. Mater.*, 10: 251 (November 1963).
57. H. Hausner, Grain Growth of UO_2, Part I, USAEC Report GEAP-4315(EURAEC-87), General Electric Co., Atomic Power Equipment Department, Apr. 15, 1963.
58. J. Mercier, Uranium Oxide Extrusion, Final Report, USAEC Report EURAEC-788, Compagnie

Industrielle des Combustibles Atomiques Frittes, July 1963.

59. A. Porneuf, Study of the Shaping of UO_2 Powders by Mechanical Compression and Their Sintering on a Pilot Scale in an Atmosphere of Cracked Ammonia, USAEC Report EURAEC-736, Compagnie Industrielle des Combustibles Atomiques Frittes, Oct. 23, 1963.
60. J. A. Christensen, High-Temperature Short-Time Uranium Carbide Metal Reactions, USAEC Report HW-72031, Hanford Atomic Products Operation, March 1963.
61. J. L. Whitton, Transmission Electron Microscopy of Uranium Monocarbide, British Report TRG-Report-612, Aug. 9, 1963.
62. J. Henney, J. W. S. Jones, and N. A. Hill, Cell-Size Variations in Thorium Monocarbide, British Report AERE-R-4456, October 1963.
63. J. E. Antill and K. A. Peakall, Mechanism of the Oxidation of a Uranium–1 Wt.% Copper Alloy, *J. Electrochem. Soc.*, 110(11): 1146-1148 (November 1963).
64. G. W. Greenwood and M. V. Speight, An Analysis of the Diffusion of Fission Gas Bubbles and Its Effect on the Behavior of Reactor Fuels, *J. Nucl. Mater.*, 10(3): 140-144 (October 1963).
65. D. Kramer, W. V. Johnston, and C. G. Rhodes, The Influence of Finely Dispersed Precipitates on Fission-Gas-Bubble Formation in Uranium-Molybdenum Ternary Alloys, paper presented at Metallurgical Society of AIME Annual Meeting, Dallas, Tex., February 1963, USAEC Report CONF-331-2, 1963.
66. Y. Quéré, Effects of Weak Irradiations on Uranium, *J. Phys.*, 24: 489-498 (July 1963).
67. Y. Quéré, Resistivity Changes in Uranium Irradiation at Low Temperatures, *J. Nucl. Mater.*, 9: 290-308 (August 1963).
68. E. King, J. A. Lee, K. Mendelssohn, and D. A. Wigley, Self-Irradiation Effects in Stabilized Delta-Plutonium, *Acta Met.*, 12: 111-112 (January 1964).
69. W. Uhlmann, Radiation Effects on Solid, Uranium-Based Nuclear Fuel Materials — A Bibliography, Vol. 3, No. 3, Swedish Report VDIT-16(3.3), September 1963.
70. R. S. Nelson, The Observation of Collision Sequences in UO_2, *J. Nucl. Mater.*, 10(2): 154-156 (October 1963).
71. H. Blank and S. Amelinckx, Some Preliminary Results on Defects in Irradiated UO_2 Single Crystals as Revealed by Transmission Electron Microscopy, *J. Appl. Phys.*, 34: 2200-2209 (August 1963).
72. B. G. Childs, Fission Product Effects in Uranium Dioxide, *J. Nucl. Mater.*, 9: 217-244 (August 1963).
73. Oak Ridge National Laboratory, Mar. 5, 1964. (Unpublished)
74. M. J. Notley, The Thermal Conductivity of Columnar Grains in Irradiated UO_2 Fuel Elements, Canadian Report CRDF-1166(AECL-1822), July 1963.

Section

II

Reactor Materials

Moderator Materials

Graphite

General Atomic has reported[1] on the physical properties of two types of fueled graphite: conventionally extruded and baked material and hot-pressed material that is typical of the fuel elements for the Peach Bottom Reactor. Coated particles contained in these matrices were UC_2 (177 to 238 μ in diameter) coated with 20 μ of pyrolytic carbon. The uranium content of the particles was 61.3 wt.%.

The strength of extruded graphite-matrix fuel elements was found to be essentially unaffected by the addition of as much as 40 vol.% coated particles (compressive strength parallel to the direction of extrusion dropped from about 4200 to 3500 psi for a fuel-loading increase from 0 to 40 vol.%, whereas shear strength dropped from approximately 1800 to 1500 psi). Hot-pressed elements showed much greater dependence of strength on fuel loading. As the loading was increased from 0 to 40 vol.% fuel particles, compressive strength dropped from 7000 to about 3800 psi, and shear strength dropped from 2800 to 1800 psi. The density of the matrix of hot-pressed elements dropped gradually from about 1.82 to about 1.68 g/cm^3 for a fuel-loading increase from 0 to 40 vol.%. In contrast, the density of the matrix of extruded elements dropped abruptly from about 1.68 to 1.57 g/cm^3, with an increase from 0 to 10 vol.% fuel. There was little change in density with increasing fuel loadings up to 40 vol.%. The addition of coated particles caused a substantial decrease in the initial high thermal conductivities of both hot-pressed and extruded fuel compacts, particularly in the lower range of fuel temperatures. Thermal conductivities measured at 1200°C in a direction perpendicular to the molding or extrusion directions were above 15 Btu/(ft)(hr)(°F) for fuel loadings of up to 40 vol.% in hot-pressed compacts and 20 vol.% in extruded compacts.

The rates of reaction of a 1-in.-diameter sphere of Speer Mod-2 graphite with helium-CO_2 mixtures having CO_2 concentrations ranging from 60 to 1650 vpm (parts per million by volume) and a total pressure of 1 atm were measured at 975°C by Oak Ridge.[2] The results, shown in Fig. II-1, indicate that the rate varies as the CO_2 concentration to the 0.7 power in the concentration range of 300 to 1650 vpm of CO_2. The rates at 60 and 110 vpm indicate an exponent approaching unity, but the precision is not very high at these low concentrations.

The same graphite sphere was also reacted with helium-H_2O mixtures having H_2O concentrations between 20 and 760 vpm at temperatures of 825 to 1025°C. It is indicated in Fig. II-1 that the reaction rate at 975°C varies as the 0.72 power of the H_2O concentration in the H_2O range of 110 to 760 vpm. This exponent was not influenced to any significant extent by changes of temperature between 825 and 1025°C in the H_2O-concentration range of 110 to 460 vpm.

The retardation of the steam-carbon reaction by hydrogen was studied at 970 to 975°C by

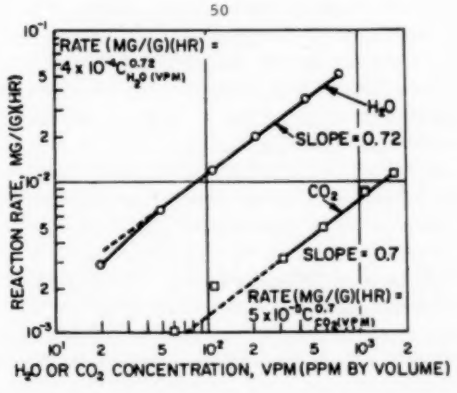
RATE (MG/(G)(HR)) = 4 x 10^{-4}C$^{0.72}_{H_2O\ (VPM)}$
H_2O
SLOPE = 0.72
CO_2
SLOPE = 0.7
RATE (MG/(G)(HR)) = 5 x 10^{-5}C$^{0.7}_{CO_2\ (VPM)}$
REACTION RATE, MG/(G)(HR)
H_2O OR CO_2 CONCENTRATION, VPM (PPM BY VOLUME)

Fig. II-1 Rates of CO_2-graphite and H_2O-graphite reactions at 975°C.[2]

introducing helium having H_2O concentrations of 110 or 460 vpm and varying concentrations of hydrogen. The experimental results are shown in Fig. II-2.

Unfueled spheres of Speer Mod-2 and ATJ graphites and of various 1.5-in.-diameter fueled graphite spheres were reacted at 800, 900, and 1000°C with steam having a partial pressure of ~730 mm Hg. The degree of burnout was observed to have a pronounced effect on the reaction rate. Reactivity of fueled spheres was not very different from that found for the unfueled Speer Mod-2 or ATJ grades of graphite. No evidence of significant attack on the pyrolytic carbon coatings of dispersed $(U,Th)C_2$ particles was observed for the fueled spheres.

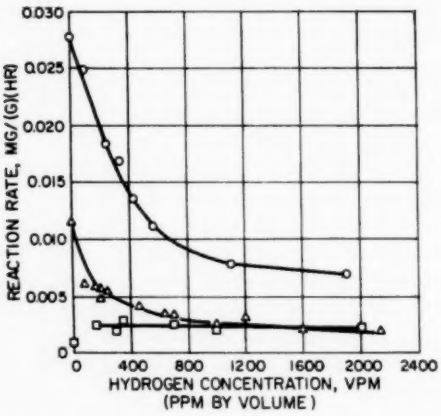

Fig. II-2 Effect of hydrogen on the H_2O-graphite reaction.[2] □, no H_2O (975°C); Δ, 110 vpm H_2O (975°C); ○, 460 vpm H_2O (970°C).

The effect of tensile load on radiation-induced contraction of graphite is under study at Hanford.[3] This investigation is adding new information concerning the proposition that radiation-induced creep is of sufficient magnitude to relieve all the differential contraction stress generated in large graphite blocks. Tensile specimens of NC-8 graphite cut parallel to the extrusion axis have been stressed to 600 or 800 psi while being irradiated at a temperature of 475°C. Over the exposure range of 3 to 8 × 10^{20} neutrons/cm^2 ($E > 0.18$ Mev), the tensile-loaded specimens always contracted but not so much as unloaded controls exposed simultaneously. The amount of restraint seemed to be dependent on load.

The rupture of two tensile samples at approximately the same strain implied the possible existence of a strain-rupture limit. The following explanation was proposed for the mechanism of failure. During neutron irradiation at these temperatures, graphite contracts. Some of this contraction can be restrained by a tensile load. The rate of restraint could be dependent on the radiation-induced creep observed by others at lower exposures. Because the creep rate is low, the differential stress in the specimen increases faster than the creep strain can relieve it. A complex internal-stress pattern develops because the graphite used in reactors is an anisotropic mixture of crystalline grains and amorphous or cryptocrystalline binder, has a porous structure, and contains both macrocracks and microcracks. Stress will not be uniform over the entire cross section, and eventually a rupture stress will be produced at some weak link, thus initiating the process of failure. This pattern will be repeated and accelerated at successive weak links until a point is reached where the accumulated stress exceeds the strength of the remaining material, and brittle fracture occurs.

Hanford has reported[4] additional information on the influence of furfuryl alcohol binder on the dimensional stability of graphite under long-term irradiation. Test samples included: (1) two series of graphites from the Armour Research Foundation, molded from mixes of No. 90 flour, Texas coke, and (respectively) 20 parts furfuryl alcohol and 37 parts pitch, and graphitized at 2900°C; (2) Dragon Project graphite, pitch bonded and furfuryl alcohol bonded, graphitized at 2700°F; (3) a proprietary needle-coke graphite, AGOT-LS. CSF reference samples were also included in the irradiations, which were performed in a series of four consecutive tests to a maximum exposure of 7.23 × 10^{21} neutrons/cm^2 ($E > 0.18$ Mev) at temperatures in the range 350 to 550°C. The exposures were sufficient to cause large dimensional changes in the graphites, the greatest contraction being 5.2%. The furfuryl alcohol-bonded graphites contracted consistently more than their pitch-bonded counterparts. The needle-coke graphite, AGOT-LS, contracted only one-fourth as much as the CSF reference sample and much less than any of the other materials.

An interim report[5] has been issued on a continuing study at Hanford on the effects of irradiation upon pyrolytic graphite. Samples were

irradiated for two periods to a maximum total exposure of 4870 Mwd/adjacent ton at 650°C. During the second irradiation period of 2200 Mwd/adjacent ton, the samples displayed a bulk expansion rate in the c direction of 0.27% per 1000 Mwd/adjacent ton and a contraction rate of −0.102% per 1000 Mwd/adjacent ton in the a direction. The accumulated changes were +0.7% in the c direction and −0.3% in the a direction. The coefficient of thermal expansion in the c direction increased steadily from an initial value of 20.5×10^{-6} to 24.6×10^{-6}/°C, but there was negligible change in the coefficient in the a direction. Dimensional changes are presented in Fig. II-3. For this study, 1 Mwd/adjacent ton is approximately equivalent to 1.2×10^{17} neutrons/cm^2 ($E > 0.18$ Mev). Because pyrolytic carbon has very nearly theoretical density and possesses a high degree of anisotropy, properties also common to crystallites, it was expected that, under irradiation, pyrolytic carbon would exhibit the same behavior as the crystallites in polycrystalline graphite. Thus the experimental data imply that during high-temperature irradiation of polycrystalline graphite to these exposures, no volume contraction occurs in the crystallites. Rather, radiation-induced shrinkage must be caused by a decrease in porosity.

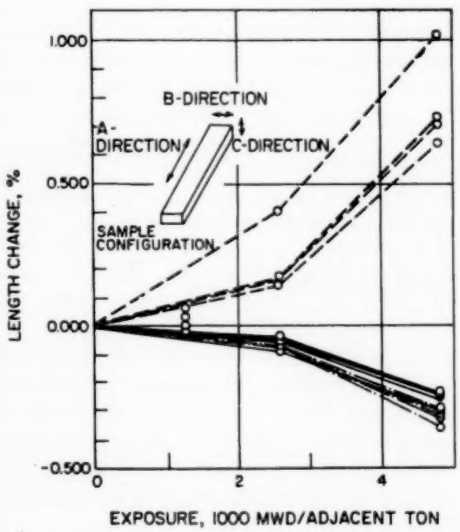

Fig. II-3 Dimensional changes for pyrocarbon samples.[5] ——, a direction (parallel); – – –, b direction (parallel); – – –, c direction (transverse).

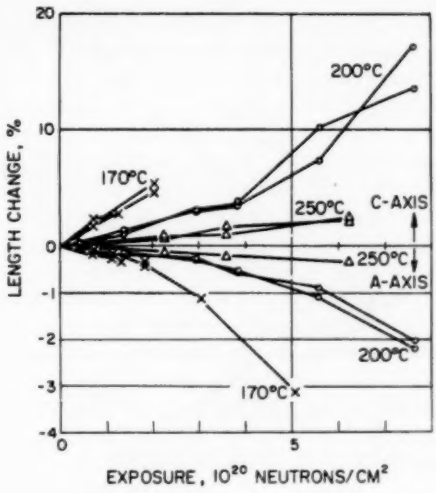

Fig. II-4 Dimensional changes with neutron dose of pyrolytic graphite at 170, 200, and 250°C.[6]

Recently British investigators[6] have compared fast-neutron-induced dimensional changes in pyrolytic graphite with those in a wide range of polycrystalline graphites. Some interesting data on the dimensional changes of pyrolytic graphite are presented in Figs. II-4 and II-5. Particularly noteworthy are the large dimensional changes in both directions under conditions represented by Fig. II-4, up to 18% growth in the c-axis direction and 3% contraction in the a-axis direction. Even at the higher temperatures represented in Fig. II-5, the dimensional changes are quite large. These dimensional changes are quite different from those observed using X rays, which generally show a saturating small increase in c spacing and a small or zero a-spacing contraction.

Of major significance in this comparison study is the conclusion that the crystallites in different polycrystalline graphites exhibit different degrees of retention of irradiation damage under the same irradiation conditions. This difference increases with increasing irradiation temperature and leads to practical difficulties in predicting the behavior of new types of well-graphitized materials.

Brookhaven researchers[7] have studied the rate of decomposition of the cesium-graphite compound C_8Cs by a tracer technique that utilizes ^{134}Cs and a sodium iodide scintillation detector. The graphite sample used in this study was a $\frac{1}{4}$-in. cube of General Electric pyrographite

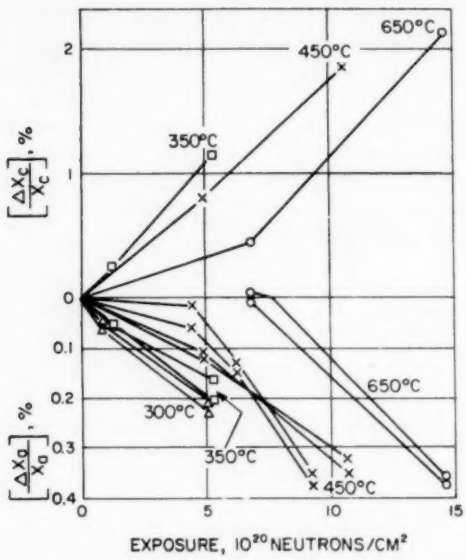

Fig. II-5 Dimensional changes with neutron dose of pyrolytic graphite at 300, 350, 450, and 650°C.[6]

annealed at 3200°C. Experiments were carried out in the temperature range 390 to 625°C. A typical decomposition curve is shown in Fig. II-6. The decomposition curves all show distinct stages. The first portion of the typical curve is linear up to 20% decomposition. At this point a break occurs, and the decomposition proceeds at a second linear rate that is slower than the first, up to 66.6% decomposition. Beyond this point, the rate of removal of cesium decreases continuously with time.

The 66.6% point corresponds to the compound $C_{24}Cs$, which is known to exist. The last stage of the decomposition appears to be diffusion controlled. The first two linear rates of decomposition may represent processes controlled by removal of cesium from the external surface of the graphite. The temperature dependence of all three regions has been established over the temperature range 390 to 625°C. The activation energies calculated for each of the three stages are similar and are in the range of 30 to 40 kcal/gram mole. (M. C. Brockway)

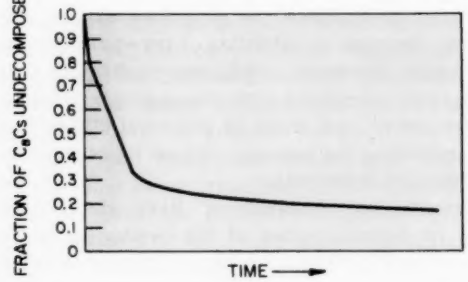

Fig. II-6 Typical decomposition curve for the cesium-graphite compound C_8Cs.[7]

Beryllium Metal and Alloys

Fabrication

A patented process[8] for forming sintered beryllium bodies uses electrolytic beryllium powder containing less than 500 ppm of aluminum and silicon. Increasing the aggregate aluminum and silicon content to 500 to 2000 ppm permits the final density of the compacts to be controlled. The specially treated powder can then be vacuum hot pressed to densities greater than 90% of theoretical.

Gross and O'Rourke have published a paper[9] reviewing fabrication techniques, tensile properties, formability, and electrical resistivity of annealed and as-drawn beryllium wires. Potential applications of beryllium wire are discussed.

A technique for producing (−50 + 60 mesh) beryllium particles was developed at Oak Ridge.[10] In a fluid-energy mill, coarse machine chips were converted by attrition to nearly spherical particles. Fines were periodically removed by screening. Although the yield was relatively low (approximately 12%), virtually no increase in impurity was noted.

Physical Metallurgy and Mechanical Properties

An article[11] in a Czechoslovakian journal concerning diffusion of uranium in beryllium presents the results of quantitative measurements and describes methods and results of quantitative metallographic evaluation and calculation of the activation energy of the diffusion process.

Ranzetta and Scott[12] used electron microscopy and electron-probe microanalysis to study the microstructure of beryllium and beryllium-iron and beryllium-chromium alloys. The effects of

thermal treatment on the distribution of impurities and of alloying elements on mechanical properties were investigated. Annealing the iron-beryllium alloys produced large iron-containing precipitates as well as a more general segregation of the iron to the grain boundaries. Some evidence of solid-solution hardening, but no precipitation aging, was found. Annealed beryllium-chromium alloys had increased high-temperature ductility, which was associated with a purification of the matrix. It was suggested that the grain-boundary regions were responsible for the ductility and coherency of the grains.

Other British investigators, Morrow and Moore,[13] have investigated the effect of testing environment on mechanical properties of beryllium. Two grades of polycrystalline beryllium were solution treated and overaged and then tested in air and in Cerrobend (a eutectic alloy of lead, tin, bismuth, and cadmium). The tensile strength of either grade of material was not susceptible to the aging treatment. However, elongation of the overaged material at 450°C increased from 50% when tested in air to 115% when tested in Cerrobend. The solution-treated material showed no change dependent on environment. It is significant that neither solution treating nor overaging produced any increase in ductility below 200°C. Neither treatment, therefore, could be used for improving the room-temperature ductility of beryllium. Two models are proposed for the improved elevated-temperature ductility.

Chemical and Nuclear Properties

Investigators at Illinois Institute of Technology[14] studied protective coatings for beryllium reflectors in SNAP-8 ground testing. Some of the coating methods investigated included enameling, metallic-slurry coating, pack-cementation inversion coatings, and commercial coatings. An anodic coating produced by Brush was the best, affording protection from 360 to 590 hr at 745°C.

The corrosion of beryllium and beryllium alloys was investigated[15] at Harwell in 325°C water and saturated steam and in 500°C dry steam. A dependence of corrosion resistance of beryllium on prior fabrication history was noted. Powder-metallurgy and tungsten-arc-melted materials appeared the best. Nickel additions ranging from 0.5 to 5.0 wt.% increased the corrosion resistance at 325°C. Corrosion in 500°C dry steam was generally lower than in 325°C saturated steam. Preexposure at 500°C increased the corrosion resistance at 325°C, presumably as a result of an anodic protective film. Calcium-rich alloys had poor resistance to 325°C water and steam. However, other investigators[16] found that a beryllium–0.7 wt.% calcium alloy was more oxidation resistant than unalloyed beryllium in (CO_2 + 2 vol.% CO)-containing water vapor. The most significant effect was the decrease in intergranular corrosion. Surface oxide scales were similar in both alloys, but the subscale in the calcium-containing alloys contained a thin layer of $Be_{13}Ca$. It was proposed that this layer added to the stability of the surface film, thereby increasing its protective nature.

British investigators[17,18] have studied by electron microscopy the nature of surface films produced by exposure to 700°C water vapor, oxygen, and CO_2. Numerous regions bounded by cracks in the oxide film appear early in CO_2 exposure, but well before breakaway. There is no evidence of preferential cracking at the grain boundaries of the substrate. However, carbide inclusions in the grain boundaries cause preferential attack, and it was postulated that these impurities play a significant role in intergranular corrosion of beryllium. (H. D. Hanes)

Beryllium Oxide

Unfueled BeO samples were irradiated by General Atomic[19] to furnish information on the effects of density, grain size, composition, shape, and temperature. Samples were prepared from UOX- or GC-grade BeO powders, using fluxing additions of 125% bentonite–1.0% MgO or a 1.0% mixture of MgO-Al_2O_3. The peak exposure was estimated as 1.0×10^{21} neutrons/cm^2 (>1 Mev). Specimen test temperatures ranged from 260 to 940°C. Visual examination of irradiated specimens indicated that 44 of 129 specimens fractured. High-density fine-grain-size specimens exhibited excellent resistance to cracking, whereas large-grained low-density specimens had poor resistance to fracture. Axial length changes in samples ranged from 0 to 1.40%. Densities decreased by about 0.25 to 6%. Strengths of irradiated specimens decreased to about 14 to 20% of the preirradiation values. Highest strength retention under irradiation was exhibited by the high-density

small-grain-size MgO-containing specimens irradiated in the high-flux–high-temperature section of the test capsule. The irradiated specimens showed a marked contraction above 850°C. This was directly related to the amount of linear growth under irradiation and was believed to be an indication of the annealing behavior of defects in the irradiated material. Preliminary measurements show a marked decrease in the thermal diffusivity of an irradiated bentonite-containing specimen to 16% of its preirradiation value. Postirradiation annealing at 1000°F increased the thermal diffusivity to about 49% of its preirradiation value.

Fueled BeO samples composed of 70 vol.% BeO–30 vol.% UO_2 were also irradiated. Half the samples contained fine (<25 μ) particles of UO_2; the others contained coarse (~150 μ) UO_2 particles. Accumulated irradiation corresponded to a peak burnup of 55% of the ^{235}U (approximately 3.7×10^{20} fissions/cm^3, or 43,000 Mwd/ton) at a peak fuel temperature of about 2000°F. The samples containing coarse fuel particles showed no gross cracks or deformation after irradiation, whereas those containing fine fuel particles broke into several pieces during irradiation. The structure of the pellets containing fine UO_2 remained relatively dense and uniform, whereas pellets fueled with the coarse UO_2 had a large-grained, severely cracked, porous matrix and fuel-particle structure. The irradiation-induced elongations in coarse-UO_2-fueled samples were less than 1%, and the decrease in density was less than 3%. Fission-gas release from samples fueled with fine UO_2 was less than 0.1% of the fission gases produced. No gas-release data were obtained from the coarse-UO_2-containing BeO.

BeO researchers may find of interest a recent translation[20] of Belyaev's book *Beryllium Oxide, Properties and Applications.* The purpose of the book is to acquaint readers with investigations of the properties of beryllium oxide and its applications which were reported in Soviet and other foreign periodicals and books through 1961.

The self-diffusion of beryllium in unirradiated cold-pressed and sintered beryllium oxide has been investigated at Oak Ridge.[21] The observed diffusion behavior between 1150 and 1800°C is described by the empirical relation

$$D = 2.49 \times 10^{-3} \exp\left(-\frac{62.5 \times 10^3}{RT}\right) \quad \text{cm}^2/\text{sec}$$

Calculated diffusion coefficients are listed in Table II-1.

This experimental study involved the development of a precision-lapping device, the deposition of ^{7}BeO on the surface of a specimen of ^{9}BeO from aqueous solution by exchange and/or adsorption, and the application of gamma autoradiography as an alternative procedure for precision lapping in the determination of penetration depths.

Table II-1 SELF-DIFFUSION COEFFICIENTS OF BERYLLIUM IN BERYLLIUM OXIDE[21]

Annealing conditions		Diffusion coefficient		Mean displacement for Be ion, μ/year
Temp., °C	Time, sec	Cm^2/sec	% deviation	
1180	4.212×10^6	5.64×10^{-13}	29	60
1245	1.639×10^6	3.02×10^{-12}	26	138
1273	2.340×10^5	2.71×10^{-12}	24	131
1273	2.340×10^5	6.83×10^{-12}	16	207
1410	3.300×10^5	1.42×10^{-11}	39	299
1500	1.602×10^5	6.01×10^{-11}	25	616
1515	2.516×10^6	1.00×10^{-10}	42	795
1600	2.509×10^6	5.85×10^{-11}	39	608
1663	2.340×10^5	3.42×10^{-10}	22	1472
1663*	2.340×10^5	2.21×10^{-10}		
1795	8.640×10^4	4.41×10^{-10}	15	1665
1795	8.640×10^4	5.96×10^{-10}	20	1940

*Analysis by gamma autoradiography.

A diffusion model is postulated on the basis of vacancy migration, which suggests identical activation energies for diffusion in both *a* and *c* directions in single crystals and predicts an activation energy of the correct order of magnitude. (M. C. Brockway)

Solid Hydrides

Zirconium Hydride

The solubility of hydrogen in zirconium-oxygen alloys has been determined by Singh and Parr,[22] who found that the hydrogen-rich boundaries of the beta-plus-delta two-phase region decrease in hydrogen content as the oxygen content increases. Extrapolation of the delta and delta-plus-epsilon boundary to zero oxygen content places it at 62 at.% hydrogen in the pure zirconium hydride, which is in good agreement with earlier data. In addition, their extrapolations indicate that the narrow delta-plus-epsilon

two-phase field lies in the following composition ranges:

Temperature, °C	Composition, at.% hydrogen
700	61.9 to 62.9
750	62.3 to 63.1
800	61.0 to 61.3

These investigators also studied the zirconium-deuterium system and found that, within the limits of experimental accuracy, the phase boundaries, eutectoid composition, and heat of solution of hydrogen are the same as for the zirconium-hydrogen system.[23]

Hydrided Zirconium Alloys

Louthan and Marshall[24] examined the effect of hydride orientation in Zircaloy. They found that, in Zircaloy hydrided at 400°C, application of stress during hydriding produced hydride platelets oriented perpendicular to the tensile stress and parallel to the compressive stress. This condition drastically reduced the ductility of the Zircaloy.

In an investigation at Hanford,[25] Zircaloy-2 reactor process tubes were hydrided to 500 and 1150 ppm hydrogen. Brittle-fracture tests were conducted on both sets, and results showed that the critical pressure for crack propagation was only one-fourth to one-half of that for non-hydrided Zircaloy-2. (H. H. Krause)

References

1. W. V. Goeddel and J. M. Pontelandolfo, The Influence of Coated Particles on the Physical Properties of Graphite-Matrix Fuel Compacts, USAEC Report GAMD-4441, General Atomic Division, General Dynamics Corp., July 23, 1963.
2. J. P. Blakely, L. G. Overholser, and J. L. Rutherford, Reactivity of Graphite and Fueled Graphite Spheres with Oxidizing Gases, USAEC Report ORNL-TM-751, Oak Ridge National Laboratory, February 1964.
3. Hanford Atomic Products Operation, Reactor and Fuels Laboratory Monthly Report, February 1964, USAEC Report HW-81019A, Mar. 13, 1964. (Classified)
4. Hanford Atomic Products Operation, Reactor and Fuels Laboratory Monthly Report, December 1963, USAEC Report HW-79999A, Jan. 15, 1964. (Classified)
5. H. H. Yoshikawa, The Effect of Radiation on Pyrolytic Graphite, USAEC Report HW-78645, Hanford Atomic Products Operation, Jan. 9, 1964.
6. W. H. Martin and B. T. Kelley, Fast-Neutron-Induced Dimensional Changes in Graphite, British Report TRG-Memo-1981, November 1963.
7. J. H. Reynolds, Nuclear Engineering Department Progress Report, May 1–August 31, 1963, USAEC Report BNL-823, Brookhaven National Laboratory, December 1963.
8. T. W. Farthing and C. A. Terry, Improvements in or Relating to Sintered Beryllium Compacts, British Patent 940,425, Oct. 30, 1963.
9. A. G. Gross and R. G. O'Rourke, Some Properties and Applications of Beryllium Wire, *Wire Production*, 38: 1087-1088, 1090-1091, 1161 (August 1963).
10. Union Carbide Corporation, Nuclear Division, Y-12 Plant, March 1964. (Unpublished)
11. E. Karnikova, M. Holnika, and V. Masivik, Uranium and Beryllium Compatibility (in Czechoslovakian), *Jaderna Energie*, 9: 277-280 (1963).
12. G. V. T. Ranzetta and V. D. Scott, The Effect of Thermal Treatment on the Metallographic Structure of Beryllium and Dilute Beryllium Alloys, *J. Nucl. Mater.*, 10: 113-126 (October 1963).
13. F. Morrow and A. Moore, Increased Ductility of Polycrystalline Beryllium Above 300°C Related to Test Environment, British Report AWRE-O-97/63, December 1963.
14. Illinois Institute of Technology, Armour Research Foundation, High-Temperature Beryllium Corrosion Protection, USAEC Report ARF-B229-17, Mar. 20, 1963.
15. J. T. Demant, R. E. Wiggins, and P. Gibson, The Corrosion of Beryllium and Some Beryllium Alloys by High-Temperature Water and Steam, British Report AERE-R-4422, October 1963.
16. V. D. Scott and G. V. T. Ranzetta, Electron Metallography of the Corrosion of Beryllium and Beryllium-Calcium Alloys, *J. Nucl. Mater.*, 9: 277-289 (August 1963).
17. W. B. Jepson and J. B. Warburton, The High-Temperature Oxidation of Beryllium and the Fate of Beryllium Carbide Inclusions, *J. Nucl. Mater.*, 10: 127-133 (October 1963).
18. W. B. Jepson, B. L. Myatt, J. B. Warburton, and J. E. Antill, Some Topographical Observations on the Oxidation of Beryllium, *J. Nucl. Mater.*, 10: 224-232 (November 1963).
19. M. T. Simnad, Part I. Irradiation Effects on Beryllium Oxide Materials; Part II. Irradiation Effects on Dispersion Type BeO-UO_2 for EBOR, USAEC Report GA-4643, General Atomic Division, General Dynamics Corp., Oct. 7, 1963.
20. R. A. Belyaev, Beryllium Oxide. Properties and Applications, USAEC Translation AEC-tr-6175, 1962.
21. H. J. deBruin and G. M. Watson, Self-Diffusion of

Beryllium in Unirradiated, Cold-Pressed and Sintered Beryllium Oxide, USAEC Report ORNL-3526, Oak Ridge National Laboratory, Jan. 29, 1964.

22. K. P. Singh and J. G. Parr, Hydrogen Solubility in Zirconium-Oxygen Alloys, *Trans. Faraday Soc.*, 59: 2248-2255 (October 1963).
23. K. P. Singh and J. G. Parr, Solubility of Deuterium in the Zirconium plus Deuterium System, *Trans. Faraday Soc.*, 59: 2256-2259 (October 1963).
24. M. R. Louthan, Jr., and R. P. Marshall, Control of Hydride Orientation of Zircaloy, *J. Nucl. Mater.*, 9(2): 170-184 (1963).
25. F. W. Albaugh, Reactor and Fuels Laboratory Monthly Report, November 1963, USAEC Report HW-79726A, Hanford Atomic Products Operation, Dec. 15, 1963. (Classified)

Section

III

Reactor Materials

Nuclear Poisons

Metallic Poison Materials

The machinability, welding properties, tensile strength, and hardness of type 430 stainless steel containing 1.5 wt.% ferroboron were evaluated at Hanford.[1] This alloy is to be used in the New Production Reactor (NPR) safety system, and ^{10}B was added to the material to make the "blackness" equivalent to 2 wt.% natural boron. An extensive report by Allis-Chalmers[2] discusses the irradiation effects on 2 wt.% boron–stainless-steel control rods.

At Chalk River,[3] experiments are under way to determine the decomposition temperature of hexagonal $GdAl_3$. The evidence thus far indicates that the hexagonal intermetallic compound is stable to at least 1000°C.

The heat content of hafnium was determined[4] up to 1073°C, with results expressed by $H_{T(°K)} - H_{298} = 5.607T - 0.911 \times 10^{-3}T^2$.

A technique for preparing thin (20 to 400 $\mu g/cm^2$) self-supporting boron films by electron bombardment is described.[5] The technique differs from those used previously in that it employs a water-cooled anode and a new method of removing the evaporated film from the backing.

(M. Kangilaski)

Dispersion Poison Materials

The ternary system hafnium-tantalum-carbon was studied[6] to determine the equilibrium-phase boundaries. Pressure-sintered or hot-pressed specimens containing 0 to 80 at.% tantalum, 0 to 50 at.% hafnium, and 0 to 60 at.% carbon at 1850°C were vacuum annealed and quenched for these experiments. Microscopic and X-ray diffraction techniques were employed to determine phase boundaries. The results are described in terms of an isothermal section through the phase diagram; the free energy of formation was computed for the carbide phases.

The fabrication and properties of hafnium carbide are discussed in a recent publication.[7] Values for room-temperature bend strength, elastic modulus, and microhardness, as well as elevated-temperature bend strength, thermal expansion, thermal conductivity, specific heat, and electrical resistance, are reported. A survey of the properties, fabrication, production, and applications of refractory boride compounds is presented in an English journal.[8]

The lattice parameters and phase structures for the system uranium oxide–europium oxide were determined by X-ray diffraction techniques.[9] In the range 38 to 64 mole % $EuO_{1.5}$, a fluorite phase exists, the lattice parameter of which drops linearly from 5.406 to 5.391 A. On the uranium-rich side of the system, crystals of the fluorite phase were found side by side with orthorhombic $UO_{2.6}$. On the europium-rich side, the fluorite phase continues, with steeply increasing lattice parameter. The transition to the *C* type of Eu_2O_3 is not observed until the $EuO_{1.5}$ content exceeds 90 mole %.

Similar lattice-parameter and phase-structure data were obtained[10] for the plutonium oxide–europium oxide system. A fluorite phase is found in the range 0 to 42 mole % $EuO_{1.5}$. For contents above 42 mole % $EuO_{1.5}$, another fluorite phase exists, and, for contents above 60 mole % $EuO_{1.5}$, the transition to the *C* type of Eu_2O_3 is found.

Fabrication processes for boron carbide and boron carbide–silicon carbide mixtures were studied at Bettis.[11] Specimens having relative densities greater than 99% were hot pressed using B_4C and SiC powder mixtures ranging from 0 to 80 vol.% SiC. The effects of starting-powder purity, particle-size distribution, SiC content, blending techniques, and hot-pressing

variables on relative density are presented. The corrosion behavior of these specimens in 680°F water is given as a function of density, B_4C particle size, and content. The fabrication of these compacts into Zircaloy-clad elements by eutectic diffusion bonding and gas-pressure bonding is discussed.

Studies at Combustion Engineering[12] indicate that UO_2 fuel elements containing 0.05 wt.% B_4C can be vibratorily compacted up to 89% relative density by electrochemical and pneumatic methods. The distribution of boron along the axis of the elements was maintained within ±20% of the nominal value by using special powder-blending and -loading techniques. The boron distribution did not change when a severe temperature gradient was imposed on the tubes.

(E. G. Smith, Jr.)

References

1. R. K. Smith, An Evaluation of Wrought 430 Boron Stainless Steel, USAEC Report HW-79081, Hanford Atomic Products Operation, Sept. 30, 1963.
2. D. A. Patterson and D. A. Nehrig, Burnup Limits for Pathfinder Two Weight Per Cent Natural Boron–Stainless Steel Control Rod, USAEC Report ACNP-63006, Allis-Chalmers Mfg. Co., Dec. 19, 1963.
3. Atomic Energy of Canada, Ltd., 1963. (Unpublished)
4. D. T. Hawkins, M. Onillon, and R. L. Orr, High Temperature Heat Content of Hafnium, *J. Chem. Eng. Data*, 8: 628-629 (October 1963); also USAEC Report UCRL-10729.
5. J. R. Erskine and D. S. Gemmell, The Preparation of Thin Self-Supporting Boron Films, *Nucl. Instr. Methods*, 24: 397-398 (October 1963).
6. E. Ruby and H. Nowatny, Investigations in the System Hafnium-Tantalum-Carbon, *Monatsh. Chem.*, 94: 507-517 (1963).
7. W. A. Sanders et al., Preliminary Investigation of the Fabrication and Properties of Hafnium Carbide, *High Temperature Materials—Part 2*, Vol. 18, Interscience Publishers, New York, 1963.
8. R. Thompson and A. A. R. Wood, Refractory Borides, *Chem. Engr. (London)*, No. 166: CE51-6 (March 1963).
9. H. Haug and F. Weigel, Mixed Oxide Systems of Lanthanide and Actinide Elements. I. Roentgen Study of the System Uranium Oxide–Europium Oxide, *J. Nucl. Mater.*, 9: 355-359 (August 1963).
10. H. Haug and F. Weigel, Mixed Oxide Systems of Lanthanide and Actinide Elements. II. Roentgen Study of the System Plutonium Oxide–Europium Oxide, *J. Nucl. Mater.*, 9: 360-363 (August 1963).
11. S. F. Kaufman, Fabrication Development of Boron Carbide and Boron Carbide–Silicon Carbide Mixtures for Possible Application as Lumped Burnable Poisons in PWR-2, USAEC Report WAPD-244, Westinghouse Electric Corp., Bettis Atomic Power Laboratory, January 1964.
12. G. Zuromsky, R. C. Brayer, and W. P. Chernock, Burnable Poison Additions to UO_2. Summary Report, July 1, 1962–June 30, 1963, USAEC Report CEND-181, Combustion Engineering, Inc., November 1963.

Section

IV

Reactor Materials

Cladding and Structural Materials

Corrosion

Zirconium Corrosion

Eight papers on the corrosion of zirconium alloys are included in the Proceedings of the USAEC Symposium on Zirconium Alloy Development held at Pleasanton, California, November 1962.[1] Among the subjects covered were: (1) oxidation in steam, oxygen, and boiling-water reactor environments, (2) composition and properties of oxide films, and (3) mechanism of hydrogen absorption and transport.

A fluorine attachment of about 0.5 mg/cm^2 has been found on Zircaloy pickled in HNO_3/HF by using radionuclide ^{18}F in studies conducted at Chalk River.[2] Of the postpickling treatments investigated, only oxidation in steam at 500°C was successful in removing the fluorides.

Long-term (336 days) exposure of Zircaloy-2, Zircaloy-4, and nickel-free Zircaloy-2 to 680°F, pH 10.5 (LiOH) water at Bettis[3] has resulted in a slight increase in corrosion rates but no increase in hydrogen absorption compared with results in neutral water under the same conditions. Bettis has also summarized corrosion and hydrogen-absorption results for long-term exposure of alpha-annealed and beta-quenched Zircaloy-4 in 750, 800, and 850°F steam and in 550 and 680°F water.

The effect of the addition of up to 850 ppm silicon on the corrosion behavior of Zircaloy-2 in high-temperature water and steam has also been reported by Bettis.[4] Silicon additions were found to render the alloy less susceptible to hydrogen absorption during corrosion and to minimize the deleterious effects on corrosion behavior of slowly cooling through the two-phase alpha-plus-beta region.

The oxidation of binary and ternary zirconium alloys containing less than 10 wt.% of antimony, beryllium, copper, germanium, molybdenum, palladium, silicon, tin, tellurium, and vanadium has been studied in 1-atm-pressure steam at 300 to 600°C at Harwell.[5] On the basis of a comparison of these results with the corrosion behavior of Zircaloy-2 and the pressure dependence of the oxidation of zirconium, it was concluded that the beneficial effect of alloying elements is not to reduce the rate of oxygen diffusion through the oxide but is to eliminate (or retard) the influence of increasing steam pressure on oxidation.

The effect of alloying with up to 3 wt.% oxygen on the steam-corrosion resistance of Zircaloy-2 has been studied at Harwell.[6] Increases in oxidation rate were attributed to inhomogeneous distribution of oxygen in the metal. With homogeneous distribution of oxygen, the oxidation rates approached those of low-oxygen material.

An analysis and correlation of data on the in-pile corrosion behavior of Zircaloy-2 in high-temperature, enriched UO_2SO_4 has been prepared by Oak Ridge.[7] It was found that corrosion rates increased with increasing fission-power density and with increasing temperature, but decreased with increasing flow velocity. On the basis of these factors, an equation was developed to express corrosion behavior in the temperature range 225 to 330°C. (W. E. Berry)

Aluminum Corrosion

Studies of the effect of high heat fluxes on the corrosion behavior of aluminum alloys under Advanced Test Reactor (ATR) conditions are being continued at Oak Ridge.[8] At heat fluxes ranging up to 2×10^6 Btu/(hr)(sq ft) and water flow rates of 25 to 45 ft/sec, it was found that oxide formation occurred at the same rate for all alloys studied, and at *p*H 5.7 to 7.0 it was 2.7 times faster than at *p*H 5. Alloys 6061 and

1100 exhibited pitting which increased in severity with increasing *p*H in the range 5.0 to 7.0. Alloy X8001 did not exhibit pitting under these conditions. Because of its better strength, it was concluded that 6061 appeared to be the optimum choice for the ATR, providing the *p*H was kept below 5.0.

Corrosion experience with aluminum-nickel-iron powder products in water at 260 to 350°C has been summarized by Argonne.[9] The corrosion resistance of Trefimetaux (French) powder products was equal to that of the wrought alloy in static 290°C water, but was poorer than that of the wrought alloy in flowing water at 315°C. Failures of other powder products were related to porosity or pickup of milling lubricant during ball milling.

A literature survey on the corrosion of aluminum and aluminum alloys in high-temperature water has been prepared by Swedish scientists.[10] The survey contains 66 abstracts (mainly on unalloyed aluminum) of reports and papers issued during the period 1949 to 1963. (W. E. Berry)

Stainless-Steel Corrosion

The effect of up to 3 to 4 ppm oxygen in 550°C, 3000-psi steam on the corrosion behavior of superheater materials has been determined by Hanford.[11] Corrosion rates ranged from about 0.5 mil/year for Incoloy and type 446 stainless steel to about 1.0 mil/year for types 304L and 406 stainless steel. There was essentially no difference in corrosion behavior between samples exposed to oxygenated steam (3 to 4 ppm oxygen) and deoxygenated steam (less than 0.05 ppm oxygen).

Irradiation was found to produce slight structural changes and no increased susceptibility to intergranular corrosion (as indicated by posttest exposure to acidified copper sulfate solution) of type 304 stainless-steel cladding on UO_2 fuel rods in studies conducted by Westinghouse.[12] Irradiation exposures were 1.7×10^{20} and 9.8×10^{20} neutrons/cm^2 (>1 Mev). Reactor-loop operating conditions were water, at 565°F and 2000 psi, containing 5 to 75 cm^3 hydrogen/kg water and 1500 ± 1000 ppm boron. On the other hand, intergranular cracking has been observed in cold-swaged type 304 stainless-steel cladding on UO_2 fuel in experiments conducted in the Vallecitos Boiling-Water Reactor.[13] Longitudnal cracks were observed in the peak-burnup region of the specimen that had a peak exposure of 7100 Mwd/ton and a maximum heat flux of 385,000 Btu/(hr)(sq ft). Posttest examinations revealed no evidence of a grain-boundary precipitate that could be correlated with the cracking behavior.

Radioactive tracers have been used to study the effect of surface finish on the stress-corrosion-cracking behavior of type 304 stainless steel in boiling chloride solutions in experiments conducted at Savannah River.[14] With no applied stress, cracking occurred in dry ground (40 grit) specimens, but not in as-received or polished specimens. Chloride-ion deposition occurred at inclusions on the ground material, but was uniform over the entire surface for the polished or as-received specimens. Silicate, phosphate, chromate, nickelous, iodide, and bromide ions were found to inhibit cracking of ground specimens in solutions containing 10 to 100 ppm chlorides. (W. E. Berry)

Corrosion of Iron- and Nickel-Base Alloys

WATER AND STEAM

Among recent publications is a compilation[15] of 20 lectures on corrosion and water treatment in water-cooled and superheat reactors presented at the Netherlands-Norwegian Reactor School held in Norway in August 1963. Materials discussed were stainless steel, high-nickel alloys, carbon and low-alloy steels, zirconium alloys, and aluminum alloys.

A radioactive tracer study of cesium and chloride deposition on mild steel, stainless steel, and Zircaloy-2 has been made by Harwell.[16] At temperatures ranging up to 60°C, deposition on stainless steel and Zircaloy-2 was low. Chloride-ion deposition on steel increased with increasing anodic activity (greater in aerated than in deareated water). Cesium-ion deposition on mild steel was greatest in room-temperature solutions and appeared to be associated with the hydrous nature of the oxide films, decreasing as the films became more crystalline.

The performance of fuel-sheath materials in superheated-steam environments has been summarized by Vallecitos.[17] Stressed and unstressed materials were exposed to flowing steam, at 550 to 1350°F, containing up to 20 ppm oxygen and up to 2.5 ppm hydrogen. Total accumulated neutron flux ranged up to 10^{22} neutrons/cm^2 (>1 Mev). On the basis of effects

on tensile properties, corrosion, structure, and physical metallurgy, Incoloy appeared most promising, followed in order by Inconel (at low stress levels), Hastelloy X, Nionel, and types 406 and 310 stainless steel.

AIR OXIDATION

Hastelloy X has been found to have better oxidation resistance than Inconel 600, Inconel 702, and Nichrome V in 300-psi air at 1750°F in work performed at Aerojet-General.[18] Internal oxidation to a depth of several mils occurred in Hastelloy X after a 10,000-hr exposure, but the alloy was free of intergranular attack. It was concluded that Hastelloy X possessed adequate oxidation resistance for use as reactor fuel cladding in the ML-1 reactor that employs nitrogen plus 0.5 vol.% oxygen as the coolant.

The extremes in environmental conditions which might be encountered in the ATR gas loop have been studied at Hanford[19] with Haynes 25, Hastelloy X, and Inconel 600. Metal-evaporation rates (extremely pure helium coolant) ranged from 0.4 to 0.8 mil/day at 1200°C in a vacuum of about 10^{-4} mm Hg. Oxidation results in air at 1200°C (most severe condition) revealed that Inconel 600 was most resistant, Haynes 25 oxidized rapidly, and Hastelloy X was intermediate, exhibiting a penetration rate of about 1 mil/day after the initial two days' exposure.

Although TD nickel is more resistant to oxidation than pure nickel, its oxidation resistance at 600 to 1000°C was found by Hanford[20] to be inferior to that reported for superalloys. Thus it was concluded that the TD nickel would probably require protective coatings at temperatures where its mechanical properties are superior. The effect of the ThO_2 on the oxidation of nickel was believed to be to lower the rate of adsorption of oxygen on the oxide film, thereby partially inhibiting the oxidation process.

(W. E. Berry)

Corrosion of Coated Refractory Alloys

Numerous investigators have found that the mechanical properties of a refractory alloy can be altered by a protective coating that is applied to it. Changes in ductility, yield strength, creep strength, and fatigue life have all been observed. The Defense Metals Information Center has recently prepared a compilation[21] of much of this information that was reported between mid-1961 and December 1963. More mechanical-property data are being generated in Navy- and Air Force-sponsored programs at Thompson Ramo Wooldridge[22] and at the University of Dayton.[23] Thompson Ramo Wooldridge is presently evaluating the Pfaudler silicide and TRW chromium-titanium-silicon coatings on D-43 and B-66 niobium alloys. Preliminary results of this program indicate that the Pfaudler coating is generally less detrimental to mechanical properties and the TRW coating is more oxidation resistant. The coatings and alloys to be evaluated at Dayton will include:

Coating Vendors

Boeing	General Telephone & Electronics Corp.
Chance Vought	The Pfaudler Co.
Chromalloy	Thompson Ramo Wooldridge Inc.
Chromizing Corp.	

Alloy Substrates

TZM molybdenum alloy
B-66, D-43, and C-129Y niobium alloys

In a fundamental investigation of the oxidation mechanism of the $MoSi_2$, Philco[24] has studied the oxidation of bulk hot-pressed $MoSi_2$ and pack-cementation silicide coatings on molybdenum. On the basis of weight changes, temperature had little effect on the rate of oxidation of bulk $MoSi_2$ under 1-atm oxygen pressure from 1120 to 2650°F. Pest oxidation occurred on $MoSi_2$ at temperatures below 1100°F; the oxidation product was identified as tiny crystals of MoO_3 and amorphous SiO_2 powder. Pest oxidation was initiated at a large number of random sites that were not related to any structural characteristics of the $MoSi_2$ (such as grain boundaries). At higher temperatures, in the neighborhood of 2200°F, oxidation exposure resulted in the formation of a thin layer of amorphous SiO_2 and tiny islands (1 to 20 μ) containing MoO_3 and cristobalite. The rate of oxidation of bulk Mo_5Si_3 was much more rapid than that of $MoSi_2$. (Mo_5Si_3 is the primary diffusion product of a $MoSi_2$ type cementation silicide coating.) (J. J. English)

Corrosion by Liquid Metals

Polythermal sodium flow systems fabricated of selected steels are being operated at Vallecitos[25] to obtain corrosion and mass-transfer data in the 1200 to 1300°F range. The systems are fabricated from type 316 stainless steel, 2¼ wt.% chromium–1 wt.% molybdenum alloy

steel, or 5 wt.% chromium–0.5 wt.% molybdenum–0.5 wt.% titanium alloy steel, or combinations of the austenitic and ferritic materials. Corrosion rates of removable samples have been less than 1 mil/year during long exposures. However, selective depletion of various alloying elements in the hot leg and deposition in the cold leg have been observed. For example, nickel and chromium are leached from type 316 stainless steel with an accompanying gamma-to-alpha transformation in a thin surface layer. In the 2¼ wt.% chromium steel systems, carbon follows the hot-zone-to-cold-zone transfer pattern. Carbon also transfers from the 2¼ wt.% chromium steel to austenitic zones in bimetallic systems.

Generally the degrees of corrosion indicated by the removable samples (tabs) agree well with pipe-wall corrosion effects. Some departure from this was observed in the case of 19,000- to 23,000-hr service-life components taken from a type 316 stainless-steel–5 wt.% chromium–1 wt.% molybdenum alloy system and from a type 316 stainless-steel–2¼ wt.% chromium–1 wt.% molybdenum steel system. Here, up to 7 mils of intergranular attack of the type 316 stainless steel in the hot zone was apparent. The surfaces of the chromium-molybdenum alloy steel cold legs of these systems exhibited a deposited surface layer high in nickel and chromium (as in the tab studies) and a semi-adherent porous layer in areas of flow turbulence or transition. Analyses indicated varying amounts of complex oxides and/or alpha iron.

Recent information from Argonne[26] indicates that the resistance of vanadium and vanadium-titanium (10 and 20 wt.%) alloys to attack by 650°C sodium is superior to that of niobium and the corresponding niobium-titanium alloys. The most conspicuous difference is that of degree of intergranular attack. Also, the vanadium and vanadium alloys exhibit relatively low weight gains or losses, whereas the niobium materials show only weight losses. These losses are higher than those exhibited by the vanadium materials.

After approximately 10,000 hr of operation, the 2000-kw Sodium Test Facility operated at Los Alamos was dismantled and systematically examined for corrosion and allied effects.[27] Some of the nominal thermal conditions during operation were as follows: sodium leaving the gas-fired primary heater, 1100°F; sodium leaving the intermediate heat exchanger, 1000°F; sodium entering the intermediate heat exchanger, 750°F; and superheated steam to the heat dump, 925°F. Among the corrosion-oriented observations were the following:

1. Type 316 stainless steel (primary and intermediate heat exchanger and superheater) increased slightly in hardness and tensile strength and decreased in ductility. Some tubes exhibited considerable carbide precipitation in the grain boundaries, but there was no evidence of sigma formation or intergranular attack. Some scale deposits appeared in the superheater tubes.

2. A 1¼ wt.% chromium–0.5 wt.% molybdenum alloy steel (evaporation and tempering heat exchanger, which was a sodium-to-sodium unit incorporated into the system to reduce temperature differences and thermal stresses in the evaporator) exhibited slight physical-property changes opposite to those for the type 316 stainless steel. Decarburization to a depth of about 10 mils and scale formation plus pitting were apparent, particularly in the evaporator tubes.

3. Transition welds between the stainless steel and the alloy steel were not damaged. Their service temperature ranged from 500 to 900°F.

4. One of the two most pronounced failures was the severe cracking of a type 316 stainless-steel thermocouple well, evidently owing to intergranular carbide precipitation. This well was located in a 900°F zone between the superheater and the tempering heat exchanger.

5. The other pronounced failure was the severe cracking of a type 304L stainless-steel pipe tee and adjacent piping used to mix two streams of secondary-loop sodium.

Battelle is investigating the possible applicability of metal-oxide ceramics and cermets as components of a high-speed rotating-shaft seal in a 1000°F potassium system.[28] The program is pursuing the idea that a low-friction potassium-compound film can be formed on a rubbing surface and, if ruptured during seal operation, can be self-healed by a reaction between the surface material and the potassium, thus allowing sustained operation. Experimental procedures include differential thermal analyses of potentially useful materials in potassium to pinpoint reaction temperatures and to give qualitative information relative to the extent of reactions. Materials have been tested both as powders and as solid bodies. Results of experiments to date suggest the following conclusions:

1. DTA data tend to verify thermodynamically derived predictions concerning potassium reactions with various materials.

2. Two single-metal type RO oxides (BeO, MgO) have been evaluated and do not appear to react with potassium in the temperature range up to 1400°F. Oxides of the types RO_2 (MoO_2, WO_2, CrO_2, TiO_2, SiO_2, ZrO_2, and ThO_2), R_2O_5 (Nb_2O_5, V_2O_5, and Ta_2O_5), and RO_3 (MoO_3 and WO_3) appear to react too extensively to form self-protecting films on solid bodies.

3. Of the R_2O_3 types that appear promising for this application, only Al_2O_3 has been examined in any detail. It has exhibited particularly promising behavior. The Al_2O_3 + K reaction appears to form a stable protective layer of potassium aluminate on the original Al_2O_3 surfaces, thus forestalling further reaction that might, as in the cases of the higher oxide bodies, fragment bodies of the material. The reaction (initiation temperature and intensity) can be influenced by impurities or additives in the Al_2O_3.

4. Potassium aluminate can be formed below 1000°F on cermet materials containing as little as 20 wt.% Al_2O_3 dispersed in metals resistant to potassium attack.

Mercury corrosion data obtained at the Lewis Research Center of the National Aeronautics and Space Administration (NASA),[29] from a reflux-capsule materials-screening program, are summarized in Fig. IV-1. As indicated, tantalum and niobium–1 wt.% zirconium alloy were found to be the most corrosion resistant, with the martensitic and low-alloy steels next. It is stated that, in alloy corrosion, specific elements are leached and that the degree of corrosive attack is approximately related to the solubility of the elements in mercury and to the total amount of soluble elements present in the alloy. The order of solubility in mercury is believed to be as follows: manganese > nickel > chromium > cobalt > iron > tungsten. Investigated at Thompson Ramo Wooldridge is the feasibility of removing by getters and by magnetic means the corrosion products in a Haynes alloy 25 system in order to minimize cold-zone deposition. Loop experiments indicated that separation of about 85% of the corroded metal is possible. Thompson Ramo Wooldridge is pursuing this scheme in mercury corrosion experiments with Croloy-9M.

Zirconium and titanium additions to boiling-mercury systems are under study at Brook-

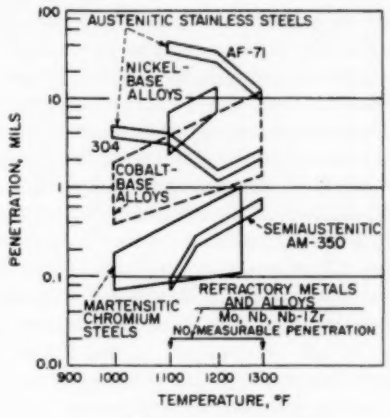

(a) Materials tested for 300 hr.

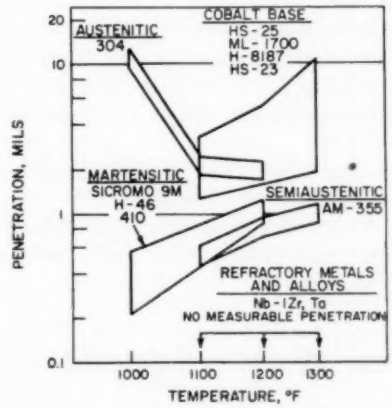

(b) Materials tested for 1000 hr.

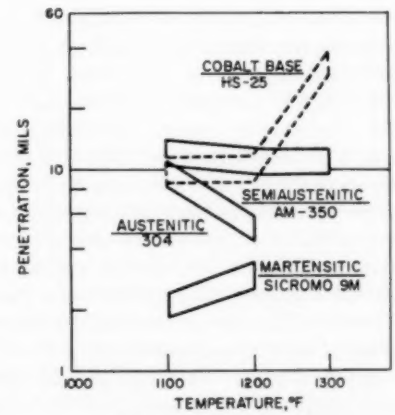

(c) Materials tested for 5000 hr.

Fig. IV-1 Corrosion penetration of various materials in mercury.[29]

haven.[30] Capsules fabricated of carbon steels and Haynes alloy 25 were first "pretreated" with 648°C mercury containing zirconium and titanium additions and then operated for 500 hr as 678°C boiling-refluxing experiments. Although data for the Haynes alloy 25 systems were not yet on hand, it was found that the carbon-steel systems displayed severe attack above the liquid level and deposition below. A zirconium-pretreated carbon-steel convection loop operated for 4568 hr with a maximum temperature of approximately 593°C in the boiler zone. Severe attack was found in the superheater section (maximum temperature approximately 705°C) and in welds near this section. Virtually no boiler-zone attack was discernible.

Attention is called to the following which present review type information in the area of liquid-metals corrosion:

1. Two panel sessions of *Materials for Sodium-Cooled Reactors* held as a part of the 1963 Winter Meeting of the American Nuclear Society[31]

2. An Oak Ridge Summary of information relating to corrosion by lithium[32]

3. A handbook summarizing the technology of liquid metals of interest to the SNAP-10A/2/8 reactor programs[33] (J. H. Stang)

Metal-Water Reactions

Additional details of the aluminum-steam reaction studies have been reported by Argonne.[34] For molten aluminum samples levitated in an induction coil and exposed to flowing steam, the aluminum-steam reaction at 1200 and 1300°C was best described by a cubic rate law. This result was evidently caused by the formation of a very protective oxide film that was not disrupted by the steam flow or the magnetic stirring produced by the induction field. Above 1400°C the reaction became approximately linear with time. The oxide film was no longer protective at these temperatures, although the reaction rates were still relatively low. Quantitative results have been reported previously.

At 1600°C and higher the aluminum pellets ignited (after a period of time) and burned to about 90% completion in steam. At 1750°C ignition was nearly instantaneous, whereas at 1700°C ignition was delayed for 5 min. At 1650 and 1600°C the delays were 9 and 18 min, respectively. The nature of the ignition and burning processes indicated that ignition occurred when aluminum vapor was able to penetrate the oxide film. Burning then took place between gaseous aluminum and water vapor.

In the Transient Reactor Test (TREAT),[35] three experiments with oxide-core (UO_2) metal-clad fuel pins have been completed. The metal cladding was Zircaloy-2 in the first experiment and type 304 stainless steel in the others. The oxide core attained a temperature of 3300°C in each of the three runs; this temperature is the vaporization point of the UO_2 in the core. Each pin underwent total destruction with the formation of globules and fine particles. It is noteworthy that, although the fuel pins were subjected to extremely energetic excursions while submerged in water, only about 30% of the molten metal reacted with the water.

Argonne[36] also completed in TREAT the first meltdown in water of a preirradiated, 20% enriched-uranium-alloy fuel pin (93.5 wt.% uranium–5 wt.% zirconium–1.5 wt.% niobium); the pin had a burnup of 1.5% of the ^{235}U and was cooled for two years. The pin was subjected to a transient having an energy input of 270 cal/g in an 84-msec period. This energy input resulted in complete melting of the fuel pin, with extensive formation of particles. The extent of the metal-water reaction was 22.6%. The physical and chemical changes noted were similar to those observed in previous experiments with cold, clean fuel of the same type at a similar energy. The results of the test with preirradiated fuel indicate tentatively that the presence of fission products does not markedly influence the behavior of uranium fuel during meltdown in water.

An interesting exercise has recently been completed[37] in an attempt to apply experimental data on metal-water reactions obtained in TREAT to the interpretation of the results of two nuclear reactor excursion incidents in which there was core meltdown and chemical reaction. The incidents, SL-1 and SPERT-I, were very similar. Each reactor had a core of aluminum-clad aluminum-uranium alloy plates. The excursion was initiated in each case by the rapid removal of a control rod. A large portion of the center of the core was melted and fragmented. Violent movement of a large portion of the coolant up and out of the reactor core occurred in each incident. In both excursions the core debris had a similar appearance. Portions of core that had been completely melted were

spongy, and considerable quantities of metallic oxides were present.

In the postexcursion analysis of both the SL-1 and SPERT-I destructive excursions, portions of the debris were analyzed for alpha alumina. (Alpha alumina is the reaction product formed at temperatures above 600°C.) On the basis of the results of these analyses, combined with an overall material balance, chemical-energy releases were estimated to be 24 ± 10 Mw-sec and 3 to 4 Mw-sec for the SL-1 and SPERT-I excursions, respectively.

The estimates of chemical-energy release calculated from TREAT data were in excellent agreement with the values obtained by the postexcursion analyses of the SL-1 and SPERT-I debris. The calculations based on TREAT data yielded values of 26 Mw-sec for SL-1 and 2 Mw-sec for SPERT-I.

In the estimation the extent of reaction was based on the peak temperatures reached by the molten core. This was necessary because the duration of the transients differed, being 40 to 1000 msec in the TREAT experiments and 2 to 4 msec in the excursions. The method is believed applicable to other materials of core construction. (A. W. Lemmon, Jr.)

Radiation Effects in Nonfuel Materials

Defects: Structure and Properties

METALS

The electron-microscope observations of neutron-irradiated molybdenum[19,38] (up to 1×10^{19} neutrons/cm^2) with 150 ppm carbon indicate that defects cluster heterogeneously at sites such as interstitial carbon atoms or large substitutional impurity atoms. The clusters in molybdenum with less than 10 ppm carbon are homogeneous. New X-ray data indicate that the increase in lattice parameter is independent of carbon content, whereas earlier data suggested a direct relation between lattice expansion and carbon content. The data now suggest that both the molybdenum with <10 ppm carbon and that with 150 ppm carbon show an average increase in a_0 from 3.1471 A to 3.1481 A for an exposure of 1.1×10^{19} neutrons/cm^2 ($E > 1$ Mev).

Recovery of high-purity proton-irradiated copper, silver, and gold was studied[39] up to 363°K. The recovery in stage III followed second-order kinetics, with an activation energy of 0.71 ± 0.04 ev for copper, 0.67 ± 0.003 ev for silver, and 0.80 ± 0.04 ev for gold. Distribution curves of the fractional concentration of defects which anneal with a given activation energy were calculated. In the case of copper and silver, they showed a complex structure followed by a large broad maximum at 0.71 ev for copper and 0.67 ev for silver. In gold there is only one large peak at 0.80 ev. The relation of these results to the various models is discussed.

Effective collision radius (R_{eff} = 0.45 to 0.58 A for 30-kev argon ions incident on copper) calculated from the anisotropy of the sputtering and emission coefficients has been shown[40] to be approximately the radius (R_{eff} = 0.41 to 0.45 A) calculated using the Born screening potential.

After irradiation to a total integrated neutron flux of 10^{20} neutrons/cm^2, an aluminum sample was placed in hot water at 96°C; an oxide film 15 to 16 μ thick was formed.[41] The oxide film on an unirradiated control sample could not be detected under a magnification of 200× under the microscope. The oxide films were separated from the samples in boric acid and subjected to X-ray analysis. The irradiated sample showed the presence of gibbsite (alpha $Al_2O_3 \cdot 3H_2O$) with a small amount of boehmite (gamma $Al_2O_3 \cdot H_2O$). Only pure boehmite could be detected in the unirradiated control sample. The corrosion rates were 0.01 g/(m^2)(hr) for the irradiated aluminum and 0.004 g/(m^2)(hr) for the unirradiated aluminum. The results show that neutron irradiation changes the structure of the oxide film and accelerates the corrosion of aluminum by allowing water to penetrate the oxide film through defects resulting from the irradiation.

A method of measuring ranges has been presented[42] which uses the change in optical-reflection coefficient of quartz due to radiation damage (by deuterons) as a means of detection. Metal films are deposited on the quartz by vacuum evaporation, and their thickness is determined with an accuracy of ±5% by weighing. If a given metal film on quartz is bombarded at a fixed flux and a number of different energies, a number of bombarded areas are formed where the deuterons have penetrated to a corresponding number of different depths in the quartz. After the metal film is chemically removed, the optical-reflection coefficients of the bombarded

areas are measured and compared with theoretical predictions to determine the bombarding energy for which exactly one-half of the incident deuterons have penetrated the metal films. The ranges obtained agree with theoretical estimates and are consistent with known ranges of protons in aluminum.

DEFECTS IN METAL ALLOYS

The critical temperature for the order-disorder transition of FeNi was studied[43] by measuring the decrease in electrical resistivity during neutron irradiation at continually decreasing temperatures. The temperature determined was $321 \pm 2°C$. The studies of the kinetics of the establishment of the short range seem to indicate the predominance of vacancy-interstitial recombination.

A uniaxial magnetic anisotropy is induced by neutron bombardment with an applied magnetic field in FeNi samples.[44,45] This anisotropy is caused by a new order-disorder transition. After irradiation at 30°C, the annealing of the defects is studied by means of the magnetic anisotropy increase. In most cases the law $\Delta E = a \log (bt + 1)$ is verified very well. This law can be explained by a second-order reaction for the annealing of the defects. Interstitials do not seem to contribute to the ordering process.

DEFECTS IN OTHER MATERIALS

Schweitzer[46–49] has presented a number of reports extending studies of the details of irradiation-produced defects in graphite. Annealing studies indicate the contribution due to interstitials and diinterstitials. Two other reports give details of reirradiation effects and the decomposition of defects.

The energy release of irradiated graphite was measured in a calorimeter[50] heated linearly with time between 50 and 450°C. Over the total recovery region, a constant value, $U = 1.8 \pm 0.1$ ev, was obtained (U is activation enthalpy). An examination of the source of energy release in relation to time showed that the model of the elementary processes with a reaction equation of first or second order and a diffusion-limited reaction rate under consideration could not be applicable. This condition, in addition to the fine structure of the recovery curve and results of other investigators, shows that the energy release in the observed recovery region is correlated with a complex defect mechanism.

These recent electron-microscopic studies of charged-particle tracks in various materials have been reported: Bowden and Caspar[51] discuss the damage resulting from collimated fission fragments; Chadderton[52] points out the diffraction contrast effects of particle tracks in crystals; Oak Ridge[53] reports successful attempts to observe fission tracks in single-crystal UO_2; Argonne[54] discusses the various aspects of their work concerning damage in foils and crystalline material; and Fleischer, Price, Walker, and Hubbard[55] report the type of track registration in various solid-state nuclear detectors.

Fast-neutron irradiation of samples of cuprous oxide results in modifications to the exciton spectrum similar to those produced by an electric field applied to the crystal.[56] The irradiation probably produces charged defects, which produce an internal electric field. The evaluation of this field allows determination of the concentration of defects produced by the irradiation. (T. G. Knorr)

Theories of Radiation Effects

The Chalk River[57] studies of the channeling of heavy ions in single-crystal material have now been extended to include body-centered cubic (bcc) tungsten single crystals. Erginsoy[58] points out that these results cannot be explained by the elastic model of channeling.

An approximate solution of the integral equation of cascade theory has been obtained[59] by the introduction of an equivalent collision distribution, for conditions in which the original collision distribution does not permit an exact solution. The method is applied to the $1/T$-collision distribution, and the influence of collision chains on the defect concentration estimated for [1 1 0] chains in copper. This calculation shows a reduction in the defect concentration of about 7%. The effect of a change in the atomic interaction potential on this correction is discussed.

A theoretical study has been presented[60] of damage effects of particle radiation in matter, and their dependence on energy, mass, and charge number of an incoming particle, as well as on the composition of the medium. Typical examples of damage effects are the number of ion pairs formed in a gas or the number of vacancies created in a crystal. The authors are particularly concerned with the consequences

of the competition between energy transfer to atomic electrons and to translatory motion of an atom as a whole. For these purposes, common integral equations are formulated and studied. The average effects resulting from an atomic particle with given energy, their average fluctuation, and probability distribution are studied. An important example is the division of the total energy dissipation, E, into energy given to recoiling atoms, ν, and energy given to electrons, $E-\nu$. Several radiation effects are accounted for from knowledge of E and ν. Comprehensive estimates of cross sections are used, and these estimates were derived elsewhere in a Thomas-Fermi treatment. Various simple approximations are introduced; analytical and numerical estimates are made of solutions to the integral equations. Only few experiments can at present be compared quantitatively with theory.

Mukherjee[61] points out an empirically determined relation between the energy of formation of monovacancies in face-centered cubic (fcc) metals and the ratio of their melting points to their atomic volume. The relation is linear for published values of the formation energy for lead, aluminum, gold, copper, and platinum, whereas silver is off the line. He uses his relation to predict formation energies of monovacancies in: iridium, 1.65 ev; nickel, 1.43 ev; thorium, 0.82 ev; calcium, 0.57 ev; and strontium, 0.52 ev.

The most recent Brookhaven[62] machine calculations concerning the dynamics of radiation damage in bcc lattices have now been published. Corciovei[63] has added additional comments to his studies of the distribution of irradiation-produced vacancies in solids. Frere[64] has published the fourth paper in his series concerning the theory of focusing chains. This paper considers the time dependence of the thermal distribution around a damage spike. (T. G. Knorr)

Surveys on Radiation-Induced Defects

Walker[65] has presented a discussion of the irradiation effects in metals. He points out that, as the energy of the incident particle increases, simple threshold theory is no longer able to explain the observed changes. In addition, these simple theories do not consider structure effects. Walker attempts to show the importance of such lattice effects both analytically and numerically. (T. G. Knorr)

Effect of Irradiation on Mechanical Properties

Harwell personnel have completed an investigation[66] on the effect of neutron dose rate and irradiation temperature on the radiation hardening of mild steels. Specimens were irradiated in the PLUTO heavy-water-moderated reactor at temperatures of 100, 150, 200, 250, 300, and 350°C. All specimens were subjected to the same total exposure. Three different fluxes were used, the relative neutron dose rates being approximately 1:4:100. Control samples were heat-treated for times comparable to the irradiation times and at the same temperatures. Tensile tests were made on the irradiated specimens. Results indicate that radiation-induced increases in tensile yield and ultimate strengths are functions of the irradiation temperature and the type of steel, but are not significantly dependent on the neutron dose rate. It was concluded that irradiation hardening of mild steels may be influenced by certain previously unrecognized metallurgical factors.

The effects of fast neutrons on the mechanical properties of stabilized austenitic stainless steels at elevated temperatures have been of considerable interest. Investigators have reported greater losses in ductility resulting from elevated-temperature irradiations than from irradiations at ambient reactor temperatures. Harwell[67] researchers have studied the effects of neutron irradiation at ~80°C on the room- and elevated-temperature tensile properties of iron–20 wt.% chromium–20 wt.% nickel, a stabilized austenitic stainless steel. Two steels of this nominal composition, stabilized with niobium and titanium, respectively, in the water-quenched and in the furnace-cooled condition, were irradiated in a hollow fuel element of the BEPO reactor. The neutron flux was not monitored, but the dosages were estimated to be 3.0×10^{18}, 9.0×10^{18}, and 1.8×10^{19} thermal neutrons/cm^2, and the ratio of thermal to fission neutron flux in these positions was estimated to be about 3 to 1. Irradiation increased the yield strength and reduced the elongation to fracture in the room-temperature and 200°C tests. No significant changes were noted at the 400°C test temperature. Marked reductions in ductility were noted upon testing at 750 and 850°C. This irradiation-induced embrittlement at 750°C was partially removed in niobium-stabilized steel by a postirradiation anneal for

15 min at 1000°C, followed by a 10-hr soak at 900°C. The same treatment on the irradiated, titanium-stabilized steel resulted in a further decrease in total elongation. The authors indicate that the factors responsible for the radiation-induced reductions in tensile ductility at 750 and 850°C are not known. They do, however, discount the fact that helium formed from the $^{10}B(n,\alpha)^{7}Li$ reaction could be directly responsible for the reduction noted.

In other studies at Harwell,[68] a representative selection of iron–20 wt.% chromium–25 wt.% nickel, niobium-stabilized steel tensile specimens from three separate Culcheth irradiation experiments were examined by Harwell workers using thin-film transmission electron microscopy. These specimens had been subjected to irradiation doses of up to 1.65×10^{20} neutrons/cm^2 (>1 Mev) and 5.7×10^{20} neutrons/cm^2 (thermal) at temperatures between 450 and 750°C. Tensile tests were made in the temperature range 650 to 800°C. Reduced ductility was apparent, and intergranular fracture had been the predominant mode of failure at the 750°C test temperature. These materials contained 0.0003 to 0.0005 wt.% boron and other impurities. On the basis of examinations of a number of thin films, it was concluded that neutron irradiation enhances the formation of a fine precipitate within the grains. No differences could be seen between the grain boundaries of the irradiated and control samples. It was suggested that the lower tensile ductility of the irradiated samples is a direct result of the enhanced precipitation within the grains.

A comparison[19] of the results of tensile tests on stainless steels (AISI 348, AISI 304, AISI 410, and AM-350SS) irradiated at approximately 50°C with data for similar specimens irradiated at 280°C indicates that the damage caused at the higher temperature is equal to or greater than that at 50°C.

Tensile properties are reported by Hanford[69] for Zircaloy-2, both before and after fast-neutron irradiation at about 60°C to about 10^{19}, 10^{20}, and 10^{21} neutrons/cm^2. The strength of specimens from the transverse and the rolling directions of cold-worked, annealed sheet increased greatly during irradiation. Transverse specimens exhibited a yield point and necking at plastic strains of less than 5% after exposures of 10^{19} neutrons/cm^2. The fracture mechanism appears to be the same for irradiated and unirradiated Zircaloy-2; however, neutron irradiation greatly reduces the total fracture energy. Work at Hanford[19] is being concluded on the in-reactor creep properties of Zircaloy-2.

The Canadians[70] have continued to study the effects of irradiation on the mechanical properties of a zirconium–2.5 wt.% niobium alloy. This alloy was irradiated at 250°C to about 10^{20} neutrons/cm^2 in both the quenched-and-tempered conditions. Relatively small changes in strength and ductility were noted following the irradiation. The alloy was, in fact, significantly better than Zircaloy-2. The quenched-and-tempered material was metallurgically stable after irradiation. The results of a more recent irradiation study on the effect of hydrogen concentration on the room temperature and 300°C tensile properties of this alloy after irradiation are shown in Table IV-1.

The irradiation of tandem-extruded tubular joints between Zircaloy-2 and stainless steel was carried out by Savannah River[71] researchers. These joints were irradiated to exposures

Table IV-1 THE EFFECT OF NEUTRON IRRADIATION* ON THE TENSILE PROPERTIES OF HYDRIDED ZIRCONIUM–2.5 WT.% NIOBIUM[70]

Test temp., °C	Hydrogen, ppm	Proportional limit, kg/cm^2	Yield strength (0.2% offset), kg/cm^2	Ultimate tensile strength, kg/cm^2	Elongation, %	Reduction of area, %
RT	0	10,500	11,300	11,600	7.5	44
RT	13	10,300	11,200	11,500	7.2	43
RT	100	9,800	11,100	11,200	5.3	30
RT	250	10,600	11,500	11,600	2.5	10
300	0	7,200	8,000	8,300	9.5	65
300	13	7,700	8,400	8,500	8.7	66
300	100	7,700	8,200	8,400	7.5	53
300	250	7,700	8,200	8,400	5.5	33

*Irradiated at 290°C to a total flux of 10^{21} neutrons/cm^2 (E > 500 ev).

between 6.0×10^{20} and 7.8×10^{20} neutrons/cm^2 (>0.1 Mev) at about 50°C. The dimensional changes occurring during irradiation were small, but some were permanent. Strengths were unchanged by irradiation, and plastic deformation or failure during testing occurred in the Zircaloy-2 segment rather than in the interface region. These results indicate that tubular joints between Zircaloy-2 and stainless steel prepared in this manner are suitable as low-temperature components of pressure tubes in power reactors.

Hanford[19] engineers have initiated a surveillance program on the Zircaloy-2 tubing which is being used in the New Production Reactor. A comparison of tensile properties after exposure to 6.7×10^{19} neutrons/cm^2 at 280°C and after exposure to the environment of the out-of-reactor section of the same loop was made. They found that exposure to the out-of-reactor loop did not alter the properties of Zircaloy-2 appreciably from the as-fabricated properties. However, neutron irradiation increased the yield strength about 40% and the tensile strength about 13%, reduced the uniform and necking strain by about a factor of 2 and decreased the reduction in area values 3 to 5%. Other room-temperature tensile tests were made on annealed, 20 and 40% cold-worked material after irradiation at about 280°C to neutron exposures in the range 1.9×10^{20} to 2.0×10^{21} neutrons/cm^2. Although there were isolated exceptions, the specimens with the greater amounts of cold work showed the highest yield and ultimate strengths and the greatest elongations, reductions in area, and plastic work.

A number of nickel and nickel-base alloy tensile specimens were irradiated by Hanford[19] in the Engineering Test Reactor at a temperature of 280°C. Neutron exposures were in the range of 4.5×10^{19} to 5.4×10^{20} neutrons/cm^2 ($E > 1$ Mev). The materials under study included Inconel 625, Inconel 718, Hastelloy X, Hastelloy N (INOR-8), Hastelloy R-235, and TD nickel. The room-temperature tensile properties after irradiation are given in Figs. IV-2 to IV-6 for all materials except TD nickel. A preliminary test on TD nickel showed an increase in yield strength from about 85,000 to 140,000 psi and a decrease in total elongation from about 10 to 1.5%. Oak Ridge workers[72] are planning to extend the Hanford studies on Hastelloy N (INOR-8) to higher temperatures (1100 to 1400°F) and higher doses (7×10^{20} neutrons/cm^2).

Hanford[73–75] reports corrosion (about a 0.05-in. decrease on a 0.125-in. diameter) in 8 of 12 refractory metals irradiated in water at 50°C. The materials that corroded were TZM (molybdenum–0.5 wt.% titanium–0.08 wt.% zirconium), molybdenum, and a tungsten–25 wt.% rhenium alloy, whereas niobium and tantalum alloys showed no signs of corrosion. They also report[5] increases in yield strength and marked decreases in elongation of a niobium–1 wt.% zirconium alloy and the niobium alloy Cb-752, after irradiations to about 9.0×10^{19}, 1×10^{20}, and 1.5×10^{20} neutrons/cm^2. These results are shown in Fig. IV-7.

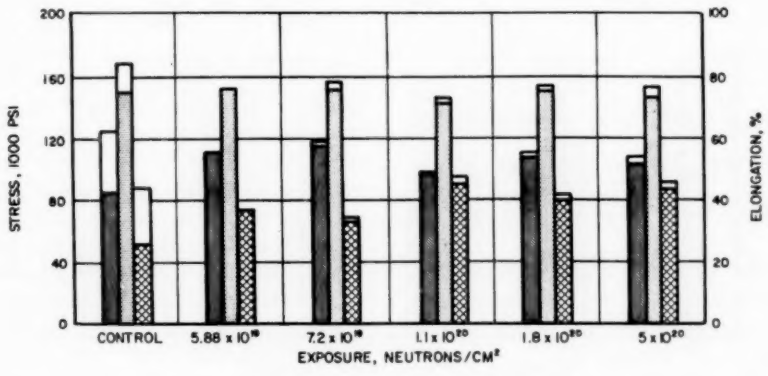

Fig. IV-2 Effects of neutron irradiation upon the room-temperature tensile and uniform elongation properties of Inconel 625 irradiated in 280°C water in the solution-treated condition.[19] ▨, 0.2% yield strength; ▭, ultimate tensile strength; ▩, % elongation.

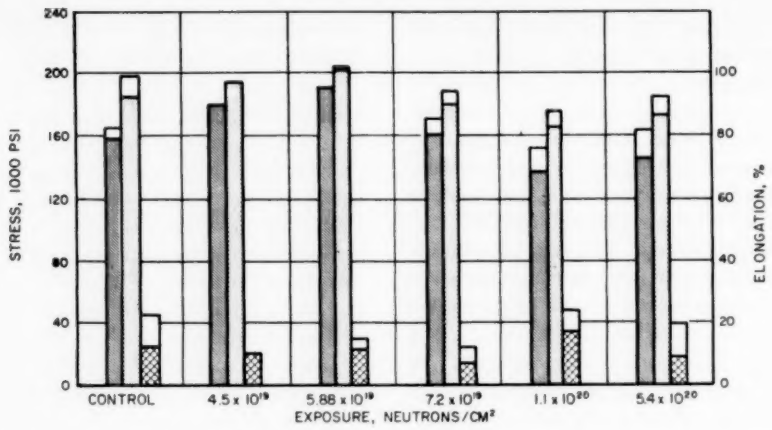

Fig. IV-3 Effects of irradiation upon the room-temperature tensile and uniform elongation properties of Inconel 718 irradiated in 280°C water in the solution-treated condition.[19] ▨, 0.2% yield strength; ▭, ultimate tensile strength; ▩, % elongation.

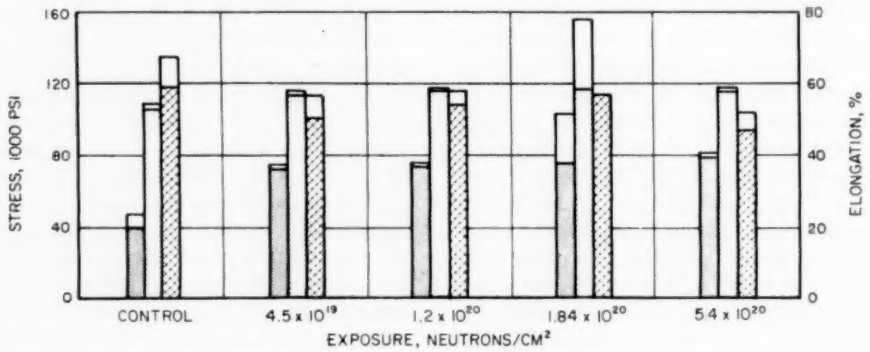

Fig. IV-4 Effects of irradiation upon the room-temperature tensile and elongation properties of Hastelloy N irradiated in 280°C water.[19] ▨, 0.2% yield strength; ▭, ultimate tensile strength; ▩, % elongation.

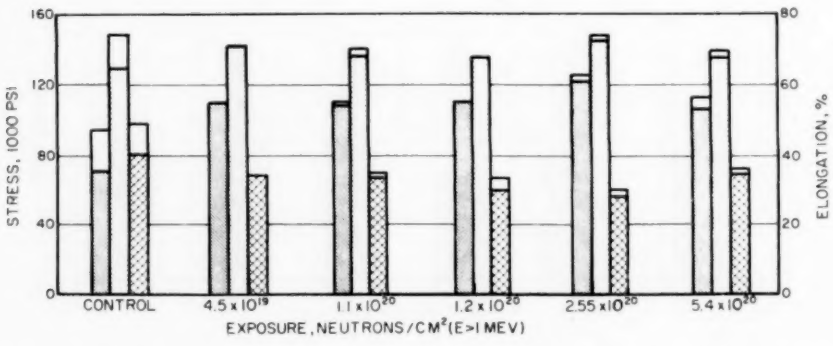

Fig. IV-5 Effects of neutron irradiation upon the room-temperature tensile and elongation properties of Hastelloy R-235 irradiated in 280°C water in the heat-treated condition.[19] ▨, 0.2% yield strength; ▭, ultimate tensile strength; ▩, % elongation.

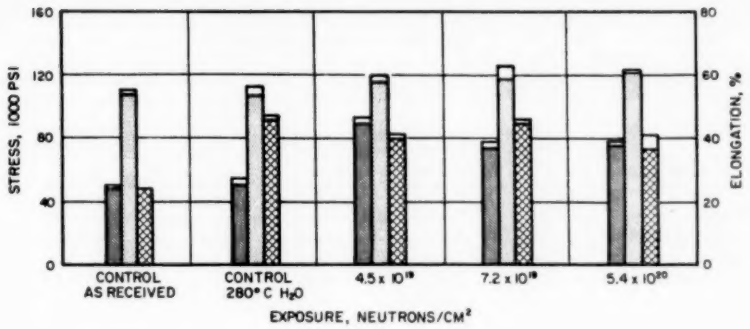

Fig. IV-6 Effects of irradiation upon the room-temperature tensile and elongation properties of Hastelloy X irradiated in 280°C water.[19] ▨, 0.2% yield strength; ▭, ultimate tensile strength; ▩, % elongation.

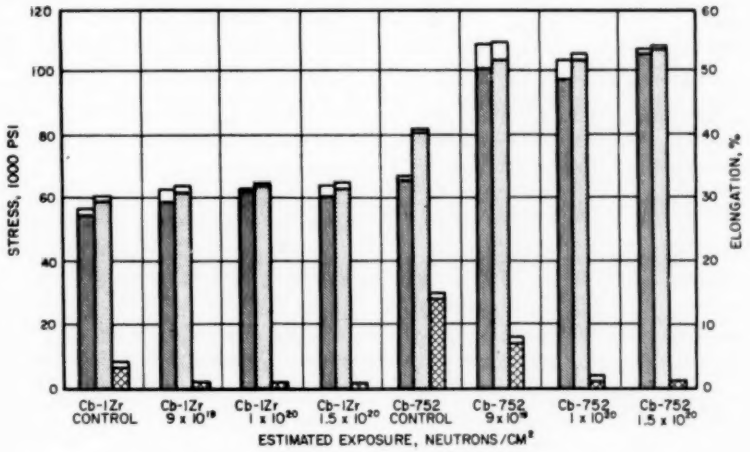

Fig. IV-7 Effects of irradiation upon room-temperature tensile properties of niobium–1 wt.% zirconium and Cb-752 irradiated at 120°F (50°C).[19] ▨, 0.2% yield strength; ▭, ultimate tensile strength; ▩, % elongation.

Workers at General Electric[76] have summarized the experimental results for 1963 from their radiation-effects program on refractory metals and alloys. The materials include tungsten, tungsten–25 wt.% rhenium, molybdenum, and TZM. The tests have included short-time tensile, creep-to-rupture, hardness, and resistivity measurements. Test temperatures have been in the 1000 to 1400°C range. The rupture times and creep rates were not altered appreciably by irradiation. Typical results from stress-to-rupture tests are summarized in Tables IV-2 to IV-4.

(F. R. Shober)

Selected Mechanical Properties of Cladding and Structural Materials

Union Carbide workers in Brussels[77] used a flash-annealing technique whereby the yield stress, σ_Y, at a strain rate, $\dot{\epsilon}$, of 1%/min can be lowered to ~3.5 kg/mm^2 to investigate the effects of strain rate on flash-annealed niobium. They found that the results can be fitted on to three linear ranges, each of the form of the equation $\sigma_Y = A + A' \log \dot{\epsilon}$. For $\dot{\epsilon} < 2$%/min, no

Table IV-2 SUMMARY OF CREEP-RUPTURE TESTS ON TUNGSTEN SPECIMENS, ROD X MATERIAL[76]

Specimen	Composition	Temp., °C	Stress, kg/mm²	Rupture life, hr	Linear creep rate, sec^{-1}	Elongation in 2.54 cm, %	Reduction in area, %
89	Control	1400	12.30	4.15		25.2	65.5
92	Irradiated ORM-4*	1400	12.30	3.95		26.4	54.5
95	Control	1400	13.01	2.60		23.0	63.6
90	Irradiated ORM-4	1400	13.01	2.55		24.2	64.7
96	Control	1400	13.36	1.90		28.3	87.7
85	Control	1200	16.87	5.00	1.1×10^{-5}	29.0	96.6
88	Control	1200	16.87	2.10	1.9×10^{-5}	26.9	96.4
91	Irradiated ORM-4	1200	16.87	2.10	2.3×10^{-5}	32.0	95.2
53	Irradiated ORM-5†	1200	17.58	2.3	2.1×10^{-5}	28.0	94.8
84	Control	1100	19.34	5.85	7.0×10^{-6}	30.8	97.0
93	Irradiated ORM-4	1100	19.34	6.74	6.3×10^{-6}	31.5	95.7
52	Irradiated ORM-5	1100	19.34	5.65	7.7×10^{-6}	31.2	97.8
54	Irradiated ORM-8‡	1100	19.34	10.2	4.2×10^{-6}	30.3	96.3
86	Control	1100	20.35	1.25	3.5×10^{-5}	33.7	97.8
50	Irradiated ORM-5	1100	20.35	1.19	3.7×10^{-5}	32.9	97.7
55	Irradiated ORM-8	1100	20.35	2.83	2.0×10^{-5}	32.1	97.1
83	Control	1100	20.74	0.55	7.6×10^{-5}	36.2	98.0
82	Control	1100	21.66	0.15	22.8×10^{-5}	38.5	97.8

*ORM-4 irradiated at 5.8×10^{17} neutrons/cm² ($E_n \geq 1$ Mev).
†ORM-5 irradiated at 3.7×10^{18} neutrons/cm² ($E_n \geq 1$ Mev).
‡ORM-8 irradiated at 2.5×10^{19} neutrons/cm² ($E_n \geq 1$ Mev).

Table IV-3 SUMMARY OF CREEP-RUPTURE TESTS ON MOLYBDENUM[76]

Specimen	Condition	Test temp., °C	Stress, kg/mm²	Rupture life, hr	Linear creep rate, sec^{-1}	Elongation in 2.54 cm, %
588	Control*	870	14.77	6.63	1.25×10^{-5}	60.6
589	Control*	870	15.47	3.55	2.20×10^{-5}	53.1
590	Control*	870	16.52	1.35	5.09×10^{-5}	49.2
585	ORM-13†	870	15.47	3.38	2.55×10^{-5}	55.5
586	ORM-13†	870	14.77	4.84	1.70×10^{-5}	57.5
891	Control*	980	11.25	2.49	3.13×10^{-5}	69.3
892	Control*	980	10.55	4.53	1.73×10^{-5}	69.7
893	Control*	980	9.84	8.18	0.9×10^{-5}	66.2
903	Control‡	980	11.25	1.88	4.33×10^{-5}	62.7
904	Control‡	980	10.55	3.02	2.40×10^{-5}	58.9
905	Control‡	980	9.84	5.90	1.28×10^{-5}	65.6
591	Control*	980	10.55	4.26	1.80×10^{-5}	65.9
584	ORM-13§	980				
587	ORM-13§	980	10.55	4.85	1.72×10^{-5}	77.2
854	Control*	1093	7.73	3.07	2.73×10^{-5}	79.3
855	Control*	1093	7.03	6.92	1.10×10^{-5}	78.6

*Arc-cast molybdenum sheet, 0.5 mm thick, recrystallized by vendor; tested as received.
†ORM-13 irradiated at 6.9×10^{18} neutrons/cm² ($E_n \geq 1$ Mev).
‡As-received sheet annealed at 1200°C for 1 hr in hydrogen.
§Invalid test, failed at pinhole.

Table IV-4 SUMMARY OF CREEP-RUPTURE TESTS ON TUNGSTEN–25 WT.% RHENIUM SPECIMENS* AT 1100°C[76]

Specimen	Ingot	Condition	Stress, kg/mm²	Rupture life, hr	Linear creep rate, sec^{-1}	Elongation in 2.54 cm, %
561	5	Control	41.5†		2.1×10^{-6}	
561	5	Control	43.6†		4.8×10^{-6}	(44.0)
563	5	Control	45.7	9.08	7.4×10^{-6}	54.9
569	5	Control	45.7	8.40	7.4×10^{-6}	52.1
566	5	ORM-13‡	45.7	9.08	6.6×10^{-6}	41.0
568	5	ORM-13‡	45.7	10.11	6.5×10^{-6}	55.1
575	1	Control	45.7	7.60	6.5×10^{-6}	33.7
573	1	ORM-13‡	45.7	7.84	5.7×10^{-6}	48.8
565	5	Control	47.5	6.92	9.8×10^{-6}	53.5
560	5	ORM-13‡	47.5	6.73	9.7×10^{-6}	30.7
564	5	Control	49.2	3.99	1.8×10^{-5}	54.4
562	5	ORM-13‡	49.2	3.98	1.5×10^{-5}	39.9
574	1	Control	49.2	3.84	1.6×10^{-5}	41.1
581	1	ORM-13‡	49.2	4.56	1.2×10^{-5}	39.1

*Specimens 0.051-cm (0.020 in.) sheet; powder batch RWS-9; recrystallized.
†Test restarted after 6 hr at lower stress levels.
‡ORM-13 irradiated at 6.9×10^{18} neutrons/cm² ($E_n \geq 1$ Mev).

yield points were observed and the yield stress was taken to be that at the apparent proportional limit. For $2 \leq \dot{\epsilon} \leq 100\%$/min, some specimens exhibited yield points and some did not. For $\dot{\epsilon} > 100\%$/min, there was always a yield drop and the ultimate strength was lower than the upper yield stress. If all the results for two of the ranges are taken together, there is some evidence for a previously proposed third range. It appears that impurities can control the deformation mechanism in niobium.

Minor (1 to 2 wt.%) additions of the reactive metals zirconium or hafnium to tantalum-tungsten-molybdenum alloys effect pronounced strengthening at 1925°C with minimal degradation of low-temperature alloy behavior, according to researchers at Battelle.[78] Additions of carbon to alloys containing reactive metals degrade both 1925°C strength and low-temperature behavior; however, dispersing ZrC in the alloys results in pronounced strengthening at lower temperatures (1480°C). Solution-process anneals for alloys containing ZrC dispersions greatly increase strength at 1480°C, but are detrimental to the fabricability and ductility. Molybdenum as an alloying addition to tantalum is less effective as a strengthener than tungsten. Tungsten additions provide higher stress-rupture strengths with less degrading effects on low-temperature ductility than do equivalent atomic percentages of molybdenum. Welding increases the ductile-to-brittle transition temperature of tantalum-tungsten-molybdenum alloys by 300 to 500°C. Rhenium and ruthenium additions showed little or no superiority to tungsten as solid-solution strengtheners, when both high- and low-temperature effects were considered.

Creep tests for 100 hr at temperatures between 950 and 1250°C were carried out by English investigators[79] on strip specimens of molybdenum–0.49 wt.% titanium, molybdenum–0.98 wt.% titanium and molybdenum–1.5 wt.% zirconium in both dispersion-hardened and recrystallized conditions. Nitrided specimens exhibited longer creep lives and lower creep rates for the same stress and temperature, compared with the nonnitrided molybdenum-titanium specimens, although the molybdenum-zirconium alloy exhibited no steady-state creep. The activation energy and stress dependence of the creep rate were evaluated for the nitrided 0.49 wt.% titanium alloy, and a metallographic and fractographic study was made of the tested specimens. The authors discussed the results in terms of current theories of creep in dispersion-hardened alloys.

Vanadium-niobium alloys that had been dispersion strengthened by additions of titanium, zirconium, or hafnium in combination with carbon were prepared by arc melting at the Illinois Institute of Technology.[80] Compositions containing 1 wt.% hafnium with small carbon additions were shown to be more difficult to fabricate and to have higher recrystallization temperatures than similar alloys containing zirconium

in place of the hafnium. Short-time creep tests were conducted in 2000°F air on siliconized vanadium–60 wt.% niobium base specimens. At stress levels of 8500 to 8850 psi, elongations of 0.5 to 1.2% were measured after $2\frac{1}{2}$ hr. Some of the specimens retained their room-temperature tensile strength and ductility after the 2000°F creep tests. Initial data indicate that a vanadium–60 wt.% niobium alloy containing 1 wt.% titanium with residual melting-stock impurities is more creep resistant at 2000°F than the alloys containing 1 wt.% zirconium with 0.1 or 0.2 wt.% carbon. (J. A. DeMastry)

Selected Metallurgical Aspects of Cladding and Structural Materials

Nickel

Russian investigators[81] have studied the structural transformations in nickel-chromium-niobium alloys with a niobium content above its solubility limit in four nickel-base solid-solution alloys containing 9.53 to 10.5 wt.% chromium; 4.82, 7.85, 10.80, and 12.54 wt.% niobium; and 0.018 to 0.23 wt.% carbon. Criteria used for structural changes included electrical resistivity, hot hardness, microstructure, and lattice parameter. Two distinct processes were found to occur; first, formation of the *K* state (in the 400 to 800°C range) and, second, the precipitation of the Ni_3Nb phase from the solid solution (in the 700 to 1000°C range). When the alloys containing 5 to 11 wt.% niobium are heated above 625°C, the *K* state is decomposed and normal aging begins. The kinetic behavior of the aging process was studied in a 13 wt.% niobium alloy. It was found that on aging at increasing temperatures in the range 850 to 1000°C, the Ni_3Nb precipitate is first seen as dispersed particles at grain-boundary regions at the lower temperatures, and then as an acicular phase throughout the matrix (probably on the {1 1 1} planes) at the higher temperatures.

Refractory Metals

Polythermal sections of the ternary systems niobium-tungsten-zirconium and niobium-molybdenum-zirconium with ratios of tungsten : zirconium = 4 : 1, 1 : 1, 1 : 3 and molybdenum : zirconium = 2.1 : 1, 1 : 1, and 1 : 3 have been studied[82] by using thermal, microstructural, and X-ray techniques. Projections of these vertical sections onto the plane of the concentration triangle, as well as isothermal sections, at the temperatures of 1100, 1800, and 2000°C were constructed. The boundary of the region of the niobium-based ternary alpha solid solution was drawn according to data of microscopic analysis and microhardness.

The tungsten-rich sections of the tungsten-boron and tungsten-beryllium systems are being studied by English investigators.[83] The solid solubility of boron is approximately 0.2 at.% at the $W\text{-}W_2B$ eutectic temperature of about 2600°C. The solubility of beryllium in tungsten is approximately 5 at.% at the $W\text{-}WBe_2$ eutectic temperature of about 2100°C. This solubility decreases to about 3 at.% in the 1000 to 1300°C range. The solid solution of boron may be interstitial *and* substitutional, whereas the solid solution of beryllium is substitutional. The WBe_2 phase is a hexagonal Laves structure.

The glide systems of pure niobium crystals in tension at 1400 to 2300°C have been investigated[84] by optical goniometry and X-ray back-reflection techniques. The metal was found to glide on the {1 1 0}, {1 1 2}, and {1 2 3} planes in the ⟨1 1 1⟩ direction. Studies of X-ray asterism confirmed the glide on the {1 1 2} and {1 2 3} planes, but in some cases the asterism suggested that glide traces were composed of slip on pairs of {1 1 0} planes.

The work-hardening properties of niobium single crystals grown by electron-beam zone melting have been studied at Cambridge University[85] over a wide range of purities, orientations, temperatures, and strain rates. Three stages of hardening are observed after the onset of plastic flow. In stage I the work-hardening rate is low and increases with increasing temperature and decreasing strain rate. This stage is absent for multiple-slip orientations. In stage II the work-hardening rate is high and approximately independent of temperature above 295°K. The rate is greater for multiple-slip orientations and increases with increasing purity. Stage III is more prominent at high temperatures, and the work-hardening rate decreases continuously until fracture. Slip-line observations show that slip occurs initially on the (0 1 1) planes and that in stage II bands of secondary slip occur.

Zirconium

Deformation twinning of pure polycrystalline zirconium has been the subject of study at the University of Florida,[1] with special emphasis on the effects of specimen orientatation and temperature. The two most prominent deformation twins in zirconium, which have quite different morphological features, are the $[1\,1\,\bar{2}\,1]$ and $[1\,0\,\bar{1}\,2]$ twins, the latter being more predominant. Tensile tests performed on longitudinal and transverse specimens at room temperature and 77°K show that the mode of deformation is slip in the longitudinal specimen and twinning in the transverse specimen. At 77°K the $[1\,1\,\bar{2}\,1]$ twin occurs more frequently than at room temperature, and second-order twinning is observed in the deformed structure.

An investigation[86] was conducted at the Illinois Institute of Technology for the purpose of determining the degree of susceptibility to delayed failure of zirconium–2.5 wt.% niobium and zirconium–2.5 wt.% niobium–0.5 wt.% copper in various metallurgical conditions. With up to 500 ppm absorbed hydrogen, the binary alloy in the annealed or the annealed and worked condition does not exhibit sensitivity to static fatigue. At the same hydrogen content and in the quenched and aged condition, moderate notch sensitivity is induced, and notched specimens at room temperature show a propensity for delayed failure. The ternary alloy with the same hydrogen content did not exhibit delayed-failure susceptibility.

The stability of various oxide and carbide dispersants in zirconium is being evaluated.[87] Dispersants of ZrC, VC, alumina, lanthana, ceria, yttria, calcia, or thoria were blended with zirconium powders, compacted, and extruded. Lanthana, yttria, and thoria remained stable in the zirconium matrix up to 1600°F and did provide some strengthening, whereas the other dispersants showed evidence of particle instability.

A compilation[88] of articles on the broad base of thorough physical metallurgy of zirconium and zirconium alloys has been prepared at General Electric.

Miscellaneous

Russian investigators[89] constructed a proposed constitutional diagram of the yttrium-tin system from thermal, microstructural, and X-ray analyses of alloys containing 30, 40, 70, and 90 at.% tin. The solid solubility of tin in yttrium does not exceed 1 wt.%, and the maximum solubility of yttrium in tin is 0.3 wt.%.

Studies are being conducted at the University of California[90] on calcium and strontium at high pressures. The only solid-solid transition in calcium below 35 kbar is that between the bcc and fcc polymorphs. The homologous transition in strontium shows a hysteresis that is a function of the pressure and becomes very large above 22 kbar. The fcc strontium exhibits a large increase in electrical resistance with pressure and a negative temperature coefficient of resistance prior to the polymorphic transition. The resistance discontinuity for the fcc to bcc transformation is a sharp increase at lower pressures, which progressively decreases in magnitude and sharpness and reverses sign at the higher pressures. (N. M. Griesenauer)

Diffusion Studies

A review of papers published in 1962 on diffusion in solids has been prepared by Winslow and Osthagen[91] and is useful for those wishing to follow general developments in the area, specific phenomena, or specific material systems. Included in the discussion are 138 references. Topics reviewed include diffusion mechanisms, solutions of diffusion equations, and diffusion in ternary systems, pure metal, and alloys. Also discussed are the effects on diffusion of strain and of gradients of temperature and pressure. Some references on diffusion in nonmetals and liquids are also reviewed.

Of interest in the field of fission-product diffusion and release in fuel-element claddings is a research program[92] being conducted for USAEC-Euratom. The objective of the research is to study the rate and mechanism of migration of fission products through cladding materials and to provide data on the magnitude of the release. Included is an investigation of the release of ^{133}Xe from iron–20 wt.% chromium alloy and an iron-nickel-base alloy. In solid-fission-product investigations, diffusion coefficients have been determined at temperatures of 600 to 1200°C for a concentration of 2×10^{13} recoils/cm^2. For diffusion in iron–20 wt.% chromium alloy, diffusion coefficients and activation energies for molybdenum, ruthenium, and high-diffusion-rate components of tellurium and zirconium are about the same as that for the

diffusion of chromium in stainless steel. Cerium, barium, iodine, and the slower zirconium component give noticeably lower diffusion coefficients and activation energies.

The diffusion kinetics of aluminum-nickel, nickel-uranium, and aluminum-nickel-uranium couples were studied by Atomics International[93] for times up to 7000 hr and temperatures of 650 to 950°F. It was found that the interdiffusion rates of aluminum and nickel and of uranium and nickel follow a parabolic relation with time, and diffusion data are presented as a function of temperature. In the aluminum-nickel system, a low-aluminum phase (AlNi or $AlNi_3$) nucleated at the Al_3Ni-Al_3Ni_2 interface when the supply of additional free aluminum into the system was restricted owing to void formation or separation between intermetallics and the aluminum. The growth of the low-aluminum phase progressed at the expense of the Al_3Ni until all this phase was consumed; then consumption of the Al_3Ni_2 phase began. Further information on these systems is reviewed in the section on diffusion bonding. (A. N. Ashurst and D. C. Carmichael)

Ceramic Technology

Some parameters affecting the mechanical behavior of ceramics have been reported by Weil,[94] using MgO, Al_2O_3, and BeO as the primary examples. He reviews the effects of thermal history, atmospheric environment, strain rate, repeated mechanical loading, stress gradient, microstructure and grain size, impurities, and porosity on the strength of ceramics.

Southern Research[95] has extended their studies of the stress-strain properties of brittle materials to higher temperatures. A 6500°F radiant-heating source has been developed. Several parametric studies in uniform tension were completed, and an investigation of the volume theory of failure for brittle materials was initiated. The effects of temperature, surface finish, strain rate, and size on the tensile properties of ATJ graphite and Al_2O_3 were investigated. On the basis of data obtained, the applicability of Weibull's theory of volume effect is considered and the degree of the effect of flaw distribution in brittle materials is questioned. Experimental data obtained for 1-in.-diameter specimens of ATJ graphite indicated a value of ultimate tensile strength at that volume significantly higher than that predicted by the volume theory.

When workers at the Jet Propulsion Laboratory[96] sought engineering information for use in the design of high-temperature structures, they determined tensile, creep, thermal expansion, and modulus of elasticity data for hot-pressed zirconium carbide. Some property data were obtained at temperatures to 2600°C. Impurities, however, of 1 to 2 wt.% nitrogen and 1 to 2 wt.% free carbon caused an unevaluated influence on the specific values obtained. Above 2100°C the tensile strength of this zirconium carbide was 2000 psi or lower, and the creep elongation was 40% or greater. The thermal-expansion coefficient varied from 5.6×10^{-6}/°C (for 25 to 400°C) to 7.6×10^{-6}/°C (for 25 to 2300°C). Room-temperature modulus of elasticity values averaged 51.6×10^6 psi.

The thermal expansion, thermal diffusivity, and elasticity of zirconia bodies with additions of MgO, Al_2O_3, CeO_2, CaO, titanium, and zirconium were measured by Burdick and Hoskyns.[97]

Kukolev and Nemets[98] have prepared a review of the modern state of research on the thermal stability of refractory ceramic materials. A detailed theoretical analysis of the mechanism and conditions of the phenomenon of thermal shock in brittle materials is included, and 140 references are given. A general survey of literature on composition, crystal structure, and preparation of carbides has been reported by Frad.[99]

Anderson and Morgan[100] at Harwell have found that H_2O vapor enhances the rates of crystal agglomeration and crystal growth of MgO. As compared to the growth rate *in vacuo* at 1050°C, the rate with water vapor at pressures lower than 5 mm Hg was more than 10^3 times faster. These effects appear to be attributable to the mobility and rapidity of exchange of H_2O molecules on the surface. Since rapid crystal growth is usually detrimental to densification, this work suggests the desirability of sintering *in vacuo* rather than in air or other H_2O-containing atmospheres. To avoid crystal growth, the ceramic should be heated slowly so that desorbed H_2O will be removed at low temperatures.

Thin-walled cylinders of Gd_2O_3 with 20 to 30 wt.% Al_2O_3 have been fabricated successfully by Oak Ridge.[72] The Al_2O_3 additions were made to minimize hydrolysis and deterioration of the Gd_2O_3. To prevent distortion during sintering, the use of prereacted materials and support of the cylinders on equally shrinking dummy shapes were found necessary. When sintered at temperatures up to 1645°C, undistorted thin-walled

cylinders with bulk densities of 5.1 to 5.2 g/cm^3 were produced.

In Avco's continuing compilation[101] of thermodynamic data on refractory compounds of 31 elements, data have been presented on hafnium diboride; the carbides of beryllium, hafnium, niobium, and tungsten; magnesium nitride; the gaseous monoxides of hafnium, silicon, titanium, uranium, and zirconium; additional oxides of hafnium, rhenium, and uranium; and uranium reference and gaseous states. A summary table provides references to thermodynamic data tables given in earlier reports. (D. J. Bowers)

References

1. H. H. Klepfer (Comp.), Proceedings of the USAEC Symposium on Zirconium Alloy Development, Castlewood, Pleasanton, California, November 12–14, 1962, USAEC Report GEAP-4089, Vol. II, General Electric Company, Vallecitos Atomic Laboratory, Nov. 30, 1962.
2. K. Beg and F. Brown, Preliminary Study of Pick-Up and Release of Fluorine by Zircaloy, Canadian Report AECL-1903 (CI-221), July 1962.
3. Westinghouse Electric Corp., Bettis Atomic Power Laboratory, Pressurized Water Reactor (PWR) Project for the Period August 24, 1963 to October 23, 1963, USAEC Report WAPD-MRP-106.
4. S. Kass, J. D. Grozier, and F. L. Shubert, Effects of Silicon, Nitrogen, and Oxygen on the Corrosion and Hydrogen Absorption Performance of Zircaloy-2, USAEC Report WAPD-283, Westinghouse Electric Corp., Bettis Atomic Power Laboratory, November 1963.
5. B. Cox, The Effect of Some Alloying Additions on the Oxidation of Zirconium in Steam, British Report AERE-R-4458, September 1963.
6. B. Cox and B. R. Harder, The Effect of Dissolved Oxygen on the Oxidation of Zircaloy-2 by Steam, *J. Electrochem. Soc.*, 110(11): 1110-1113 (November 1963).
7. G. H. Jenks, Zircaloy-2 Corrosion in Aqueous Homogeneous Reactor Solutions, *Trans. Am. Nucl. Soc.*, 6(2): 367-368 (November 1963).
8. J. C. Griess, H. C. Savage, and J. L. English, Effect of Heat Flux on the Corrosion of Aluminum by Water, Part IV. Tests Relative to the Advanced Test Reactor and Correlation with Previous Results, USAEC Report ORNL-3541, Oak Ridge National Laboratory, February 1964.
9. J. E. Draley, W. E. Ruther, and S. Greenberg, Corrosion Experience with Aluminum Powder Products, USAEC Report ANL-6785, Argonne National Laboratory, November 1963.
10. W. Uhlmann, The Corrosion of Aluminum and Some Aluminum Alloys in High-Temperature Water, A Literature Survey, Swedish Report VDIT-81, November 1963.
11. Hanford Atomic Products Operation, Metallurgy Research Operations, Quarterly Progress Report, October–December 1962, USAEC Report HW-76228, Jan. 15, 1963.
12. W. S. Hazelton, C. J. Kubit, and D. R. McClintock, A Study of the Structural Changes of Corrosion Susceptibility of Irradiated 304 Stainless Steel, *Trans. Am. Nucl. Soc.*, 6(2): 388 (November 1963).
13. E. A. Lees, Analysis of Failure of Type 304 Stainless Steel Clad Swaged Powder Fuel Assembly, USAEC Report GEAP-4400, General Electric Company, Vallecitos Atomic Laboratory, Oct. 3, 1963.
14. R. F. Overman and R. P. Jackson, Utilization of Radioactive Tracers in Studying Chloride Stress-Corrosion Cracking of Stainless Steel, USAEC Report CONF-329-1, Savannah River Laboratory, Oct. 23, 1963.
15. Advanced Course on Corrosion and Water Treatment Problems in Water Cooled Power Reactors Organized by the Netherlands-Norwegian Reactor School at Institutt for Atomenergi, Kjeller, Norway, August 19–August 30, 1963, Norwegian Report KR-53.
16. E. Hesford, J. M. Williams, and G. N. Walton, A Radiotracer Study of Cs^+ and Cl^- Deposition on Steels and Zircaloy-2 in Alkaline Water Systems, British Report AERE-R-4069, February 1963.
17. F. A. Comprelli, D. F. MacMillan, and C. N. Spalaris, Materials for Superheat Fuel Sheaths. Relative Performance of Alloys in Superheated Steam Environments, USAEC Report GEAP-4351, General Electric Company, Atomic Power Equipment Department, July 1963.
18. G. W. Titus and J. S. Brunhouse, Long Term Air Corrosion of Several Nickel-Based Alloys, *Corrosion*, 19(10): 339t-344t (October 1963).
19. Hanford Atomic Products Operation, Metallurgy Research Operation. Quarterly Progress Report, October–December 1963, USAEC Report HW-79766, Jan. 15, 1964.
20. D. A. Jones and R. E. Westerman, Oxidation of a Nickel–2% ThO_2 Alloy and the Logarithmic Rate Law of Oxidation, USAEC Report HW-79350, Hanford Atomic Products Operation, October 1963
21. W. A. Gibeaut and E. S. Bartlett, Properties of Coated Refractory Metals, Report DMIC-195, Battelle Memorial Institute, Defense Metals Information Center, Jan. 10, 1964.
22. D. B. Warmuth, Design Data Study for Coated Columbium Alloys, II. Bimonthly Report No. 5, November 1, 1963 through January 1, 1964, Report TM-3866-67, Thompson Ramo Wooldridge Inc., Feb. 1, 1964.

23. J. C. Wurst and J. A. Cherry, The Evaluation of High Temperature Materials, Quarterly Progress Report, September 1–November 30, 1963, on Contract AF33(616)-7838, University of Dayton, Dec. 13, 1963.
24. R. W. Bartlett, Investigations of Mechanisms for Oxidation Protection and Failure of Intermetallic Coatings for Refractory Metals, Report ASD-TDR-63-753, Philco Aeronutronic Division, Ford Motor Company, June 1963.
25. R. W. Lockhart and R. S. Young, Sodium Mass Transfer Program, presentation at the AEC Sodium Components Development Program Information Meeting, Hollywood, California, April 15, 1964.
26. Argonne National Laboratory, Reactor Development Program Progress Report, February 1964, USAEC Report ANL-6860, Mar. 15, 1964.
27. H. I. Bowers and W. E. Ferguson, Structural Materials in LASL Liquid Sodium Systems, USAEC Report LADC-5783, Los Alamos Scientific Laboratory, Oct. 18, 1964.
28. S. J. Basham, C. M. Allen, and W. A. Glaeser, Quarterly Progress Report on Development of a Long-Life Contact Seal for a High-Speed Rotating Shaft in Liquid-Metal Dynamic Power Systems, January 1–April 1, 1964, Battelle Memorial Institute report on Contract AF 33(657)-10961, Apr. 15, 1964.
29. C. M. Scheuermann, C. A. Barrett, W. H. Lowdermilk, and L. Rosenblum, SNAP-8 Materials, *Astronaut. Aerospace Eng.*, 1(11): 40-43 (December 1963).
30. Brookhaven National Laboratory, Nuclear Engineering Department Progress Report, May 1–Aug. 31, 1963, USAEC Report BNL-823, December 1963.
31. W. C. Hayes, W. J. Anderson, P. E. Elkins, and D. L. Johnson, Materials for Sodium/Graphite Reactors, *Trans. Am. Nucl. Soc.*, 6(2): 365 (November 1963).
32. J. R. DiStefano, Corrosion of Refractory Metals by Lithium, USAEC Report ORNL-3551, Oak Ridge National Laboratory, March 1964.
33. G. F. Burdi, SNAP Technology Handbook, Vol. 1, Liquid Metals, USAEC Report NAA-SR-8617, Atomics International, Dec. 30, 1963. (Classified)
34. R. E. Wilson, Kinetics of the Molten Aluminum–Steam Reaction by the Levitation Method, USAEC Report CONF-39-105, February 1963.
35. Argonne National Laboratory, Reactor Development Program Progress Report, January 1964, USAEC Report ANL-6840, Feb. 15, 1964.
36. Argonne National Laboratory, Reactor Development Program Progress Report, December 1963, USAEC Report ANL-6810, Jan. 15, 1964.
37. Argonne National Laboratory, Chemical Engineering Division Summary Report, April–June 1963, USAEC Report ANL-6725.
38. T. K. Bierlein, H. E. Kissinger, B. Mastel, and J. J. Laidler, Damage in Molybdenum Associated with Neutron Irradiation and Subsequent Post-Irradiation Annealing, USAEC Report HW-SA-2953, Hanford Atomic Products Operation, Mar. 14, 1963.
39. E. Dworschak, K. Herschbach, and J. S. Koehler, Experiments on Stage III Annealing in the Noble Metals, *Phys. Rev.*, 133: A 293-303 (Jan. 6, 1964).
40. E. S. Mashkova and V. A. Molchanov, Value of the Effective Collision Radius in Sputtering and Ion-Electron Emission Experiments on Single Crystals, *Soviet Phys. Solid State, English Transl.*, 5(8): (February 1964).
41. A. V. Byalobzheskii, The Effect of Neutron Irradiation on the Corrosion Behavior of Aluminum in Water, *Dokl. Akad. Nauk SSSR*, 152: 899-900 (Oct. 1, 1963).
42. R. L. Hines, Ranges of 5- to 27-kev Deuterons in Aluminum, Copper, and Gold, *Phys. Rev.*, 132: 701-706 (October 15, 1963).
43. A. Marchland, J. Pauleve, and D. Dautreppe, Resistivity of the Ordered Alloy Fe-Ni (50%-50%) Under Neutron Irradiation, *Compt. Rend.*, 257: 2987-2989 (Nov. 13, 1963).
44. J. Pauleve and D. Dautreppe, Study of the Annealing of Defects in an Iron-Nickel Alloy by Post-Irradiation Determination of the Magnetic Anisotropy, *J. Phys.*, 24: 522-524 (July 1963).
45. L. Neel, J. Pauleve, R. Pauthenet, J. Laugier, and D. Dautreppe, Magnetic Properties of an Iron-Nickel Single Crystal Ordered by Neutron Bombardment, *J. Appl. Phys.*, 35: 873 (March 1964).
46. S. Aronson, D. G. Schweitzer, and R. M. Singer, Properties of Irradiated and Periodically Annealed Graphite, *Nucl. Sci. Eng.*, 17: 192-193 (October 1963).
47. D. G. Schweitzer, R. M. Singer, S. Aronson, J. Sadofsky, and D. H. Gurinsky, Decomposition of Defects by Neutrons in Reirradiated Graphite, *Nucl. Sci. Eng.*, 18: 406-408 (March 1964).
48. D. G. Schweitzer, Di-interstitial Annealing During the First Neutron Irradiation of Graphite: The Mobility of C_2, USAEC Report BNL-6558, Brookhaven National Laboratory, 1962.
49. D. G. Schweitzer, Determination of Single Interstitial Migration Energy from Stored Energy and Thermal Resistivity Changes in Irradiated Graphite, USAEC Report BNL-6809, Brookhaven National Laboratory, 1963.
50. M. Kaltenbrunner, R. Sizmann, and H. Wenzl, Reaction Kinetics Analysis of the Energy Release of Irradiated Graphite, *Nukleonik*, 5: 269-274 (October 1963).
51. F. P. Bowden and P. E. Caspar, The Damage of Crystals by Collimated Fission Fragments, *Phil. Mag.*, 8: 2091 (December 1963).

52. L. T. Chadderton, On Diffraction Contrast at Particle Tracks in Crystals, *Phil. Mag.*, 8: 2085 (December 1963).
53. Oak Ridge National Laboratory, Solid-State Division Annual Progress Report for Period Ending May 31, 1963, USAEC Report ORNL-3480, Aug. 23, 1963.
54. Argonne National Laboratory, Metallurgy Division Annual Report for 1962, USAEC Report ANL-6677.
55. R. L. Fleischer, P. B. Price, R. M. Walker, and E. L. Hubbard, Track Registration in Various Solid-State Nuclear Track Detectors, *Phys. Rev.*, 133: A 1443 (Mar. 1, 1964).
56. S. Nikitine and M. Grosmann, Effect of Defects Produced by Neutron Bombardment on the Exciton Spectrum of Cu_2O, *J. Phys.*, 24: 525-531 (July 1963).
57. B. Domeij, F. Brown, J. A. Davies, G. R. Piercy, and E. V. Kornelsen, Anomalous Penetration of Heavy Ions of kev Energies in Monocrystalline Tungsten, *Phys. Rev. Letters*, 12: 363 (Mar. 30, 1964).
58. C. Erginsoy, Anomalous Penetration of Rare Gas Atoms in Lattice Channels, *Phys. Rev. Letters*, 12: 366 (Mar. 30, 1964).
59. G. Diener, D. Heinrich, and R. Lenk, Corrections to the Cascade Theory of Defect Production, *Phys. Status Solidi*, 3: 2069-2082 (1963).
60. J. Linhard, V. Nielsen, M. Scharff, and P. V. Thomsen, Integral Equations Governing Radiation Effects (Notes on Atomic Collisions III), *Kgl. Danske Videnskab., Mat.-Fys. Medd.* (Denmark), 33(10): 42 (1963).
61. K. Mukherjee, Correlation Between the Absolute Melting Temperatures and the Activation Energy of Formation of Monovacancies in Face-Centered Cubic Metals, *Phys. Letters*, 8: 17 (Jan. 1, 1964).
62. C. Erginsoy, G. H. Vineyard, and A. Englert, Dynamics of Radiation Damage in A Body-Centered Cubic Lattice, *Phys. Rev.*, 133: A 595-606 (Jan. 20, 1964).
63. A. Corciovei and A. Babcenco, Distribution des Vacancies Produites dans un Solide par Irradiation, *Phys. Status Solidi*, 4: 587 (1964).
64. R. Frere, Theorie des Chaines de Collisions Focalisantes (IV), *Phys. Status Solidi*, 3: 2281 (1963).
65. R. M. Walker, Irradiation of Metals, *J. Phys.*, 24: 474-481 (July 1963).
66. P. J. Barton, D. R. Harries, and I. L. Mogford, Effects of Neutron Dose Rate and Irradiation Temperature on Radiation Hardening in Mild Steels, British Report AERE-R-4489, December 1963.
67. J. Fennell and A. C. Roberts, Effects of Neutron Irradiation on the Room and Elevated Temperature Tensile Properties of 20% Chromium, 20% Nitrogen: Stabilized Austenitic Steels, British Report AERE-R-4465, November 1963.
68. D. R. Arkell and P. C. L. Pfeil, Transmission Electron Microscopical Examination of Irradiated Austenitic Steel Tensile Specimens, British Report AERE-R-4405, November 1963.
69. A. L. Bement, Jr., Effects of Cold Work and Neutron Irradiation on the Tensile Properties of Zircaloy-2, USAEC Report HW-74955, Hanford Atomic Products Operation, April 1963.
70. J. H. Foley and M. Nasim (Eds.), Heavy-Water Reactors: International Newsletter No. 6, Canadian Report NP-13395, September 1963.
71. J. W. Joseph, Jr., Irradiation of Tandem-Extruded Joints Between Zircaloy and Stainless Steel, USAEC Report DP-859, E. I. du Pont de Nemours & Co., October 1963.
72. Oak Ridge National Laboratory, Molten-Salt Reactor Program Semiannual Progress Report for Period Ending July 31, 1963, USAEC Report ORNL-3529, Jan. 7, 1964.
73. F. W. Albaugh, Reactor and Fuels Laboratory Monthly Report, February 1964, USAEC Report HW-81019A, Hanford Atomic Products Operation, Mar. 13, 1964. (Classified)
74. Hanford Atomic Products Operation, Reactor and Fuels Laboratory Monthly Report, January 1964, USAEC Report HW-80560A, Feb. 19, 1964. (Classified)
75. Hanford Atomic Products Operation, Reactor and Fuels Laboratory Monthly Report, December 1963, USAEC Report HW-79999A, Jan. 15, 1964. (Classified)
76. General Electric Company, Advanced Technology Services, Third Annual Report, High-Temperature Materials and Reactor Component Development Programs, Vol. 1, Materials, USAEC Report GEMP-270A, Feb. 28, 1964.
77. A. Fourdlux and A. Wronski, The Effect of Strain Rate on the Room Temperature Yield Stress of "Flash-Annealed Niobium," *Acta Met.*, 11: 270-273 (November 1963).
78. F. F. Schmidt, E. S. Bartlett, and H. R. Ogden, Investigation of Tantalum and Its Alloys, Report ASD-TDR-62-594 (Part II), Battelle Memorial Institute, March 1963.
79. A. K. Mukherjee and J. W. Martin, The Effect of Nitriding Upon the Creep Properties of Some Molybdenum Alloys, *J. Less-Common Metals*, 5: 403-410 (October 1963).
80. F. C. Holtz, Dispersion-Strengthened Vanadium Alloys, Bimonthly Report No. 5, August 14, 1963–October 13, 1963, Report IITRI-B6007-5, Illinois Institute of Technology Research Institute, Nov. 8, 1963.
81. B. G. Livshits and V. B. Ovenskii, Study of Structural Transformations in Nickel-Chromium-Niobium Alloys, *Izv. Akad. Nauk SSSR, Otd. Tekhn. Nauk Met. i Toplivo*, No. 1: 139-146 (1962).
82. E. M. Savitskii, Investigation of the Ternary Systems Niobium-Tungsten-Zirconium and Niobium-

Molybdenum-Zirconium, Russian Report JPRS-22593 [translated from *Issled. Splavov Tsvetn. Metal., Akad. Nauk SSSR, Inst. Met.*, No. 4: 108-116 (1963)].

83. H. J. Goldschmidt, E. A. Catherall, W. M. Ham, and D. A. Oliver, Investigation into the Tungsten-Rich Regions of the Binary Systems Tungsten-Carbon, Tungsten-Boron, and Tungsten-Beryllium, Report ASD-TDR-62-25 (Part II), Birmington Small Arms, Ltd., June 1963.
84. B. Harris, Glide Systems in Niobium Single Crystals in the Range 1400 to 2300°C, *J. Inst. Metals*, 92(Part 3): 89-92 (November 1963).
85. T. E. Mitchell, R. A. Foxall, and P. B. Hirsch, Work-Hardening in Niobium Single Crystals, *Phil. Mag.*, 8(8): 1895-1920 (November 1963).
86. D. Weinstein and F. C. Holtz, Research Designed to Evaluate Zr-2.5Nb and Zr-2.5Nb-0.5Cu Alloys for Delayed Failure Hydrogen Embrittlement, Final Report, October 15, 1962–October 14, 1963, USAEC Report IITRI-B6005-11, Illinois Institute of Technology Research Institute, Nov. 14, 1963.
87. D. Weinstein and F. C. Holtz, On Dispersion Strengthening of Zirconium, USAEC Report TID-18430, Armour Research Foundation, Jan. 14, 1964.
88. H. H. Klepfer (Comp.), Proceedings of the USAEC Symposium on Zirconium Alloy Development, Castlewood, Pleasanton, California, November 12–14, 1962, USAEC Report GEAP-4089 (Vol. I), General Electric Company, Vallecitos Atomic Laboratory, Nov. 30, 1962.
89. V. F. Terekhova, I. A. Markova, and E. M. Savitskii, Constitution Diagram of Yttrium-Tin Alloys, *Zh. Neorgan. Khim.*, 8: 1991-1993 (August 1963).
90. A. Jayaraman, W. Klement, Jr., and G. C. Kennedy, Phase Diagram of Calcium and Strontium at High Pressures, *Phys. Rev.*, 132: 1620-1624 (Nov. 15, 1963).
91. F. R. Winslow and K. H. Osthagen, Diffusion Today, *J. Metals*, 15(11): 855-860 (November 1963).
92. T. S. Elleman, G. G. Cocks, J. Bugl, and A. A. Bauer, Fission-Product Release From Fuel-Element Claddings, Quarterly Progress Report October–December 1963, USAEC-Euratom Report, BMI-X-10072 (EURAEC-936), Battelle Memorial Institute, Jan. 1, 1964.
93. R. A. Harlow and O. Gamba, Diffusion Kinetics Studies in the Aluminum-Nickel-Uranium System, USAEC Report NAA-SR-8387, Atomics International, Nov. 30, 1963.
94. N. A. Weil, Parametric Effects Governing the Mechanics of Ceramic Materials, USAEC Report CONF-135-4, Cummins Engine Company, Inc., September 1963.
95. Southern Research Institute, The True Stress-Strain Properties of Brittle Materials to Very High Temperatures, Final Report, 1962–1963, USAEC Report TID-19812.
96. M. H. Leipold and T. H. Nielsen, Mechanical and Thermal Properties of Hot-Pressed Zirconium Carbide Tested to 2600 C, Report JPL-TR-32-452, California Institute of Technology, Jet Propulsion Laboratory, Sept. 15, 1963.
97. R. B. Burdick and W. R. Hoskyns, Research on the Thermal Properties of Zirconia, Report ARL-63-170, Materiadyne Division, Pfaudler Permutit, Inc., May 17, 1963.
98. G. V. Kukolev and I. I. Nemets, Modern Concepts of Thermal Stability of Refractory Ceramic Materials and Means of Increasing It, *Zh. Vses. Khim. Obshchestva im. D. I. Mendeleeva*, 8: 155-162 (1963).
99. W. A. Frad, Carbides, USAEC Report IS-722, Ames Laboratory, Iowa State University, August 1963.
100. P. J. Anderson and P. L. Morgan, The Effects of Water Vapor on Sintering of MgO, British Report AERE-R-4495, January 1964.
101. H. L. Schick, D. F. Anthrop, R. E. Dreikorn, P. L. Hanst, and M. B. Panish, Thermodynamics of Certain Refractory Compounds. Part II. Continued Theoretical and Experimental Studies on an Extended List, Report RAD-SR-63-105, Avco Corp., June 15, 1963.

Section V

Reactor Materials

Special Fabrication Techniques

Melting, Casting, and Hot and Cold Working

Investigators studying the thermodynamics of cold-mold arc melting at the Bureau of Mines[1] are now employing a segmented water-cooled copper crucible divided into upper and lower sections, as an aid for determining the heat-transfer characteristics of the systems during consumable melting. A typical summary of the data from one heat of titanium is shown in Fig. V-1. It has been noted that the heat transfer through the mold wall is distributed over a much larger area in consumable-electrode melting than in nonconsumable-electrode melting and that the amount of heat conducted along the length of the ingot changes abruptly as the arc is terminated.

High-temperature sensing devices are being investigated by National Lead Co. of Ohio[2] and Bridgeport Brass[3] for process-control applications. Tests at National Lead indicate that infrared pyrometry can be used to control their remelt furnace operations. Bridgeport Brass has met with little success in adapting any commercially available temperature-sensing instruments for use in the exit end of their extrusion presses. These two sites are also continuing their production studies of uranium fuel cores. Bridgeport Brass studies are concerned with reducing the amount of machining stock on extruded uranium tubes. Increases in yield should be obtainable, since it is feasible to reduce the machining allowance on the outside diameter from the present 0.125 to 0.050 in.

National Lead[2] has utilized an improved induction-coil assembly for vacuum induction melting. More than 350 melts have been made with no arcing between the coil turns. This higher thermal efficiency has made it possible to reduce the furnace power cycle.

Electrochemical machining as a method of boring fuel slugs is also being investigated at both of the above-mentioned sites. Tool penetration rates of up to 0.55 in./min are employed at National Lead. Tool penetration rates of 0.4 to 0.5 in./min are employed by Bridgeport Brass, and good dimensional and surface quality (which are the same for unalloyed uranium and low-additive uranium) are reported. Further studies in this area are contemplated at both sites.

As in the past, most of the reports covered during this period are concerned with the production of specific shapes from refractory alloys. The refractory-metal facility of Du Pont at Baltimore has issued three reports[4–6] concerning the preparation of shapes from niobium-base alloys. Of these reports, two deal with the extrusion of H and T sections. A complete account of the development program from the initial ingot preparation to the final extrusion is reported. Because the foil rolling program has just been initiated, the report covers only the ingot preparation of alloys D-43, B-66, and Cb-752 plus two tantalum alloys, tantalum–10 wt.% tungsten and tantalum–8 wt.% tungsten–

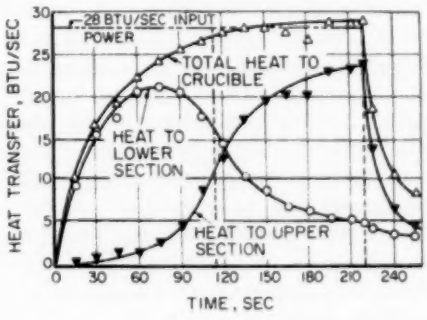

Fig. V-1 Typical heat distribution for consumable-electrode heat-sectioned crucible.[1] Run was conducted at 200 torrs furnace pressure.

2 wt.% hafnium (T-111). Of particular importance are the results of microprobe analyses of the cast structure, which revealed microsegregation in the niobium-base alloys on the order of ±25%, and the fact that high-temperature homogenization heat-treatments did not remove this segregation.

At Argonne[7] the TZM alloy is of primary interest. Reduction ratios of from 7.2:1 to 9.9:1 were employed at temperatures of 1100 to 1150°C, utilizing type 304 stainless steel for both the jacket and the core.

Nuclear Metals and General Electric are interested in tungsten and tungsten-base alloys in the form of tubing. At Nuclear Metals,[8–10] both tungsten and tungsten–25 wt.% rhenium tube blanks produced by powder metallurgical techniques are being extruded to sleeves. For the tungsten extrusions, Nuclear Metals is now employing steel fillers in place of the molybdenum formerly used, and resistance-heated furnaces in place of the induction-heating units that were used. It is believed that a more uniformly heated extrusion is obtained by resistance heating, and therefore recrystallization during heat-treatment is more uniform and can be controlled more closely. Recrystallization studies have been conducted at temperatures of 1200 to 1600°C for 1 hr. At 1200°C a small but detectable increase in both the width of the fibrous bands and the number of clearly defined grains is detected. At 1600°C the specimens appear to be fully recrystallized. Extrusion temperatures of the tungsten–25 wt.% rhenium alloy sleeves are reported as 1500, 1600, and 1800°C. There are indications that the 1500°C extrusion temperature yields the best surfaces.

The above-mentioned tungsten-rhenium alloy is being investigated at General Electric.[11] Their studies have shown that interstitial impurity content of finished sheet is low and not influenced by the composition of the starting tungsten powder or by processing variables. They have compacted and sintered several tube blanks. A piece of this tubing was found to be ductile at room temperature and free of sigma phase. (N. E. Daniel)

Cladding

Cladding by Rolling, Swaging, Coextrusion

At Hanford,[12] plutonium-containing, 19-rod-cluster fuel elements have been fabricated for the Plutonium Recycle Test Reactor (PRTR) by swage compacting loose, mixed oxide powders in Zircaloy cladding. Some elements contained physical mixtures of UO_2 and PuO_2, and others contained high-energy-rate pneumatic-mechanical-impaction-densified fuel particles in which PuO_2 is dispersed throughout UO_2. Swageable end caps eliminated machining after swaging and maintained high fuel density over the entire fuel length. (R. J. Diersing)

Pressure Bonding

A detailed study of cleaning Zircaloy components for pressure bonding has been reported by Bettis.[13] This investigation was conducted as a part of the development of the pressure-bonding method for fabricating PWR core-2 plate type fuel elements. Zircaloy-to-Zircaloy bonds were examined as a function of cleaning procedures and abrasion coolants for prior surface-conditioning compatibility. Both laboratory and shop tests were performed, leading to the selection of commercially available cleaning materials and abrasion coolants. Alkaline-emulsion cleaning was most effective for removing particulate soil, with the greater degree of scrubbing producing better bonds. For abrasion, a mineral oil with 10 to 15% of saponifiable oil was satisfactory. (S. W. Porembka)

Diffusion Bonding

An analysis has been made of diffusion bonds for the system aluminum-nickel-uranium, where the nickel is a thin intermediate layer between the aluminum cladding and the uranium core. At Atomics International[14] the specimens were bonded at 750°F and 120 psi and subsequently held at that temperature for 1000, 2000, and 4000 hr. The nickel layer was consumed almost exclusively by the aluminum-nickel interdiffusion. The products formed were identified as Al_3Ni and Al_3Ni_2. Diffusion between the nickel and uranium was at a significantly lower rate. After the nickel was consumed, the uranium-nickel and nickel-aluminum phases interacted to form a ternary phase, identified by the investigators as UNi_7Al_{13}. When the aluminum diffuses through the zones to the uranium component, the UAl_3 intermetallic is formed. The resulting zones in sequence are: $U/UAl_3/UNi_7Al_{13}/Al_3Ni_2/Al_3Ni/Al$. It was observed that there was a continuous separation between the Al_3Ni and the aluminum, and it was postulated

that the separation resulted from differences in thermal contraction upon cooling. A complementary study of the diffusion kinetics of the aluminum-nickel-uranium system is reviewed in Sec. IV under Diffusion Studies. In a study at Pyromet[15] of the self-bonding of uranium, it has been reported that a layer of gold at the bond interface has promising characteristics as an aid to diffusion bonding.

Two very useful reviews on diffusion bonding have been issued which should be of considerable interest to those working in this field. An annotated bibliography of 89 selected references has been issued by Lockheed.[16] References from 1940 to 1962 on the subjects of hot-pressure bonding (welding) and diffusion bonding are covered, and a subject index is provided. Also, an excellent literature survey has been reported by Solar[17] on diffusion bonding, especially of refractory metals, and related subjects. Extended abstracts are included, and the literature is summarized and analyzed in some subject areas. In addition to these two reviews, a brief, generalized review[18] of diffusion-bonding principles and techniques has been published.

(D. C. Carmichael)

Canning

Efforts at Combusion Engineering[19] have been directed toward obtaining better process control and reproducibility, and increased compact density for 4- to 6-ft-long vibration-compacted rods. Several process parameters were studied. Calibration of pneumatic vibrators with respect to g levels and frequencies improved control and reproducibility. The optimum three particle-size group for pneumatic compaction consists of 60 wt.% of −6 +16 mesh, 15 wt.% of −30 +100 mesh, and 25 wt.% of −200 mesh. The coarse powder component of the UO_2 breaks down at an appreciable rate during pneumatic vibratory compacting; therefore the initial powder distribution is altered significantly. Regardless of the initial distribution used, the final distribution tended to be the same for densities of 90% of theoretical or higher.

Powder segregation and low-density regions within 1 to 2 in. of the bottom end cap of the fuel rods were reduced to acceptable levels by incorporating controlled predensification techniques. High vibrator-power settings were used during predensification to reduce the time necessary to achieve densities in excess of 89% of theoretical during subsequent compaction. Higher fuel-rod densities were obtained during final compaction by increasing table loadings and accelerations.

More recently at Combustion Engineering,[20] a 37-tube projection-welded cluster was compacted to an average density of 84.8% of theoretical.

A purely mathematical approach to predict achievable vibratory-packing densities of spherical shapes is reported by Argonne.[21] Equations are given whereby the packing efficiency of any multicomponent system of spheres can be calculated as a function of the ratio of diameter of container to first component, first component to second, second to third, etc. The limiting packing fraction for a ternary system is 0.951, with the average difference between the calculated fraction and that achieved by experiment being 0.014.

Recent design changes in a NAVCO BH-3 pneumatic device at Oak Ridge[22] produced an acceleration in excess of 30,000 g, which is required to achieve uniform density in 10-ft-long fuel rods.

A British patent[23] describes the process for the manufacture of fuel elements in which a fuel rod is enclosed in a tubular can that is closed at each end. The can has a coefficient of thermal expansion which is greater than that of the fuel rod. The process includes heating the can and subsequently bringing it into intimate contact with the fuel rod by the application of an enveloping pressure. While being heated, the can is mounted in a clamp that applies end restraint.

(V. D. Linse)

Nonelectrolytic Chemical-Plating Techniques

Deposition of nickel from the carbonyl[24] and that of tungsten by hydrogen reduction of WF_6 (Ref. 25*a*) still attract interest for various applications. Thermal decomposition of mixed nickel and iron carbonyls was used in alloy deposition studies.[26] Homogeneous alloys were obtained for use in low-temperature phase-equilibria investigations. Vapor-formed shapes of tungsten were prepared on stainless-steel or copper mandrels by hydrogen reduction of WF_6 (Ref. 27*a*). Deposition conditions included a temperature of 600°C, a pressure of 10 torrs, and a H_2:WF_6 ratio of 140:1. Metal-recovery efficiency was 95%. Tungsten tubes of various lengths were formed in a size range of 0.040 in. in inside diameter by 0.001 in. in wall

thickness to 0.750 in. in inside diameter by 0.040 in. in wall thickness. Tungsten shapes, spheres, and wires and cloth made from refractory fibers are being joined by chemical vapor deposition (Refs. 27*b*, 27*c*, 28, and 29). Although fine-grained deposits can be secured, further development will be required to obtain better mechanical properties.

High-purity boron can be prepared from boron triiodide[30] and from mixed boron hydride and halide vapors.[31] Fluidized-bed techniques were used to prepare UO_2 from UF_6, steam, and hydrogen.[32] Uranium dioxide particles, in a size range of −16 to +140 mesh, with a density of 9.5 to 9.75 g/cm^3, were prepared.

Refractory fibers of Al_2O_3 (Ref. 33), BeO (Ref. 34), boron, B_4C, and TiC (Ref. 35) can be formed by chemical vapor deposition. Such fibers are especially useful in current development of strong composite materials for use under conditions of high-temperature oxidation.

In the area of overlay and diffusion coatings, the following developments and applications are described. Vapor-deposited tungsten coatings on UC thermionic cathodes were subjected to diffusion-emission tests.[36] To secure deposits of refractory metals on temperature-sensitive substrates, new metal-organic compounds are being investigated as source materials.[37,38] The metals involved are molybdenum, tungsten, niobium, tantalum, titanium, hafnium, zirconium, silicon, and boron. A method of depositing composite coatings of hard and very hard pyrolytic carbon was patented.[39] Theory[25] and practical application[40] of the fluidized-bed method for forming silicide coatings on large refractory-metal shapes were discussed. Multilayer diffusion coatings appear to afford some advantages over single-layer diffusion coatings.[41–43]

(E. M. Sherwood)

Ceramic Coatings

A patent[44] has been issued to the U. S. Atomic Energy Commission on an oxidation-resistant coating for metallic yttrium. The coatings consist of a silicate or phosphate glass plus 5 to 35 wt.% CeO_2. (B. W. King)

Metals Joining

Welding

Most of the welding studies continue to be concerned with the adaptation of existing processes and techniques to the joining of specific component designs.

A rather extensive study of gas–tungsten-arc welds in dissimilar-metal tubes is in progress at Hanford.[45,46] Several of the Hastelloy alloys, Haynes alloys, and stainless steels have been welded in various combinations. Hastelloy W is being used as the filler metal where superalloys are involved; type 316L stainless-steel filler metal is used in other combinations.

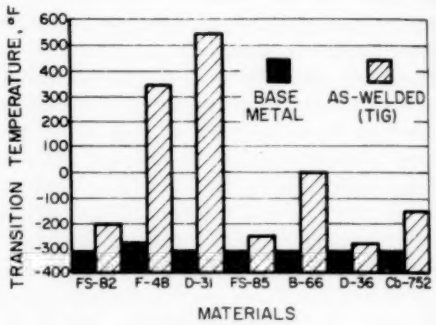

Fig. V-2 Ductile-to-brittle transition temperatures of several niobium alloys.[48]

Much attention should be paid the cleanliness of joints to be welded. This has been demonstrated recently in numerous cases where pressure vessels are fabricated for the aerospace programs. Reactor technologists have realized this for a long time, but periodically its importance must be reiterated. Mere touching of the joint area of aluminum fuel-element end caps with leather gloves prior to welding caused porosity in the joint, which was eliminated in later joints by the simple expedient of using tongs.[47]

Continuing their evaluation of the weldability of niobium alloys, Thompson Ramo Wooldridge[48] has reported on four additional alloys. The transition temperatures for wrought sheet and welded sheet of these alloys and of alloys previously studied are compared in Fig. V-2. Two thicknesses were included for each alloy, about 0.020 and 0.060 in. The effects of tungsten–inert-gas, electron-beam, and resistance spot-welding variables on weld properties were determined. Increases in the ductile-to-brittle transition temperature were recorded for tungsten–inert-gas and electron-beam welds in all alloys. Electron-beam welds were usually

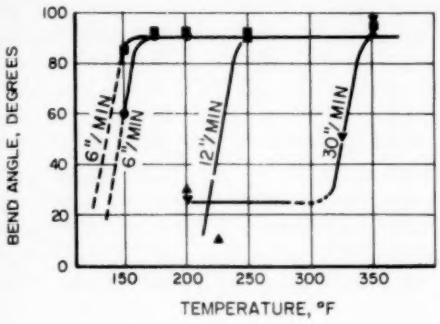

Fig. V-3 The effect of welding speed and amperage on the bend transition temperature of TZM.[49] Conditions: speed, variable; amperage, variable; weld width, constant (approximate); electrode, standard.

more ductile and stronger than the tungsten–inert-gas welds. Aging of the tungsten–inert-gas welds at 1800 and 2000°F raised the transition temperature further, especially for welds in B-66 and Cb-752.

The effects of various tungsten-arc–inert-gas welding parameters on bend ductility of welds in TZM alloy sheet have been reported by Universal Cyclops,[49] as shown in Figs. V-3 to V-5. It was concluded that the narrowest weld and lowest welding speeds would give the lowest bend transition temperature. Solar reports[50] that, when welding TZM foil (0.006 and 0.010 in.), it is necessary to preheat to 600°F to prevent cracking. In addition, the edges must be crimped to furnish filler, or else filler wire is necessary. Electron-beam welds were also made successfully in these foils. A major criterion for minimization of cracking and brittleness problems was absolute cleanliness.

The results of diffusion-bonding, electron-beam-, tungsten–inert-gas-, and resistance-welding studies on TD nickel have been published by NASA–Langley Research Center.[51] Sandwich structures held in an evacuated stainless-steel retort at 1×10^{-4} mm Hg for 24 hr at 2025°F contained diffusion-bonded joints that were stronger than the base metal. There was no agglomeration of the dispersed thoria. Electron-beam welds in 0.025- and 0.050-in. sheet showed minor agglomeration. The welds had some bend ductility but little tensile ductility. They were about 80% as strong as the base metal at room temperature. Tungsten–inert-gas welds made with nickel filler metal showed some diffusion of thoria into the filler metal and agglomeration at the grain boundaries. The joint efficiency was about equal to that of electron-beam welds. Welds made by the same process without filler metal were porous and only 50% as strong as the base metal at room temperature.

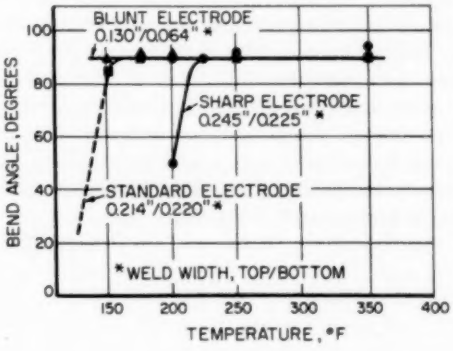

Fig. V-5 The effect of electrode configuration and weld width on the bend transition temperature of TZM.[49] Conditions: speed, 6 in./min; amperage, 125 amp; weld width, variable; electrode, variable.

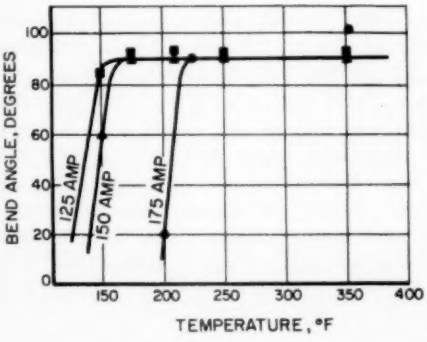

Fig. V-4 The effect of amperage and weld width on the bend transition temperature of TZM.[49] Conditions: speed, 6 in./min; amperage, variable; weld width, variable; electrode, standard.

Brazing

Brazing-technique- and brazing-alloy-development studies directed toward the fabrication of complex lightweight, high-temperature components persist as a major interest of metals-joining technologists.

The brazing of refractory-metal foils to be used in heat shields and other structures is the

subject of several research programs now in progress. One facet of these investigations is the determination of the effect of the thermal treatments involved in brazing on the properties of the foil. The effect of simulated brazing cycles on the room-temperature properties of several niobium alloys, TZM molybdenum alloy, and T-111 tantalum alloy as reported by Solar[52] is shown in Fig. V-6. Base-metal properties are given in Table V-1.

The titanium–13 wt.% vanadium–11 wt.% chromium–3 wt.% aluminum (B120VCA) alloy and a titanium-chromium alloy have been proven suitable for brazing D-36 niobium joints that are to be subjected in use to temperatures[53] above 2000°F. A novel technique for producing the titanium-chromium alloy in foil form was reported. Titanium foil 0.0015 in. thick was coated with chromium by vapor deposition. Following coating, the foil was given a diffusion treatment for less than 1 min at 2450°F to give a homogeneous alloy. In initial brazing tests it was found that the diffusion treatment could be included as a step in the brazing thermal cycle. Brazing at 2700°F without the diffusion step caused liquation of the alloy.

(R. M. Evans)

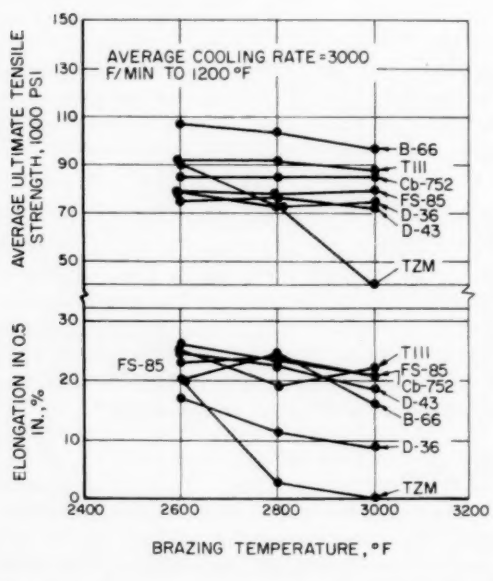

Fig. V-6 Room-temperature tensile properties of 0.006-in. foils[52] following various 5-min vacuum-brazing cycles in the 2600 to 3000°F temperature range.

Table V-1 ROOM-TEMPERATURE TENSILE PROPERTIES OF FOILS USED IN STUDY OF SIMULATED BRAZING CYCLES[52]

(As-Received Condition)

Alloy*,†	Ultimate tensile strength, 1000 psi	Elongation in 0.5 in., %
TZM	135.1	19
	128.7	19
B-66	104.2	16
(Heat DX-544)	102.1	20
D-36	79.8	19
	81.2	
Cb-752	134.0	4
	132.8	4
D-43	103.8	6
	103.0	8
FS-85	93.6	15
	95.8	14
T-111	91.6	21
	91.7	22

*Strain rate: 0.003 in./(in.)(min) (elastic range).

†Nominal gauge dimensions: 0.006 by 0.125 by 0.50 in.

Nondestructive Testing

Ultrasonic Techniques

General Electric[54] has been using an immersion ultrasonic testing facility in their Radioactive Materials Laboratory at Vallecitos to examine irradiated fuel rods. The equipment was designed especially for in-cell use, with most setup and maintenance done remotely by manipulators. It is claimed that cracks as small as 5% of the wall thickness may be detected under favorable conditions; however, if scratches, gouges, and scale are present, the test may be limited to cracks 30% of the wall or greater. The tester uses a pulse-echo technique.

The variety of useful techniques and the quantity of information possible with the employment of ultrasonics are indicative of its value to the field of nondestructive testing. Realization of its fullest potential is possibly far in the future. Hanford[55] and others[56] have been conducting studies that are expected to lead to improvements in interpreting received signals and in developing new techniques. Hanford[55] has been studying two-layered media, one layer

being the incident medium, the other the refracting medium. They claim that, whenever attenuation is considered either in the refracting medium or in both layers, the refracted waves are always inhomogeneous, whereas, without attenuation, inhomogeneous boundary waves are generated only at incidences equal to or exceeding the critical angles. Attenuation also resulted in a complex wave leading to a modified form of Snell's law which did not exhibit a critical angle. This study makes good use of schlieren photography.

Battelle[56] incorporates a variably delayed stroboscope in its schlieren system which is capable of "stopping" an ultrasonic pulse at any position in its travels. Movies have been produced of traveling pulses incident on various objects in water. This is a very valuable technique for studying the propagation characteristics of ultrasonic energy.

Argonne[21] is continuing work with image conversion. On round stock, the method will be useful for relatively large diameters (4 cm or more). Round stock acts as an ultrasonic lens which makes the image information from smaller-diameter material difficult to interpret. Argonne claims that visual flaw detection in flat material is much improved by orienting the sample at an angle of 15 to 20° from the direction of the ultrasonic beam. This is presumably because multiple reflections between the transducer and the specimen are eliminated.

(D. Ensminger)

NDT Methods Other Than Ultrasonic

The use of eddy-current instrumentation for separation of four test-specimen parameters independently has been demonstrated by investigators at Hanford. A "multiparameter" eddy-current unit[57] was employed, with a three-layered specimen composed of stainless steel on brass with carbon steel below the brass. The separation of parameters was good over the following ranges:

Parameter 1, probe spacing	0.0035 to 0.0115 in.
Parameter 2, stainless thickness	0.001 to 0.006 in.
Parameter 3, brass thickness	0.004 to 0.006 in.
Parameter 4, steel thickness	0.002 to 0.006 in.

The complex calculations and adjustments necessary to separate four parameters independently were found to be nearly an order of magnitude greater than those required to separate three parameters. The simultaneous separation of four parameters required multifrequency techniques. Frequencies of 6 kc, 22 kc, 70 kc, 250 kc, and 3 Mc were employed. The 3-Mc signal was used to check probe spacing. With one frequency, "several" parameters could be separated when only one parameter was varied at a time. The investigators feel that the concept used—transformations of parameters and signals in n-dimensional space—is new in its application to eddy-current testing and also has valuable potential applications in other areas of nondestructive testing.

Eddy-current techniques have also been used at Hanford[58] to detect the presence of hydride in Zircaloy-2 reactor process tubes. According to the investigators, hydride concentrations of about 100 ppm are positively identified by a single measurement. Further, the existence of 100 ppm hydride in a given sample can be determined positively if the eddy-current readings are referenced to previous measurements obtained when the sample was known to be in the nonhydrided state. Improvement of the stability, and thus the accuracy, of the instrument is being achieved by use of a special chopper technique believed to be new to eddy-current testing. A 60-cps chopper is employed in a signal comparator arrangement such that the effects of probe-spacing variations (and variations in instrument voltages) are reduced by the action of a center-of-curvature bridge reference circuit.

A pulsed electromagnetic test method using a differential encircling coil was developed[59] by investigators at Argonne to detect small cracks in Zircaloy-2 thermocouple tubing 0.080 in. in outside diameter with a 0.015-in. wall. The encircling coil consisted of three windings—a center winding that generated the field and a pickup winding located on each side. The center coil was driven with pulses approximately 6 μsec in duration and shaped like a half sinusoid. In its final form the instrument had sufficient sensitivity to detect cracks under 0.001 in. in depth emanating from the inner circumference. Inspection proceeded at a linear tube velocity of about 2 in./sec. (A. F. Leatherman)

References

1. Bureau of Mines, Albany Metallurgy Research Center, Quarterly Metallurgical Progress Report

No. 21, October 1–December 31, 1963, USAEC Report USBM-U-1091.

2. R. Burgett (Ed.), Summary Technical Report on Feed Materials, October 1–December 31, 1963, USAEC Report NLCO-900, National Lead Co. of Ohio, Feb. 17, 1964.
3. Bridgeport Brass Co., Quarterly Progress Summary on Fuel Development, April–June 1963, USAEC Report BRB-78, Dec. 13, 1963. (Classified)
4. E. V. Peterson, Columbium "H" Section Program. Phase I, Extrusion. Phase II, Drawing. Interim Report I, July 1–October 1, 1963, Report NP-13410, E. I. du Pont de Nemours & Co., Inc.
5. J. S. Clark and A. W. Dana, Jr., Final Report on Columbium Alloy Extrusion Program, Report ASD-TDR-63-637(Vol. I), E. I. du Pont de Nemours & Co., Inc., June 1963.
6. E. I. du Pont de Nemours & Co., Inc., Refractory Alloy Foil Rolling Development Program, Interim Report No. 2, October 15, 1962–January 15, 1963, Report AD-297246, Mar. 5, 1963.
7. Argonne National Laboratory, Reactor Development Program Progress Report, October 1963, USAEC Report ANL-6801, Nov. 15, 1963.
8. Nuclear Metals, Inc., Fundamental and Applied Research and Development in Metallurgy, September 1963, USAEC Report NMI-2121, Nov. 19, 1963.
9. Nuclear Metals, Inc., Fundamental and Applied Research and Development in Metallurgy, October 1963, USAEC Report NMI-2122, Dec. 10, 1963.
10. Nuclear Metals, Inc., Fundamental and Applied Research and Development in Metallurgy, November 1963, USAEC Report NMI-2123, Jan. 10, 1964.
11. General Electric Company, Advanced Technology Services, High-Temperature Materials Program, Progress Report No. 31, Part A, USAEC Report GEMP-31A, Jan. 24, 1964.
12. Hanford Atomic Products Operation, Specifications for Swage Compacted, Mixed Oxide (UO_2-Pu_2), Fuel Elements for the PRTR (MARK I-M), USAEC Report HW-79290, Oct. 1, 1963.
13. J. Weber, R. Lloyd, and W. L. Frankhouser, Cleaning Zircaloy Components for Pressure Bonding, USAEC Report WAPD-TM-375, Westinghouse Electric Corp., Bettis Atomic Power Laboratory, September 1963.
14. J. J. Auleta, D. B. Finch, L. Goodman, D. E. Lew, H. Mandel, and H. J. Rubenstein, Piqua Nuclear Power Facility Operations Analysis Program, Progress Report No. 2, Fiscal Year 1963, USAEC Report NAA-SR-8722, Atomics International, Nov. 30, 1963.
15. R. C. Bertossa, Feasibility Study on the Diffusion Bonding of Uranium, USAEC Report UCRL-13075, Pyromet Co., Oct. 15, 1962.
16. S. J. Buginas (Comp.), Diffusion Bonding: An Annotated Bibliography, Report AD-423723, Lockheed Missiles & Space Co., March 1963.
17. A. G. Metcalfe and T. B. Lindemer, Diffusion Bonding of Refractory Metals, Interim Technical Documentary Progress Report No. 1, Solar Aircraft Co., Oct. 1, 1962.
18. D. C. Carmichael, Diffusion Bonding, *Iron Age*, 192(3): 81-83 (July 18, 1963).
19. B. E. Murtha and W. P. Chernock, The Development and Testing of UO_2 Fuel Systems for Water Reactor Applications. Summary Report, July 1, 1961–June 15, 1962, USAEC Report CEND-157 (EURAEC-597), Combustion Engineering, Inc., 1962.
20. B. E. Murtha and W. P. Chernock, The Development and Testing of UO_2 Fuel Systems for Water Reactor Applications. Summary Report, June 15, 1962–July 31, 1963, USAEC Report CEND-186 (EURAEC-904), December 1963.
21. Argonne National Laboratory, Reactor Development Program Progress Report, January 1964, USAEC Report ANL-6840, Feb. 15, 1964.
22. Oak Ridge National Laboratory, Mar. 5, 1964. (Unpublished)
23. L. F. Gazeley and W. H. Mackie, Improvements Relating to Fuel Elements for Nuclear Reactors, British Patent 939,721, Oct. 16, 1963.
24. L. W. Owen, Recent Developments in the Technique of Nickel Plating from the Vapor of Nickel Carbonyl, *Plating*, 50(10): 911-915 (October 1963).
25. Papers presented at the 93rd AIME Annual Meeting, New York, Feb. 16–20, 1964.
    a. F. W. Hoertel, Vapor-Phase Deposition of Tungsten from Tungsten Hexafluoride.
    b. J. M. Gunderson and W. G. Dreisbach, Proposed Mechanism of Silicide Coating Formation on Molybdenum Alloys by Reaction with Silicon Iodides.
26. T. Heumann and G. Karsten, A Carbonyl Technique and an Evaporation Technique for the Determination of Phase Equilibria in Temperature Ranges of Low Mobility, Discussed in the Examples of Iron-Nickel Alloys, *Arch. Eisenhuttenw.*, 34(10): 781-785 (October 1963).
27. Papers presented at the AIME Technical Conference on Applied Aspects of Refractory Metals, Dec. 9–10, 1963.
    a. R. L. Heestand and C. F. Leitten, Jr., Parameters for the Production of Refractory Metal Tubing by the Vapor Deposition Process.
    b. N. R. Koenig, Vapor Deposition Bonding of Tungsten.
    c. M. J. Desckind and S. Maszy, Joining Tungsten by Chemical Vapor Deposition.
28. Aerojet-General Corp., Vapor-Deposition Bonding of Tungsten Spheres and Wires, Report MF-510 (Polaris Propulsion Research and Development), Oct. 31, 1963.
29. C. E. MacNeill, Chemical Joining of Aerospace Fibrous Materials, paper presented at the Sixth National SAMPE Symposium, Nov. 18–20, 1963.
30. A. F. Armington, G. F. Dillon, and R. F. Mitchell, The Preparation of High-Purity Boron via the

Iodide, *Trans. Met. Soc. AIME*, 230(2): 350-354 (March 1964).

31. W. L. Robb, Process for Boron Production, U. S. Patent 3,115,393, Dec. 24, 1963.
32. I. E. Knudsen, N. Levitz, and A. A. Jonke, Preparation of Dense Uranium Dioxide Particles from Uranium Hexafluoride in a Fluidized Bed, USAEC Report CONF-117-33, Sept. 1, 1963.
33. W. B. Campbell, Feasibility of Forming Refractory Fibers by a Continuous Process, Report AD-426713, Aug. 25, 1963.
34. E. I. Ryshkewitch and A. R. Sheets, Method for Producing High Purity Monocrystalline Beryllia Fibers and Platelets, U. S. Patent 3,125,416, Mar. 17, 1964.
35. L. G. Davies and J. C. Withers, A Study of High-Modulus, High-Strength Filament Materials by Deposition Techniques, First Bi-Monthly Progress Report Covering Period November 1 to December 31, 1963, General Technologies Corp., Jan. 15, 1964.
36. General Atomic Division, General Dynamics Corp., Investigations of Carbides as Cathodes for Thermionic Space Reactors, Report GA-4391, Sept. 25, 1963.
37. G. J. Burcal and H. C. Sumner, Research on Metal-Organic Compounds for Vapor-Plating Applications, Quarterly Progress Report No. 2, August 1–October 31, 1963, Report GR-63-61, Ethyl Corp. Research Laboratories.
38. G. J. Burcal and J. D. Odenweller, Research on Metal-Organic Compounds for Vapor-Plating Applications, Quarterly Progress Report No. 3, November 1, 1963–January 31, 1964, Report GR-64-11, Ethyl Corp. Research Laboratories.
39. R. J. Diefendorf and R. M. Williams, Method for Depositing Carbon Coatings on High-Temperature Material Members, U. S. Patent 3,120,450, Feb. 4, 1964.
40. G. Michaelson, Fabricating and Coating Molybdenum Alloy Parts, *Metal Progr.*, 85(3): 88-91 (March 1963).
41. P. J. Chao, Multilayer Diffusion Coatings and Method of Applying the Same, U. S. Patent 3,117,846, Jan. 14, 1964.
42. TAPCO, Division of Thompson Ramo Wooldridge Inc., Oxidation Resistant High Temperature Protective Coatings for Tungsten, First Quarterly Progress Report for Period May 15–August 15, 1963, Report TM-3792-67.
43. W. A. Gibeaut and E. S. Bartlett, Properties of Coated Refractory Metals, Report DMIC-195, Battelle Memorial Institute, Defense Metals Information Center, Jan. 10, 1964.
44. D. R. Wilder and C. D. Wirkus, Oxidation-Resistant Coating on Articles of Yttrium Metal, U. S. Patent 3,109,752 (to USAEC), Nov. 5, 1963.
45. R. L. Knecht, Dissimilar Metal Welds of Certain Superalloys and Stainless Steels, USAEC Report HW-78574, Hanford Atomic Products Operation, August 1963.
46. Hanford Atomic Products Operation, Metallurgy Research Operation, Quarterly Progress Report, April–June 1963, USAEC Report HW-77954, July 15, 1963.
47. Hanford Atomic Products Operation, Reactor and Fuels Laboratory Monthly Report, January 1964, USAEC Report HW-80560A, Feb. 14, 1964. (Classified)
48. J. M. Gerken and T. L. Fullerton, Investigation of Weldability of Additional Columbium Alloys, Report ASD-TDR-63-843, Thompson Ramo Wooldridge, Inc., July 1963.
49. F. D. Seaman and D. J. Seman, Welding of Refractory Metals, Interim Technical Documentary Report No. 4, Universal-Cyclops Steel Corp., October 1963.
50. J. W. Welty, P. J. Valdez, C. E. Smeltzer, and C. P. Davis, Joining of Refractory Metal Foils, Report ASD-TDR-63-799, Part I, Solar, Subsidiary of International Harvester Co., July 1963.
51. C. R. Manning, D. M. Royster, and D. N. Braski, An Investigation of a New Nickel Alloy Strengthened by Dispersed Thoria, Report NASA-TN-D-1944, Langley Research Center, July 1963.
52. Solar, A Division of International Harvester Co., Joining of Refractory Metal Foils, Quarterly Progress Report No. 5, Report RDR/1324-5, Oct. 25, 1963.
53. D. B. Hugill and B. Gainnie', Quartz Lamp Radiant Heat Brazing of Large Refractory Metal Honeycomb Panels, IR-7-937a (IV), Fourth Interim Engineering Progress Report, April 10 to July 10, 1963, NORAIR Division, Northrop Corp.
54. T. G. Lambert, Ultrasonic Inspection of Irradiated Fuel Rods, in *Proceedings of the 11th Conference on Hot Laboratory Equipment*, pp. 255-265, New York, 1963.
55. C. E. Fitch, Jr., Ultrasonic Wave Propagation Models for Nondestructive Testing: Liquid-Liquid Interfaces, USAEC Report HW-78701, Hanford Atomic Products Operation, October 1963.
56. D. F. Fox, D. Ensminger, and D. E. Stutz, Ultrasonic Testing of Thin Plates, paper presented at 1964 Spring National Convention of the Society for Nondestructive Testing, Mar. 19, 1964.
57. H. L. Libby and K. W. Atwood, Broadband Electromagnetic Testing Methods, Part III. Parameter Extraction, USAEC Report HW-79553, Hanford Atomic Products Operation, November 1963.
58. M. M. Hendrickson and J. K. Green (Eds.), Research and Development Programs Executed for the Division of Reactor Development, USAEC Report HW-78388, Hanford Atomic Products Operation, July 1963.
59. R. H. Selner, C. J. Renken, R. B. Perry, and K. Balaramamoorthy, Nondestructive Tests of Components of EBR-I, Core IV, USAEC Report ANL-6632, Argonne National Laboratory, October 1963.

LEGAL NOTICE

This journal was prepared under the sponsorship of the U. S. Atomic Energy Commission. Neither the United States, nor the Commission, nor any person acting on behalf of the Commission:

A. Makes any warranty or representation, expressed or implied, with respect to the accuracy, completeness, or usefulness of the information contained in this journal, or that the use of any information, apparatus, method, or process disclosed in this journal may not infringe privately owned rights; or

B. Assumes any liabilities with respect to the use of, or for damages resulting from the use of any information, apparatus, method, or process disclosed in this journal.

As used in the above, "person acting on behalf of the Commission" includes any employee or contractor of the Commission, or employee of such contractor, to the extent that such employee or contractor of the Commission, or employee of such contractor prepares, disseminates, or provides access to, any information pursuant to his employment or contract with the Commission, or his employment with such contractor.

NUCLEAR SCIENCE ABSTRACTS

The U. S. Atomic Energy Commission, Division of Technical Information, publishes *Nuclear Science Abstracts (NSA)*, a semimonthly journal containing abstracts of the literature of nuclear science and engineering.

NSA covers (1) research reports of the U. S. Atomic Energy Commission and its contractors; (2) research reports of government agencies, universities, and industrial research organizations on a world-wide basis; and (3) translations, patents, books, and articles appearing in technical and scientific journals.

Complete indexes covering subject, author, source, and report number are included in each issue. These are cumulated quarterly, semiannually, and annually providing a detailed and convenient key to the literature.

Availability of *NSA*

SALE *NSA* is available on subscription from the Superintendent of Documents, U. S. Government Printing Office, Washington, D. C., 20402, at $30.00 per year for the semimonthly abstract issues and $22.00 per year for the four cumulated-index issues. Subscriptions are postpaid within the United States, Canada, Mexico, and all Central and South American countries, except Argentina, Brazil, British and French Guiana, Surinam, and British Honduras. Subscribers in these Central and South American countries, and in all other countries throughout the world, should remit $37.00 per year for subscriptions to semimonthly abstract issues and $25.00 per year for the four cumulated-index issues.

EXCHANGE *NSA* is also available on an exchange basis to universities, research institutions, industrial firms, and publishers of scientific information. Inquiries should be directed to the Division of Technical Information Extension, U. S. Atomic Energy Commission, P. O. Box 62, Oak Ridge, Tennessee, 37831.